NASA/TM–20240009657
NESC-RP-19-01482

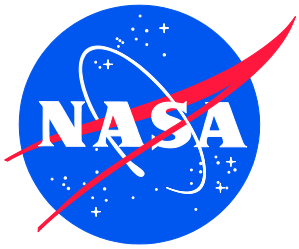

Characterization of Internal Insulation Thermal Performance

Jonathan E. Jones/NESC
Langley Research Center, Hampton, Virginia

Heath T. Martin
Marshall Space Flight Center, Huntsville, Alabama

James M. Womack
Northern Nevada Statistical Consulting, LLC, Agoura Hills, California

Andrew T. Hiatt
Marshall Space Flight Center, Huntsville, Alabama

July 2024

NASA STI Program Report Series

Since its founding, NASA has been dedicated to the advancement of aeronautics and space science. The NASA scientific and technical information (STI) program plays a key part in helping NASA maintain this important role.

The NASA STI program operates under the auspices of the Agency Chief Information Officer. It collects, organizes, provides for archiving, and disseminates NASA's STI. The NASA STI program provides access to the NTRS Registered and its public interface, the NASA Technical Reports Server, thus providing one of the largest collections of aeronautical and space science STI in the world. Results are published in both non-NASA channels and by NASA in the NASA STI Report Series, which includes the following report types:

- TECHNICAL PUBLICATION. Reports of completed research or a major significant phase of research that present the results of NASA Programs and include extensive data or theoretical analysis. Includes compilations of significant scientific and technical data and information deemed to be of continuing reference value. NASA counterpart of peer-reviewed formal professional papers but has less stringent limitations on manuscript length and extent of graphic presentations.

- TECHNICAL MEMORANDUM. Scientific and technical findings that are preliminary or of specialized interest, e.g., quick release reports, working papers, and bibliographies that contain minimal annotation. Does not contain extensive analysis.

- CONTRACTOR REPORT. Scientific and technical findings by NASA-sponsored contractors and grantees.

- CONFERENCE PUBLICATION. Collected papers from scientific and technical conferences, symposia, seminars, or other meetings sponsored or co-sponsored by NASA.

- SPECIAL PUBLICATION. Scientific, technical, or historical information from NASA programs, projects, and missions, often concerned with subjects having substantial public interest.

- TECHNICAL TRANSLATION. English-language translations of foreign scientific and technical material pertinent to NASA's mission.

Specialized services also include organizing and publishing research results, distributing specialized research announcements and feeds, providing information desk and personal search support, and enabling data exchange services.

For more information about the NASA STI program, see the following:

- Access the NASA STI program home page at http://www.sti.nasa.gov

- Help desk contact information:

https://www.sti.nasa.gov/sti-contact-form/
and select the "General" help request type.

NASA/TM–20240009657
NESC-RP-19-01482

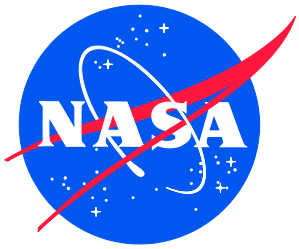

Characterization of Internal Insulation Thermal Performance

Jonathan E. Jones/NESC
Langley Research Center, Hampton, Virginia

Heath T. Martin
Marshall Space Flight Center, Huntsville, Alabama

James M. Womack
Northern Nevada Statistical Consulting, LLC, Agoura Hills, California

Andrew T. Hiatt
Marshall Space Flight Center, Huntsville, Alabama

National Aeronautics and
Space Administration

Langley Research Center
Hampton, Virginia 23681-2199

July 2024

Available from:

NASA STI Program / Mail Stop 050
NASA Langley Research Center
Hampton, VA 23681-2199

NASA Engineering and Safety Center
Technical Assessment Report

Characterization of Internal Insulation Thermal Performance

TI-19-01482

NESC Lead – Jonathan Jones

Technical Lead – Heath Martin

June 25, 2024

Report Approval and Revision History

NOTE: This document was approved at the June 25, 2024, NRB.

Approved:	Timmy Wilson Digitally signed by Timmy Wilson Date: 2024.07.09 11:19:51 -04'00'		
	NESC Director		Date

Version	Description of Revision	Office of Primary Responsibility	Effective Date
1.0	Initial Release	Dr. Jonathan E. Jones, NASA Technical Fellow for Propulsion, MSFC	06/25/2024

Table of Contents

Technical Assessment Report

List of Figures

List of Tables

Technical Assessment Report

1.0 Notification and Authorization

In the thermal analysis of solid rocket motor (SRM) internal insulation, current models are generally inadequate for predicting the performance of ablative materials. For systems in which hot-fire test data are available, these models can be calibrated to produce reasonably accurate results for small variations of important parameters (e.g., chamber pressure, firing duration, or propellant composition); however, for untested systems, significant uncertainty exists in insulation performance predictions. Though it is not yet possible to incorporate the necessary physics into a predictive fundamental-physics model of material ablation, a semi-empirical approach incorporating data from widely used internal insulation materials under a range of relevant environments can produce many of the same benefits faster and with fewer resources.

This proposed approach includes: 1) characterization of an internal-insulation test bed; 2) compilation of a thermal performance database for common insulation materials in the characterized test bed; and 3) correlation of material performance with thermal environmental variables for use in SRM performance predictions.

The key stakeholders for this assessment are the Space Launch System (SLS) Program and other programs using SRMs.

2.0 Signature Page

Submitted by:

JONATHAN JONES
Digitally signed by JONATHAN JONES
Date: 2024.07.08 09:24:15 -05'00'

Dr. Jonathan E. Jones

Significant Contributors:

Heath Martin
Digitally signed by Heath Martin
Date: 2024.07.08 08:27:48 -05'00'

Dr. Heath T. Martin

James Womack (affiliate)
Digitally signed by James Womack (affiliate)
Date: 2024.07.02 09:19:23 -07'00'

Dr. James M. Womack

Andrew Hiatt
Digitally signed by Andrew Hiatt
Date: 2024.07.03 13:32:01 -05'00'

Mr. Andrew T. Hiatt

Signatories declare the findings, observations, and NESC recommendations compiled in the report are factually based from data extracted from program/project documents, contractor reports, and open literature, and/or generated from independently conducted tests, analyses, and inspections.

3.0 Team List

Name	Discipline	Organization
Core Team		
Jonathan Jones	NASA Propulsion Technical Fellow	MSFC
Dan Dorney	NASA Propulsion Technical Fellow (ret.)	MSFC
Jeff Rayburn	NASA Propulsion Deputy Technical Fellow	MSFC
Heath Martin	Technical Lead	MSFC
John Sharp	Thermal	MSFC
Paul Dumbacher	Test Engineer	MSFC
Bradley Lawrence	Technician (M&P)	MSFC
Andrew Hiatt	Early Career Engineer	MSFC
Shelby Westrich	Materials	MSFC
James Womack	Statistician	LaRC
Business Management		
Pamela Stacy	Program Analyst	LaRC/MTSO
Katherine King	Program Analyst	LaRC/MTSO
Assessment Support		
Linda Burgess	Planning and Control Analyst	LaRC/AMA
Erin Moran	Technical Editor	LaRC/AMA
Betty Trebaol	Project Coordinator	LaRC/AMA

3.1 Acknowledgments

The assessment team would like to acknowledge the significant contributions made by Chloe Bower and Shelby Westrich for engineering, planning, executing, and evaluating the Solid Fuel Torch (SFT) tests.

4.0 Executive Summary

In the thermal analysis of solid rocket motor (SRM) internal insulation, current models are generally inadequate for accurately predicting the thermal performance of ablative materials. For systems in which hot-fire test data are available, these models can be calibrated to produce reasonably accurate results for small variations of important parameters (e.g., chamber pressure, firing duration, or propellant composition), but for untested systems, significant uncertainty exists in insulation performance predictions. A semi-empirical approach—incorporating data from an array of widely used internal insulation materials under a range of thermal environments relevant to SRMs—can be used to accurately model material ablation in new SRM designs.

A test campaign was completed to hot-fire test four commonly used SRM internal insulation materials in the Marshall Space Flight Center (MSFC) Solid Fuel Torch (SFT) and to test Polybenzimidazole-Nitrile Butadiene Rubber (PBI-NBR) insulation at three non-standard fuel-aluminum (Al) loadings. All seven tests were successfully performed, along with subsequent data analysis that revealed the thermal performance differences among these tested materials as well as among materials tested in other efforts. Functional data analysis (FDA) was used to create a model of insulation material decomposition rates (MDRs) as a function of six covariates: oxygen (O_2) mass flow rate, nitrogen (N_2) mass flow rate, oxidizer-to-fuel ratio, alumina (Al_2O_3) mass fraction, average chamber pressure, and material group. This MDR model was then used to interrogate the relationships among these covariates and insulation thermal response.

From this NESC assessment, it was concluded that for all materials, MDR is most sensitive to O_2 mass flow rate among the FDA covariates and, in the sample region where the flow is attached, its correlation is positive, meaning greater O_2 mass flow rates produce greater MDRs. Increasing amounts of condensed-phase alumina in the SFT combustion products were determined to increase insulation MDRs for all but the forward-most locations of an insulation sample, but this effect was relatively weak. The functional regression model revealed a counter-intuitive negative correlation between MDR and pressure in the attached-flow region, but a positive correlation in the separated-flow portion of the sample. The standard SFT configuration produces irregular flow environments in the forward portion of the sample that seem to erroneously influence the MDR correlation.

Uncertainties in the precise fluid, thermal, and chemical environment in the insulation test sample complicate the effort to use SFT MDRs to predict insulation performance in SRMs. Coupled thermal-fluid-chemical modeling of the SFT and additional testing at non-standard conditions (e.g., other fuel Al loadings, pressures) would reduce uncertainties and increase the usefulness of the SFT material database for SRM design and material development.

5.0 Assessment Plan

The objective of the proposed effort was to compile a material thermal performance database from a well-characterized subscale test bed that can be used to validate, calibrate, or construct thermo-ablative models with improved fidelity and/or predictive capability over existing processes and tools.

As a well-characterized subscale test bed, the MSFC SFT was used to perform hot-fire testing of commonly used SRM internal insulation materials for the collection of material response data in the form of time-averaged MDRs. The result of this effort was a NASA-owned database of thermal performance for several internal insulation materials that can improve thermal models, be shared with industry, and fill important gaps in NASA's knowledge.

6.0 Background and Current Effort

6.1 Background

New solid/hybrid motor designs often encounter issues. Recent examples include:

- Peregrine – Motor case failure during testing and redesign challenges [ref. 1]
- Mars Ascent Vehicle (MAV) – Unexpected performance during testing [refs. 2-7]
- Super Strypi (Sandia, Aerojet Rocketdyne, University of Hawaii) – First-stage failure during inaugural flight [refs. 8-9]
- Landspace Zhuque-1 (China, private) – Third-stage failure during inaugural flight [refs. 10-11]
- Northrop-Grumman OmegA – Explosion near the throat/nozzle during a static test fire [refs. 12-13] (see Figure 1)
- Other solid/hybrid rocket failure studies, including those associated with insulation [refs. 14-18]

Figure 1. Nozzle Failure During the OmegA SRM Test [ref. 13]

6.1.1 MSFC SFT

The MSFC SFT [ref. 19] is a 6-inch-diameter hybrid rocket motor that is used primarily to generate SRM-like internal thermochemical environments for lab-scale testing of SRM internal

insulation materials. The insulation test sample is designed so that it experiences a range of heating and viscous shear rates that roughly bound those occurring within SRMs. The hybrid nature of the SFT makes it safer and, consequently, much cheaper to manufacture, assemble, and operate than a comparably sized SRM and provides a more convenient means of controlling inputs to produce atypical environments. Prior to the current effort, the SFT had been fired 74 times with various materials and in various configurations.

Though it has been fired in a multiplicity of configurations, the standard variant is shown in Figure 2. This variant employs a solid fuel grain that consists of hydroxyl-terminated polybutadiene (HTPB) rubber and 50% by mass of Al powder that is combusted with an oxidizer consisting of gaseous oxygen (GOx) diluted with 55% by mass gaseous nitrogen (GN_2) (oxidizer-to-fuel ratio (O/F) = 2.7) to produce a combination of temperature, pressure, and chemical species (the non-geometric factors supposed to drive ablation) that is analogous to that of the SLS SRM. Table 1 provides a comparison of these important internal environmental parameters between the standard SFT configuration and the SLS SRM.

The SFT nozzle comprises a series of four tungsten rings surrounded by a copper water-cooling jacket, which does not erode under typical test conditions. This non-eroding nozzle combined with the limited O/F shift that occurs over the standard 10-s test duration generates a stable, near-constant pressure environment that facilitates post-test data analysis and interpretation.

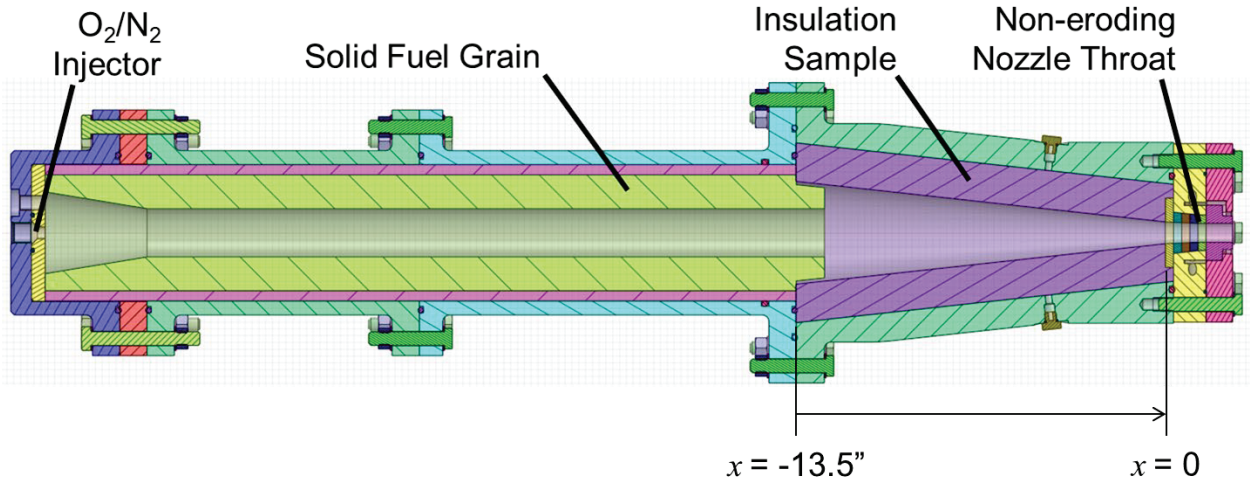

Figure 2. Standard Converging-cone SFT Configuration Cross-section

Table 1. Comparison of SFT and SLS Booster Internal Environment Parameters

Parameter	SLS Booster (Block I)	SFT, Standard Configuration
Average Pressure, psia	720	810
Flame Temperature, K	3400	3700
Al_2O_3 Content in Products (%)	28	24

The insulation sample in this configuration is a simple cone that converges in the flow direction; thus, it is denoted the converging-cone insulation configuration. This geometry causes the combustion-product mass flux to increase steadily in the flow direction until it reaches its maximum at the nozzle throat. As mass flux correlates positively with viscous shear stress and convective heat transfer in an internal flow, the converging-cone geometry serves as a means of testing an insulation material over a smoothly varying range of heating and shear rates and

producing a smoothly varying ablation-rate curve in a single test firing. One issue with the standard configuration is the relatively small fuel-grain port diameter, combined with its penetration into the forward end of the insulation sample cone, produces a significant region of separated flow (i.e., a recirculation zone) in the forward portion of the sample. In the separated-flow region, heating, viscous-shear, and mass-transfer rates differ from those that would occur for attached flow in ways that are difficult to quantify. Though this type of environment is relevant to SRM interiors (e.g., forward domes), the existence of this zone complicates analysis of material performance in this region.

Fine resolution of the material-response data is enabled by using structured-light scanning to measure the pre- and post-test dimensions of the insulation sample. This technique produces thousands of circumferential measurements of the insulation sample inner radius for each of the 0.1-in-spaced axial stations. These measurements are circumferentially averaged to generate a single radius measurement for each axial station for both pre- and post-test cases. Prior to the post-test scan, the char is manually scraped from the fired surface, as consistent with historical practice. The pre-test average radius is then subtracted from the post-test radius at each axial station to produce the material decomposition depth (MDD). The response parameter of interest, the MDR or ablation rate is computed by dividing these MDDs by the test duration, which is defined as the time during which the insulation sample is exposed to a hot-gas flow. The MDR is the customary metric of thermal performance for internal insulation materials because the low thermal diffusivity of typical rubber-matrix materials ensures that, in normal use cases, the thermal front does not proceed far beyond the pyrolysis zone. Therefore, the MDR multiplied by the insulation exposure time in a given motor location provides a reasonable estimate of the thickness required for adequate thermal protection.

6.2 Assessment

Originally, it was planned to use the SFT to perform hot-fire testing of seven commonly used insulation materials in the standard SFT configuration for the collection of material response data in the form of time-averaged MDRs; however, in the period between the assessment proposal and initiation, two of the proposed materials were tested in the SFT under another program and one of the proposed materials became obsolete. Therefore, it was decided to use the three tests that would have been performed for those materials to study the effect of propellant Al loading on the insulation ablation. Table 2 lists each of the test materials and examples of its current application. Specification sheets are included in Appendix D.

Table 2. Test Materials and Application Examples

PBI-NBR	Primary insulation used in SLS Booster – These tests will be used to assess the sensitivity of insulation material performance to different environmental parameters
Silica filled - ethylene-propylene-diene monomers (SF-EPDM)	Used in SLS Booster and material that exhibited unexpectedly poor performance in the Peregrine sounding rocket
SF-NBR	Used in SLS Booster
FM-5504 Silica-Cloth Phenolic (SCP)	Used as a nozzle material and as an internal insulation material in high-convection environments (e.g., MAV-Hybrid and Peregrine 2.0 and small test motors)
MXSE-55 Rubber-Modified SCP	Employed in SLS-LAS-ACM, Black Brant, and Peregrine 2.0

Two of the test materials are from the family of SCPs, which have a plastic matrix material rather than the rubber typically used in internal insulation materials and whose fiber content is in the form of woven cloth rather than chopped fibers. This makes the SCP denser and less elastic than powder- or fiber-filled EPDMs and NBRs and therefore more suited as nozzle liners than as internal insulation. Nevertheless, these materials have been used as internal insulators in strong shear flow regions in flight and test motors. The different properties of the phenolic materials require different methods for fabricating test samples. As shown in Figure 3, the phenolic sample cones retain the interior dimensions of the rubber cones but are made as two separate parts. The larger-diameter cone is tape-wrapped, but the smaller-diameter part is press molded, as its diameter is too small for proper tape wrapping. Both parts are surrounded by reusable SCP liners, and the gap between the parts and the liners is filled with silicone RTV sealant. The test sample plies are aligned 30° to the motor's centerline, which results in their having a 23.8° angle to the inner sample surface. The SCP plies were not aligned parallel to the exposed surface as the SCP's properties cause it to be vulnerable to ply separation and sloughing upon heating when configured with extremely low ply angles to the heated surface.

There were manufacturing-related anomalies for the phenolic samples reported by the manufacturing personnel following the curing operation, which are shown in Appendix A. After examination of these areas by the technical lead, it was determined that these areas would have an inconsequential effect on the MDR measurements and were allowed to proceed through the remaining manufacturing process and into test.

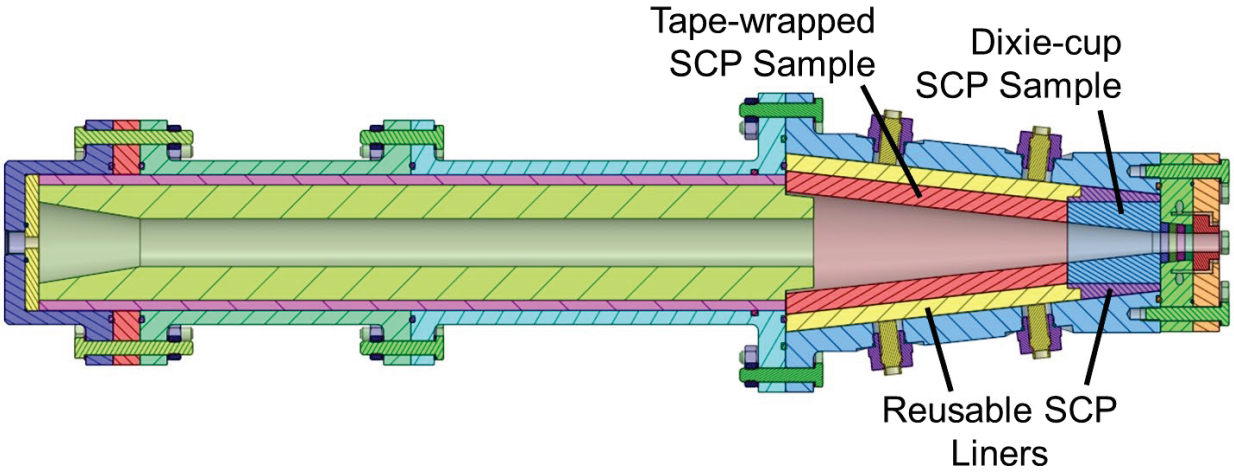

Figure 3. Phenolic-Composite-Sample SFT Configuration Cross-section

Though always a topic of interest, the effect of propellant Al loading on insulation performance became particularly salient when the SLS Booster Obsolescence and Life Extension (BOLE) motor was designed to use a 19% Al by mass propellant, rather than using the heritage Space Shuttle Program and SLS SRMs' 16% Al formulation. The first subscale SRM static test that included the BOLE propellant formulation resulted in increased ablation of the control insulation material above that attributable to the increase in average chamber pressure alone from the previous 16%-Al tests. The primary product of Al combustion is liquid-phase Al_2O_3 droplets. The presence of these droplets in the combustion-product flow could increase the rate of insulation ablation in some scenarios but could decrease it in others depending on the types and magnitudes of the interactions between the Al_2O_3 droplets and the insulation/char surface. The

uncertainty surrounding these interactions and their net effect prompted the sub-series of SFT tests performed at various Al loadings in this assessment.

The size, simplicity, and safety of the SFT grain casting operation made casting fuel grains at varied Al loadings straightforward, and grains were cast at 0, 13, and 60% by mass of Al. The hybrid fuel grains have higher Al percentages than comparable solid-propellant grains because the hybrid grains do not contain the oxidizer. The ability to vary the O_2 and N_2 flow rates independently in the SFT allowed the chamber pressure and flame temperature to vary minimally for each of the different Al loadings. The test material selected was PBI-NBR, as it is the most thoroughly tested SRM internal insulation material at MSFC; therefore, results from multiple SFT tests at standard conditions exist with which to compare those from the non-standard Al loading tests. Table 3 shows the complete test matrix for this assessment.

Table 3. Characterization of Internal Insulation Thermal Performance Test Matrix

Test No.	Material	Al% in Solid Fuel	O_2 mass flow rate [lbm/s]	N_2% of Oxidizer	O/F	Pressure [psia]	Flame Temp. [K]	Al_2O_3% in products
1	PBI-NBR	0	1.10	23	3.50	810	3582	0.0
2	PBI-NBR	13	0.95	34	3.36	809	3574	5.3
3	PBI-NBR	60	0.55	63	2.68	819	3647	27
4	SF-EPDM	50	0.65	55	2.72	810	3700	24
5	SF-NBR	50	0.65	55	2.72	810	3700	24
6	MXSE-55 SCP	50	0.65	55	2.72	810	3700	24
7	FM-5504 SCP	50	0.65	55	2.72	810	3700	24

The ultimate goal of this effort is to produce an empirical correlation of insulation material thermal performance with thermal and chemical environmental parameters that can be used to predict insulation MDRs for a given material in untested systems or conditions. To that end, FDA techniques were applied to data collected from all SFT tests using the "converging cone" insulation sample configuration (not merely the NESC-funded ones). The regression model produced by this analysis was examined to identify the factors with the greatest influence on insulation MDR.

7.0 Results and Discussion

7.1 Al Loading Study

The SFT test firings were performed in three rounds on different days: Tests 1 and 2 on April 28, 2022, Tests 3, 4, and 5 on July 27, 2022, and Tests 6 and 7 on July 11, 2023. Table 4 provides the notable test parameters for each test of this series, which vary slightly from the values given in Table 3. The first three tests were those performed for studying Al content effects on insulation performance, and the resulting MDRs are plotted against axial location in Figure 4 alongside the average result for three tests of PBI-NBR at standard conditions (50% Al). The error bars on the 50% Al curve represent two sample standard deviations ($\pm 2\sigma$) and illustrate the test-to-test variation in MDR for this material under consistent conditions. The axial coordinate, x, is defined as shown in Figure 2, with the zero location being the aft extent of the samples and the forward-most location being x = -13.5 in. The MDR decrease occurring aft of x = -0.5 for the high-MDR cases reflects the influence of the slower-eroding SCP ring directly downstream.

These data indicate that the differences among the MDRs for the various Al levels in the low-mass-flux/separated-flow region of the test sample may not be significant, but those in the high-mass-flux/attached-flow region likely are. These differences indicate a negative correlation between Al loading and MDR (i.e., increasing Al loadings lead to decreasing insulation ablation rates). This result seems counter-intuitive, especially given that the HTPB fuel regression rate in these tests is positively correlated with Al loading (as consistent with results in the literature [ref. 20]). Additionally, the physics driving hybrid fuel regression, diffusion-limited thermal polymer decomposition [ref. 21], is essentially identical to that driving insulation ablation. The positive correlation between Al loading and fuel regression is typically understood as resulting from increased heat feedback from the flame to the fuel surface through thermal radiation from burning Al and hot Al_2O_3 droplets [ref. 20]. In Figure 5, this correlation is illustrated by plotting fuel mass-loss ratio against fuel Al percentage by mass. Fuel mass-loss ratio is defined as the difference between the fuel grain's post-test mass and its pre-test mass divided by its pre-test mass, which provides a density-independent, non-dimensional correlative of regression rate. Fuel mass-loss ratio increases monotonically with Al loading and practically linearly for the non-zero Al loadings. The same plot reveals a monotonic decrease in insulation mass loss with increasing fuel Al loading. However, the data in Figure 4 suggest the mass loss difference between the 0 and 13% results is not significant, which is another departure from the fuel mass-loss data where there is a substantial difference between having no Al and some Al in the fuel.

It appears from these data that the enhancement of the radiative heat transfer from the propellant flame to the fuel surface (on the emission and absorption sides) enhances fuel regression, but not insulation recession. This supports two non-exclusive possibilities: 1) the fuel-regression enhancement is produced primarily by the effects of having Al in the fuel (e.g., increased radiation absorption, higher thermal conductivity, etc.) than by the effects of having burning Al or hot Al_2O_3 in the combustion product stream, and 2) that incident radiation to the insulation surface is substantially reduced through absorption and scattering by condensed-phase pyrolysis products and, therefore, not a significant contributor to the total heat absorbed by the insulator. Furthermore, the inverse relationship between fuel-Al loading and insulation ablation rates means, not only radiation effects, but also effects from droplet impingement or slag films must be insignificant compared to gas-phase effects.

Table 4. As -Measured Parameters for Internal Insulation Thermal Performance Tests

Test No. iSFT-	Material	Al% in Solid Fuel	O_2 mass flow rate [lbm/s]	N_2% of Oxidizer	O/F	Pressure [psia]	Flame Temp. [K]	Al_2O_3% in products
075	PBI-NBR	0	1.063	22	4.25	765	3530	0.0
076	PBI-NBR	13	0.923	34	3.58	837	3574	5.1
077	PBI-NBR	60	0.540	62	2.46	812	3606	27
078	SF-EPDM	50	0.610	55	2.43	815	3674	25
079	SF-NBR	50	0.610	55	2.51	809	3681	25
086	MXSE-55 SCP	50	0.636	54	2.59	782	3719	24
087	FM-5504 SCP	50	0.634	55	2.64	769	3717	24

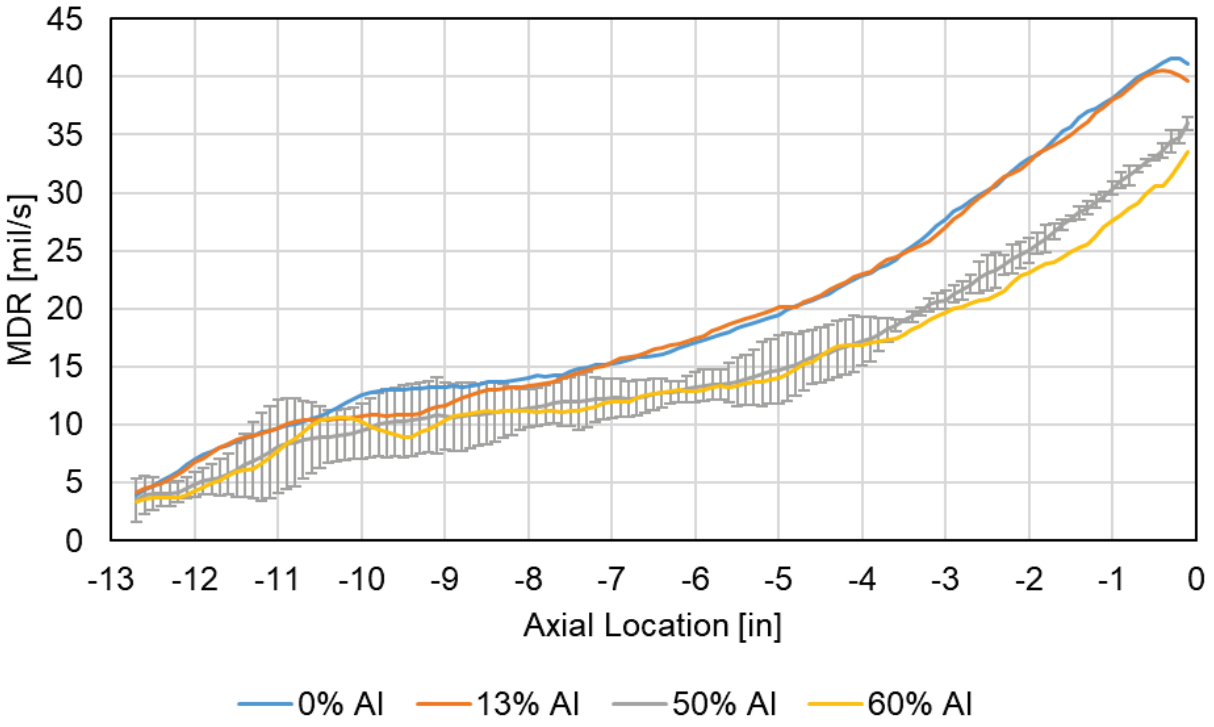

Figure 4. PBI-NBR MDRs versus Axial Location for Different Fuel-Al Loadings

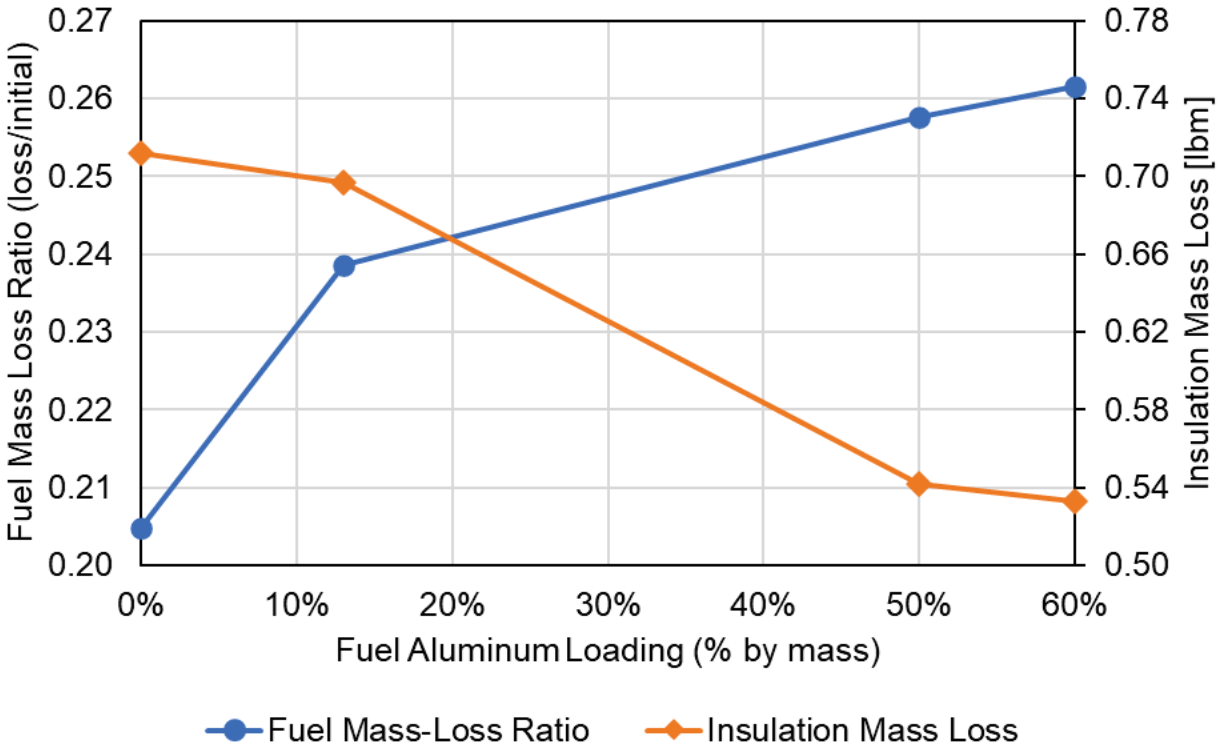

Figure 5. Fuel Mass-Loss Ratio and Insulation Mass Loss for Different Fuel-Al Loadings

Though the test conditions were designed such that the only factor significantly affecting the insulation MDRs would be the amount of Al_2O_3 in the combustion-product flow, it was not possible to completely limit the effect of varying fuel-Al loading to a single factor. The mass

flow rate of oxidizer and the proportion of that consisting of N_2 were varied to compensate for the higher temperatures and pressures that would otherwise result from increasing Al loading, which additionally affected O/F. Furthermore, Al combustion inevitably affects the product species mixture even for the same product temperature and pressure. Finally, the target conditions were not precisely replicated because of test variability, overprediction of fuel regression rate for low Al loadings, and differences in nozzle erosion behavior induced by the different concentrations of Al_2O_3 in the combustion products. As illustrated in Figure 6, the consequence of these realities is that the mass flow rate of the gas-phase products through the insulation sample is lower for the tests with higher Al loadings as is the mass percentage of strong oxidizing species (O_2, OH, and O) in the product stream. Surface oxidation is not considered to significantly influence rubber-matrix insulation recession as its weak char is thought to be more readily removed by mechanical than thermochemical effects. The gas-phase mass flux, through its correlation with convective heat and momentum transfer rates, is regarded as the dominant factor.

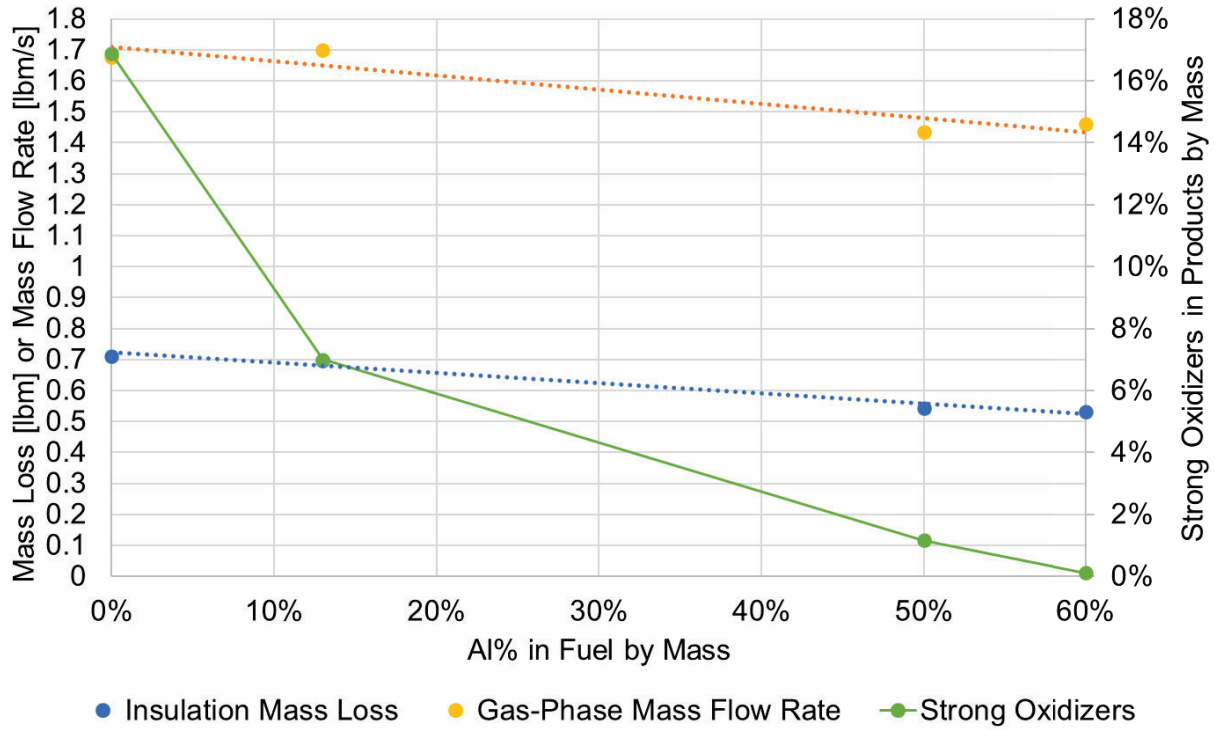

Figure 6. Insulation Mass Loss, Gas-Phase Mass Flux, and Strong Oxidizer Content in Products by Mass versus Fuel-Al Loading

It is worth noting the effect that the presence of Al in the propellant has on the tungsten nozzle and thereby the chamber pressure. Without Al to bind O_2 into the condensed phase, the nozzle undergoes substantial thermochemical erosion, as evidenced by the steadily decreasing chamber pressure history for the 0% Al test (iSFT-075) plotted in Figure 7. Post-test measurements of the nozzle throat rings confirm erosion commensurate with the pressure decrease exhibited in the pressure history. For the 13% Al test (iSFT-076), negligible nozzle erosion occurred, suggesting that an oxidation-potential threshold had been crossed. For the 50 and 60% Al tests (iSFT-029, -031, -064, and -077), 'negative erosion' was observed, as alumina slag (the precise chemistry of which was not characterized) coated the inner diameter of the cooled nozzle throat and effectively decreased the flow area. The slag flowing through the throat can introduce

unpredictable blips in the pressure histories of the higher-Al-loaded cases as observed in those for iSFT-031 and -077 in Figure 7. This difference in nozzle erosion behavior explains why time-average chamber pressure remained steady with increasing Al loading though gas-phase mass flow rate did not.

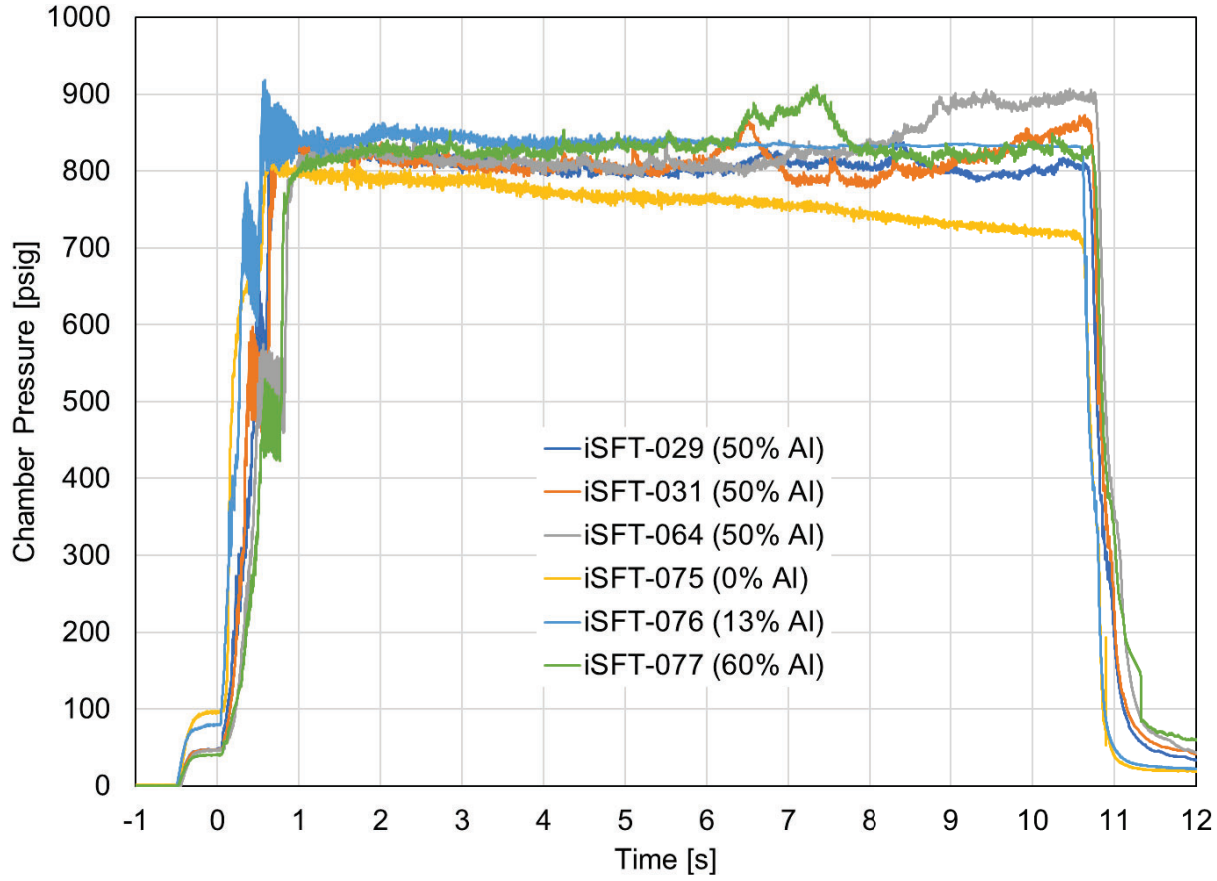

Figure 7. Chamber Pressure Histories for Tests Included in the Al Loading Study

7.2 Material Database Expansion

SFT insulation test section MDRs as a function of axial location are shown in Figure 8 for the standard-condition test series subset consisting of SF-NBR (iSFT-078), SF-EPDM (iSFT-079), MXSE-55 SCP (iSFT-086), FM5504 SCP (iSFT-087), as well as reference results from prior SFT testing for PBI-NBR and RDL-7565 aramid-filled EPDM (AF-EPDM). The PBI-NBR curve is the average MDR of three different tests at standard conditions, and that of the RDL-7565 is the average of four different tests at standard conditions. The SCP insulation materials, MXSE-55 and FM5504, had the lowest MDRs for the tested materials shown in this comparison. The baseline PBI-NBR average had the second lowest MDRs, and the SF-EPDM results were unexpectedly like the baseline PBI-NBR values. The RDL-7565 average results showed the second highest MDRs. The SF-NBR test had the highest MDRs.

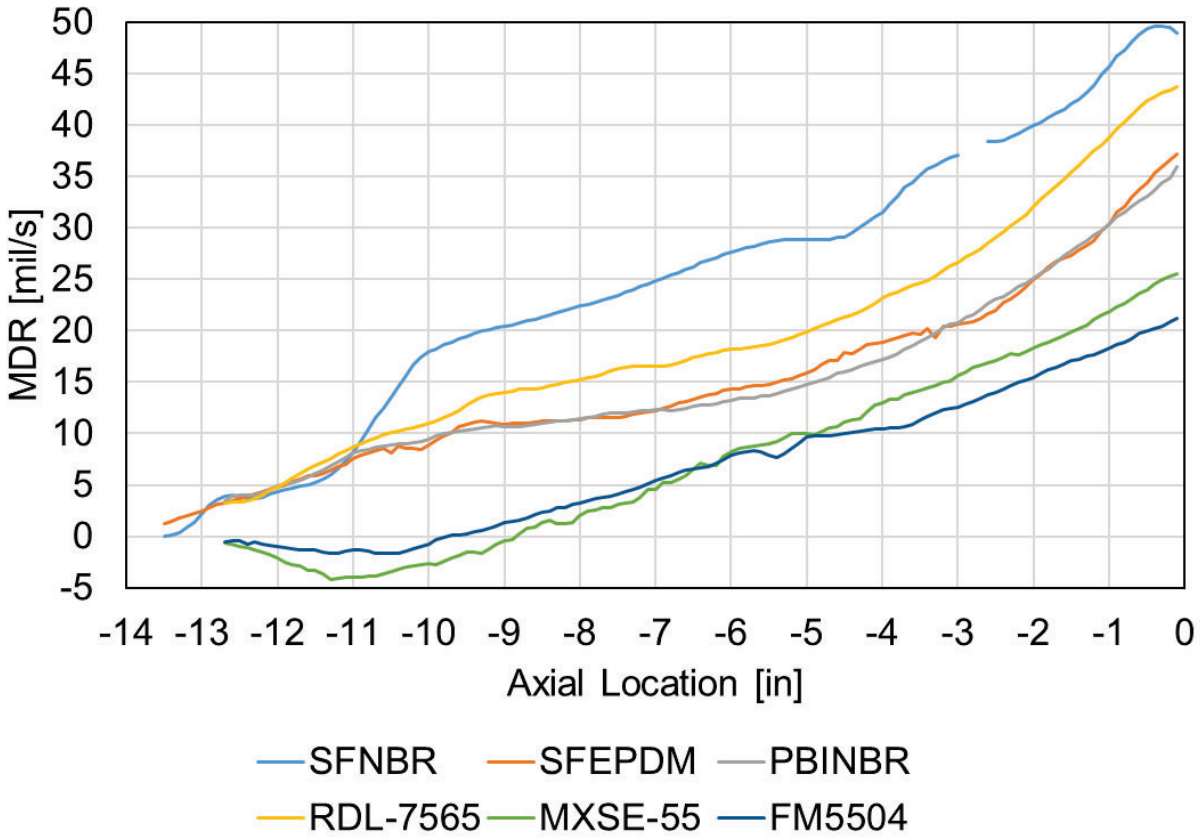

Figure 8. SFT Insulation Test Section MDR as a Function of Axial Location for Several Commonly Used Materials

One consequence of the low MDRs of the SCP samples seems to be enhanced nozzle erosion, as can be deduced from the lower time-average pressures shown in Table 4. Post-test measurements of the nozzle throat rings confirm that greater erosion occurred for the SCP-sample tests (iSFT-086 and -087) than for the 0% Al test with PBI-NBR (iSFT-075). It is hypothesized that the reduced insulation MDRs correlate with reduced injection of cool, fuel-rich chemical species into the boundary layer upstream of the nozzle throat, which, in turn, promotes thermochemical erosion of the tungsten. Stated differently: it could be that the ablation of the insulation samples protects the nozzle throat from erosion, and when the ablation rate is diminished, throat erosion is augmented.

The MXSE-55 MDR results were lower compared with those of FM5504 for the forward half of the insulation test section, but the MDR curves crossed near the midpoint such that the FM5504 had the lower MDRs in the aft half of the sample. This observed behavior in the calculated MDR is likely correlated in part to the regions of separated flow, transition, and attached flow as defined at axial locations forward to aft within the insulation test section coupled with the material composition and thermal response characteristics. Additionally, the SCP insulation materials showed negative MDRs, which are associated with material swelling, along the forwardmost third of the insulation test section. Material swelling, also reported as negative MDR, results from thermal expansion and pore pressure produced by in-depth heat penetration and subsequent pyrolysis and charring. In the absence of sufficient oxidation rates of the char surface and mechanical stresses to cause material erosion, ablating materials can become thicker,

rather than thinner, upon heating, despite losing mass through pyrolysis. The separated-flow region at the forward end of the SFT test section likely imposes these conditions: heating sufficient to pyrolyze the material at an appreciable rate, but insufficient heating, viscous-shear, mass-transfer rates, and particle impingement to cause substantial surface erosion. In this way, the "more negative" MDRs of the MXSE-55 in the forward portion of the test section likely indicate greater sensitivity to the thermal environment relative to the FM5504, just as its higher MDRs in the aft section do. There was no evidence of hot-gas intrusion to the back side of the MXSE-55 or FM5504 material samples.

The MXSE-55 SCP is an elastomeric formulation using a silica fabric impregnated with a rubber-modified phenolic resin whereas legacy SCP formulations (e.g., MX2600 and FM5504), use a phenolic resin that does not contain a rubber modifier. Compared with the FM5504 SCP formulation that was tested, the lower MDR values exhibited by the MXSE-55 material in the recirculation zone in the forward section of the insulation test section may be due to the lower temperatures, lower gas flow velocities, and lower shear stresses of this environment. A less severe environment and material properties at the less severe conditions may contribute to the probability of material swelling resulting from char layer retention and inter-layer expansion via pyrolysis gases. The expanded char layers will be increasingly removed as the environment becomes more severe and the material properties become less favorable with increasing temperature. In short, a greater propensity to swell in less severe environments likely correlates to higher rates of ablation in more severe environments, as observed in the MXSE-55 MDRs vis-à-vis those of FM5504 in this study.

The PBI-NBR is a fiber-reinforced rubber-based insulation material that has consistently demonstrated good thermal performance in multiple testing environments. The chemical composition provides a favorable thermal response via the pyrolysis reactions and the reinforcing fibers aid in char layer retention in high shear stress environments. The cooling effect of the pyrolysis gas coupled with the effectiveness of the retained char layer to insulate the virgin material from the hot combustion gases results in low MDR values.

The RDL-7565 insulation material is an AF-EPDM. The aramid fibers provide structural reinforcement to assist in retaining the char layer that serves as a good thermal insulator. Historically, AF-EPDM materials have had higher MDRs and greater variability in MDR values compared with PBI-NBR results.

The SF-EPDM test produced an unexpected outcome in that the SF-EPDM MDRs were very similar to the PBI-NBR MDR values throughout the length of the test section. The pretest expectation was that the SF-EPDM would have a MDR trend like that of SF-NBR, where the lack of reinforcing fibers in the composition results in high MDRs under high flow velocities. Both materials have a silica-filled rubber-based formulation that does not include reinforcing fibers, and differences in the chemical formulation were not expected to have an effect of this magnitude on the MDRs. The reason for the difference in the MDRs has not been identified and may be due to formulation effects or simple material performance variability. Additional testing would be required to investigate the results given only one test has been completed for each of the SF-EPDM and SF-NBR materials.

Regarding the unexpected SF-EPDM MDR similarity to PBI-NBR, the PBI-NBR was expected to be a better performer in high shear-stress environments, such as in the aft portion of the SFT test sample, due to the presence of the reinforcing fibers and the formulation composition.

SF-EPDM contains silica powder but no fibers and so was expected to perform well in low-velocity-to-static-flow regions where the viscous shear stress is low (e.g., the forward portion of the SFT test sample). Therefore, silica-filled, rubber-matrix insulation materials are typically not used in environments having high flow velocity and subsequent high shear stress such as are present in the aft end of a motor, aft dome, nozzle, or where gas flows change direction at high velocity. However, silica-filled, rubber-matrix insulation materials are often well suited for low flow velocity, low shear stress environments (i.e., forward dome locations).

7.3 Low-Mass-Flux Tests

Under a different test program, four SFT firings were conducted at lower mass flow rates and, therefore, lower pressures than standard. The objective of these tests was to gather insulation MDRs at lower mass fluxes than occur for the standard conditions and, as each insulation sample produces a range of mass fluxes along its length for a given mass flow rate, an understanding of the effects of pressure independent of mass flux. These "low-mass-flux" tests were iSFT-080, -081, -084, and -085 and were operated at lower mass flow rates and pressures than the balance of the SFT tests included in the database. To eliminate the region of separated flow within the insulation sample, a short section of insulated pipe, the so-called "flow straightener", was inserted between the aft end of the fuel grain and the forward end of the insulation sample, as shown in Figure 9.

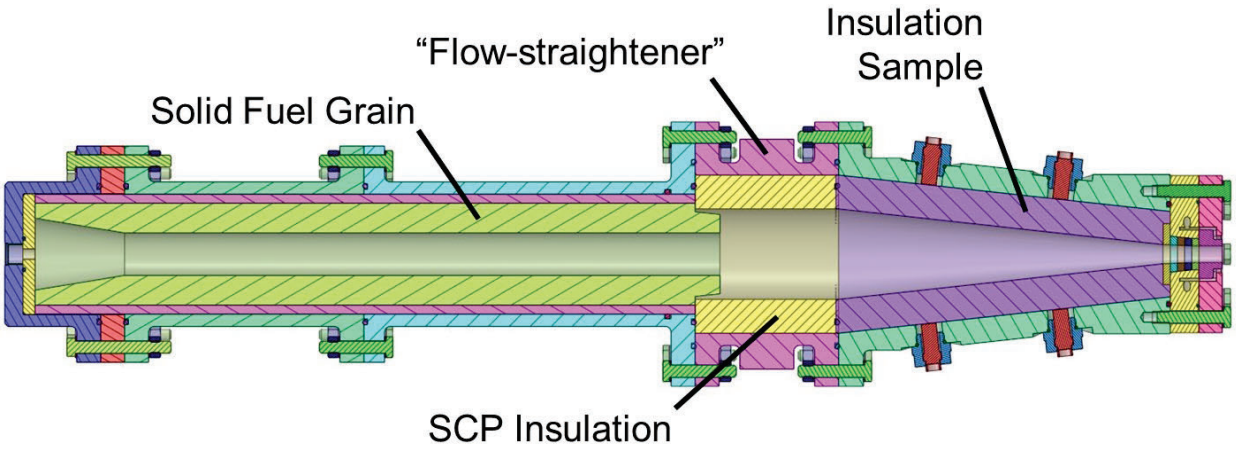

Figure 9. "Flow-Straightened" SFT Configuration used in Low-Mass-flux Tests

Table 5 contains key as-measured parameters for the low-mass-flux tests. Compared with standard conditions, such as targeted in iSFT-078 and iSFT-079 and displayed in Table 5, not only are pressures and mass flow rates lower for the low-mass-flux tests, but the O/F is significantly reduced, and the percentage of N_2 and flame temperature are also slightly lower. The fraction of Al_2O_3 in the products tends to be a bit greater than that for standard conditions owing to the lower O/F.

Table 5. As-measured Parameters for Low-Mass-Flux Tests

Test No. iSFT-	Material	Al% in Solid Fuel	O_2 mass flow rate [lbm/s]	N_2% of Oxidizer	O/F	Pressure [psia]	Flame Temp. [K]	Al_2O_3% in products
080	PBI-NBR	50	0.261	40	1.65	297	3617	27
081	PBI-NBR	50	0.376	49	1.94	464	3563	26
084	RDL-7565	50	0.262	41	1.49	313	3350	23
085	RDL-7565	50	0.369	51	1.99	472	3515	25

The MDR curves for the low-mass-flux tests including PBI-NBR, iSFT-080 and iSFT-081, are shown in Figure 10, where MDR is plotted against axial location and Figure 11, where MDR is plotted against gas-phase mass flux. The curves labeled "Baseline" represent the average result for three tests of PBI-NBR at standard conditions and employ the same data as those in Figures 4 and 8. It is evident from Figure 10 that the MDR behavior for the baseline tests is different than that for the low-mass-flux tests in the forward portion of the sample: a fact imputed to the existence of separated flow in this region for the "Baseline" PBI-NBR tests. For low-mass-flux tests, the MDRs are roughly constant for much of the sample length, with steep increases occurring toward the aft end. Figure 11 reveals that above about 0.3 lbm/in^2-s, the three curves nearly consolidate into one, indicating that gas-phase mass flux is the dominant driver of MDR. For lower gas-phase mass fluxes (less than about 0.3 lbm/in^2-s) where the MDRs are roughly constant for a given test, higher pressures correlate to higher MDRs.

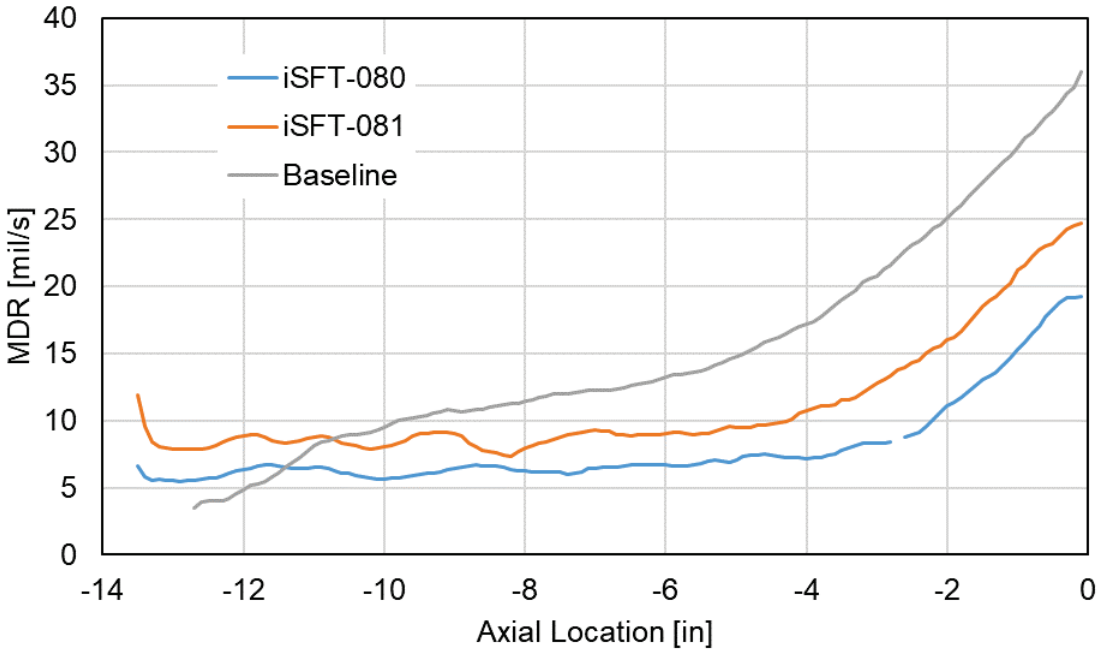

Figure 10. MDR versus Axial Location for PBI-NBR Low-Mass-Flux Tests

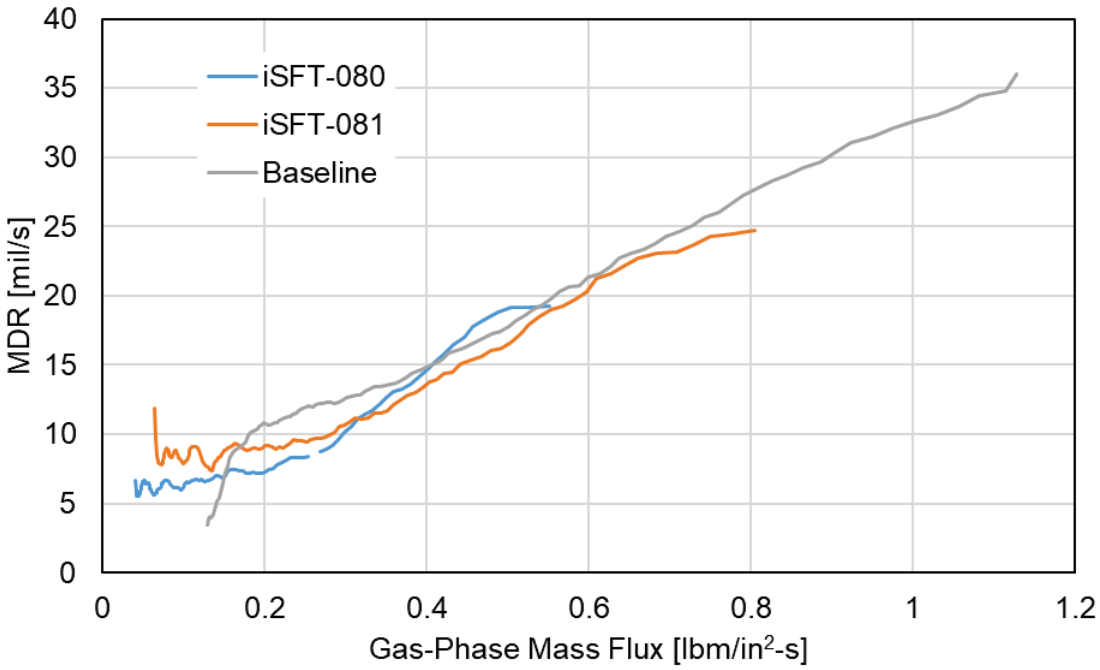

Figure 11. MDR versus Gas-Phase Mass Flux for PBI-NBR Low-Mass-Flux Tests

Figures 12 and 13 display the same curves as Figures 10 and 11, respectively, but for RDL-7565 and with the baseline being the average of four different tests at standard conditions as in Figure 8. Though the curves in Figure 12 display similar trends to those of PBI-NBR, the curves in Figure 13 do not merge for higher mass fluxes, and the MDR correlation with pressure is less evident. RDL-7565 has exhibited substantial test-to-test variability among standard-condition tests, so it is possible that this variability is masking an underlying behavior like that exhibited by PBI-NBR.

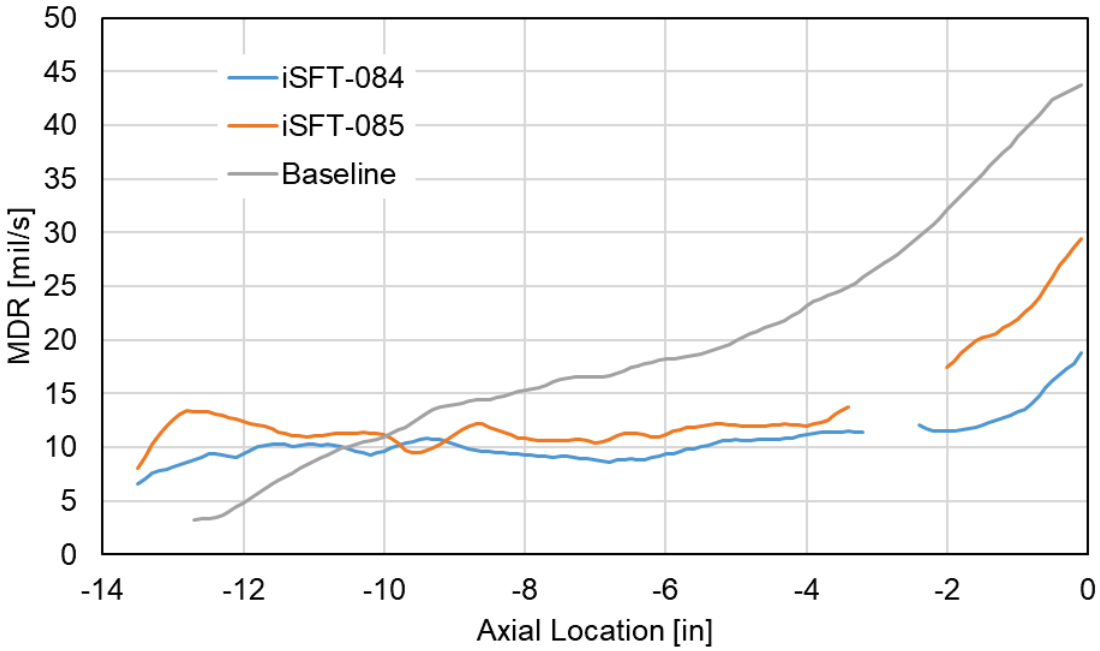

Figure 12. MDR versus Axial Location for RDL-7565 Low-Mass-Flux Tests

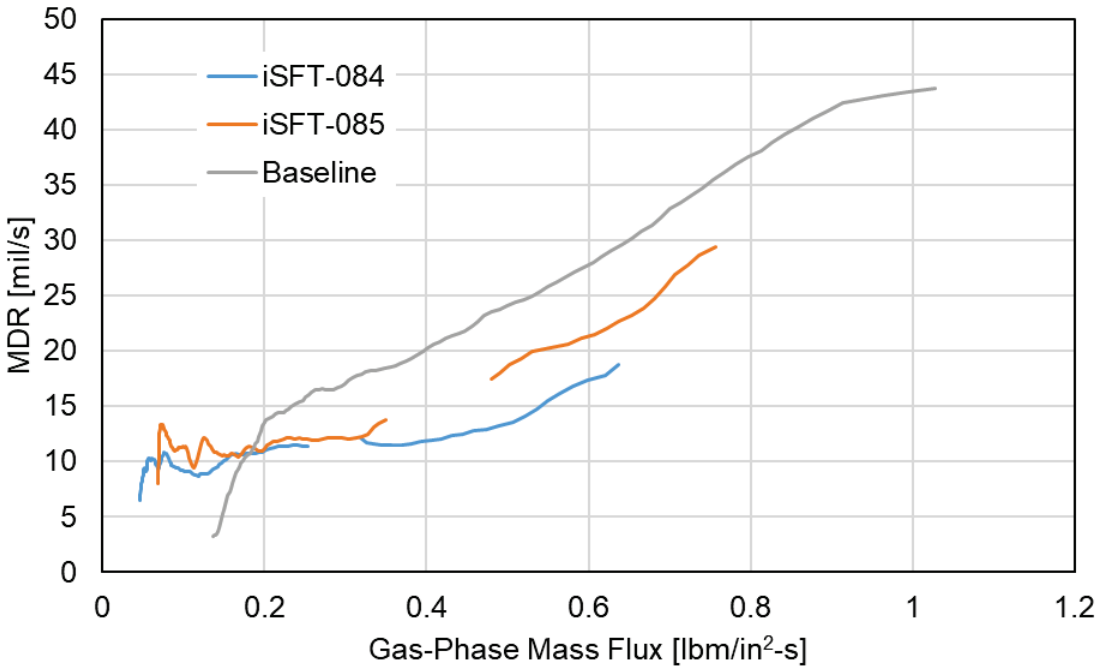

Figure 13. MDR versus Gas-Phase Mass Flux for RDL-7565 Low-Mass-Flux Tests

7.4 MDR Data Analysis

The objective of this statistical analysis is to determine what factors affect the MDR and develop an applicable regression function (based on the factors) to predict MDR. Since MDR is a continuous function of axial location, FDA [ref. 22] was used to model MDR for the 43 test cases. The statistical analysis was performed using the JMP statistical software [ref. 23].

7.4.1 Overview of Test Data

Data were collected for 43 test cases. In each test case, MDR is computed at 128 locations along the test specimen axis. Figure 14 shows the MDR by location data for each test case.

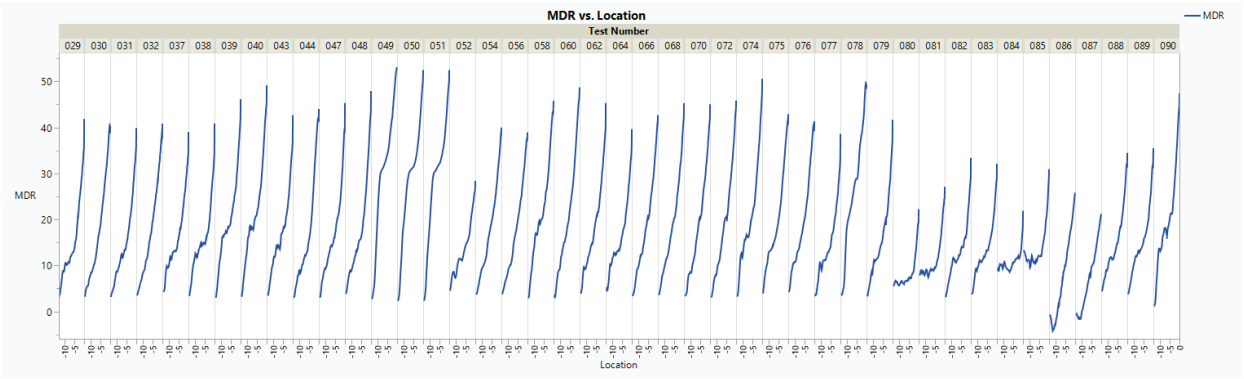

Figure 14. MDR versus Location Data

Eighteen factors specific to each test case are recorded. Table 6 lists the covariates.

Table 6. Covariates Measured for Each Test Case

Covariate Name	Test Ballistics Name
1. Aluminum	Al Content in Fuel (%)
2. Burntime	Burn Time (s)
3. FuelBurned	Fuel Burned (lbs)
4. GOxFlow	GOx flow (lbs/s)
5. N_2Flow	N_2 flow (lbs/s)
6. OtotFTotalAvg	$\frac{O}{F} = \frac{\dot{m}_{O_2} + \dot{m}_{N_2}}{\dot{m}_{fuel}}$ *time averaged*
7. TflameTheore	Tflame (theoretical) (K)
8. Al_2O_3Content	Al_2O_3 Content in Products (%)
9. StrongOx	Strong Ox (O_2, OH, O) in Products (%)
10. MaxPressure	Max Pressure (psi)
11. MaxSmoothedPress	Max Smoothed Pressure (psi)
12. TotalAvgPress	Total Avg Pressure (psi)
13. BulkcEff	Bulk c* efficiency
14. RegRate	Regression Rate Coefficient
15. Configuration	Configuration
16. InsulMaterial 2	Recoded insulation material
17. TotalMassFR	Total Mass Flow Rate (lbm/s)
18. GasPhaseMassFR	Gas Phase Flow Rate (lbm/s)

The covariate InsulMaterial 2 is recoded based on grouping the values of InsulMaterial into 10 levels. The original covariate, InsulMaterial, has 29 levels which is too many levels to be of much use in regression modeling with this limited database of MDR curves. Table 7 shows how InsulMaterial was recoded. These groupings are based on engineering judgement from the experimenters.

Table 7. Recoding InsulMaterial into InsulMaterial 2

Original Covariate Values for InsulMaterial	Original Frequency	Recoded Covariate Values for InsulMaterial 2
40BL0181 (REDAR EPDM)	1	3
40BL0182 (REDAR EPDM)	1	3
40BL0183 (REDAR EPDM)	1	3
FM5504 (SCP)	1	7
MFD-121-1R	1	4
MFD-121-2	2	4
MFD-121-3K	2	4
MFD-174-1K	2	5
MFD-174-1R	1	5
MFD-1223-1R	2	6
MFD-1223-2R Batch 1	1	6
MFD-1223-2R Batch 2	1	6
MXSE55 (SCP)	1	7
PBI-NBR	10	1
PBI-NBR - Overcured	1	1
RDL 7565 Burke	1	2
RDL7565c (Chinese Chlorez)	1	2
RDL7565-Calendered	1	2
RDL 7565 Kirkhill	1	2
RDL7565-WEI	1	2
RDL7566d-WEI	1	10
RDL7576b-Calendered	1	10
RDL7576b-WEI	1	10
RDL7588-WEI	1	10
RDL7589-WEI	1	10
RDL-7565	2	2
RDL-7749	1	10
SF-EPDM	1	9
SF-NBR	1	8

Only six of the covariates can vary independently in setting up the experiment. These are GOxFlow, N_2Flow, OtotFTotalAvg, Al_20_3Content, TotalAvgPress, and InsulMaterial 2. The other covariates are dependent on these six independent covariates which are called control variables (i.e., variables that can be selected by the experimenter).

Figure15 plots the six independent covariates by test number and Figure 16 plots the six independent covariates against each other in a scatter plot matrix.

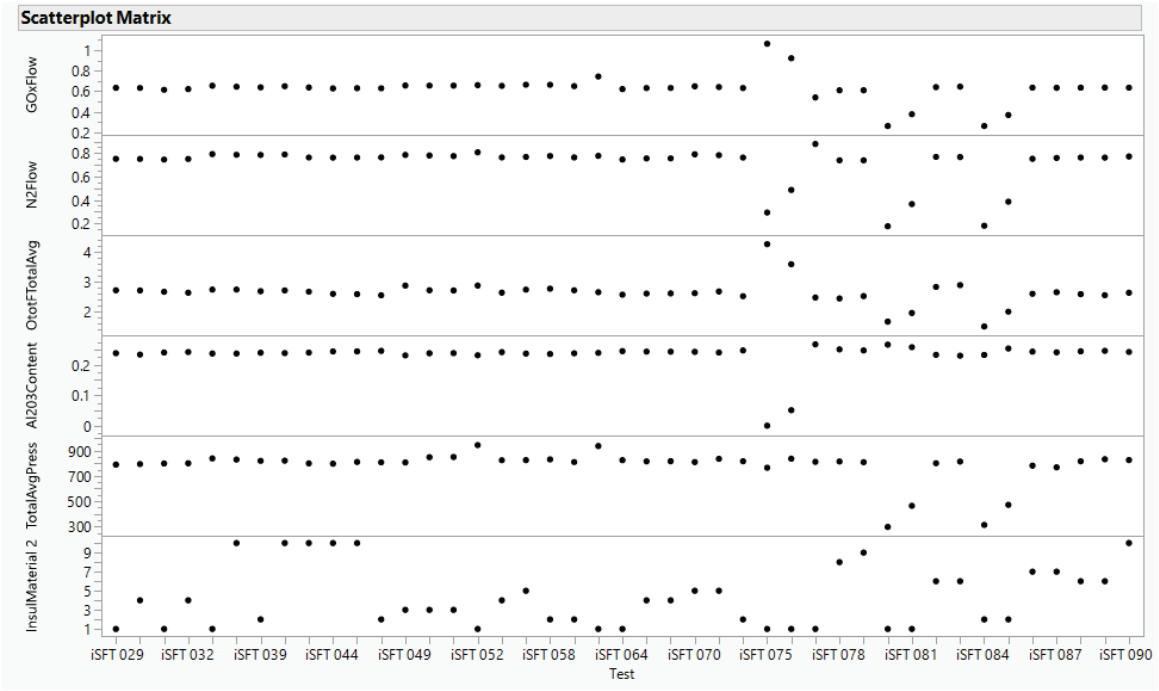

Figure 15. Covariates Plotted by Test Case

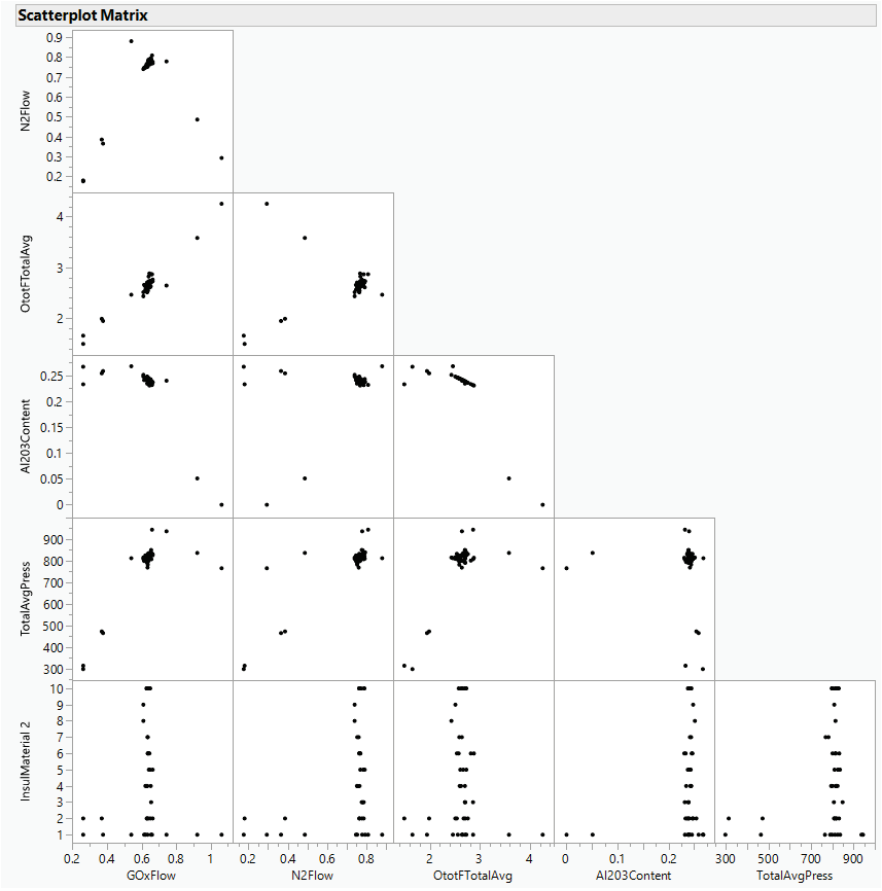

Figure 16. Scatter Plot of Covariates

In an optimal test design, these points would be spread uniformly across the full range of the covariates, but testing was limited in this assessment (see Section 6.2).

7.4.2 FDA

FDA is a branch of statistics where data analyses provide information about curves, surfaces, or other parameters varying over a continuum. Since MDR is measured at 128 equally spaced axial locations, FDA is an appropriate method to determine what covariates are important and for developing a MDR model as a function of covariates.

Each FDA sample element (i.e., a test) is considered as a random function. The MDR axial locations are considered as a function which contains noise due to experimentation and measurement. This means that if a case was repeated under the exact conditions, the MDR would be different due to measurement error and experimental noise. Basis functions are used to model each sampled MDR function. The fitted basis functions are used to determine functional regression models. In this case, the test response is MDR, a function of location, and the six independent covariates are scalers.

Before fitting basis-functions to MDR, first process the data to remove outliers. It is noted that the measured MDR at location 0 are discontinuous because it is adjacent to an SCP ring that erodes much more slowly than the test materials, so location 0 is removed from the data. Figure17 is a MDR plot as a function of location for all 43 test cases after location 0 was removed. Notice some of the test cases have missing measurements of MDR. Another benefit to using FDA is the individual MDR measurements will be fitted by a continuous curve and the missing data will not have a major impact on the results. Figure 18 is a summary of the MDR functions.

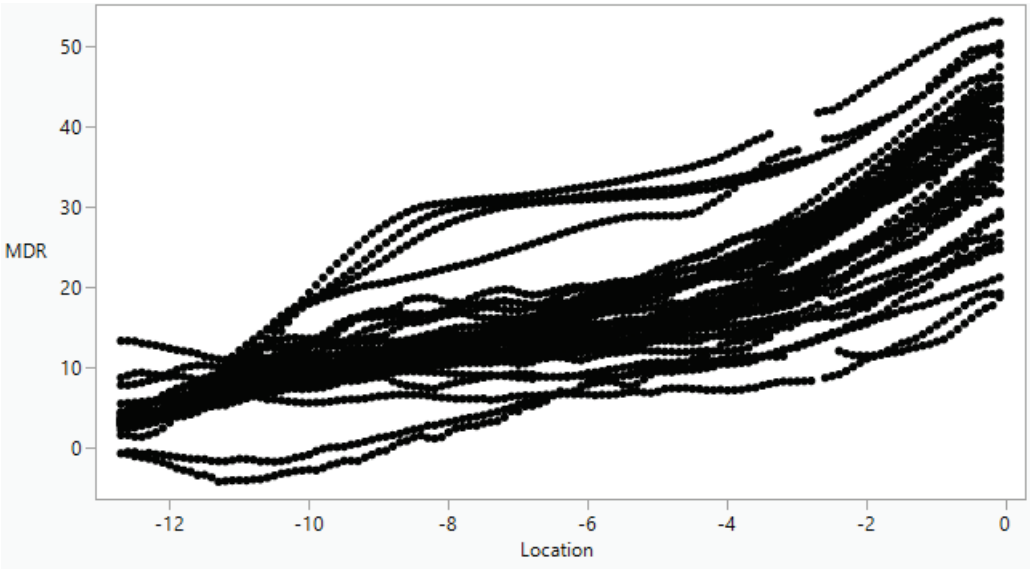

Figure 17. MDR by Location Plots

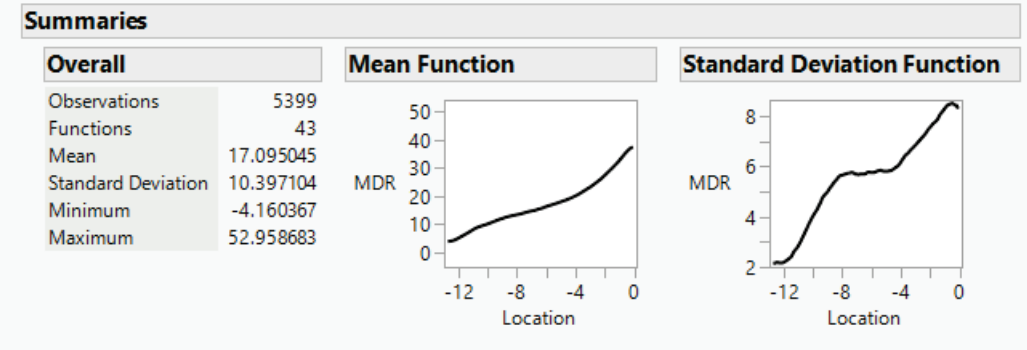

Figure 18. Summary of MDR Curves

7.4.2.1 Fitting Wavelet Basis to MDR Curves

The next step is to convert these 127-point curves into continuous functions computable for any desired location value. Because the MDR measurements contain observational errors that need to be removed, the conversion from discrete data to functions involves smoothing. This is accomplished using a system of basis functions. A basis function system is a set of known functions φ_k that are mathematically independent of each other and that have the property that can approximate arbitrarily well any function by taking a weighted sum or linear combination of a sufficiently large number K of these basis functions. For the MDR curves it was determined a wavelet basis was an excellent basis which combines the frequency-specific approximating power of Fourier basis with the spatially localized spline basis features [ref. 24].

A wavelet is a continuous wave-like oscillation with an amplitude that begins at zero, increases or decreases, and then returns to zero one or more times. Wavelets can be used as a basis by selecting a suitable mother wavelet function (ψ) and then considering dilations and translations of the form

$$\psi_{jk}(t) = 2^{j/2}\psi\left(2^j t - k\right)$$

For integers j and k, the best mother wavelet was determined to be the Symlet 4 wavelet shown in Figure 19. The wavelet is a continuous function but has sharp peaks to be able to fit the sharp peaks in the MDR functions.

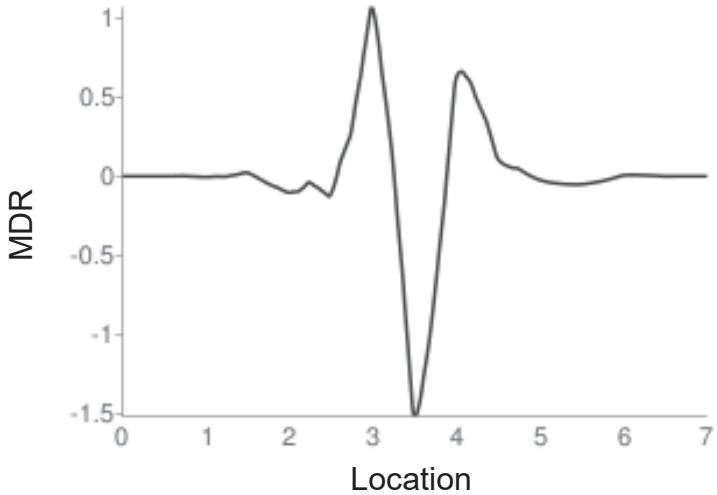

Figure 19. Symlet 4 Wavelet

To model MDR curves, the wavelet width and its central frequency are changed by adjusting *j* and moving it along the location of MDR by changing *k*. This allows simultaneous modeling high and low frequency components of the MDR curve. Wavelets are selected because MDR has some sharp peaks and the Symlet 4 wavelets are great with data with sharp peaks. Figure 20 shows the actual MDR functions and the fitted MDR functions using the wavelet basis model for each test case. In the plots, the y-axis is MDR and the x-axis is location.

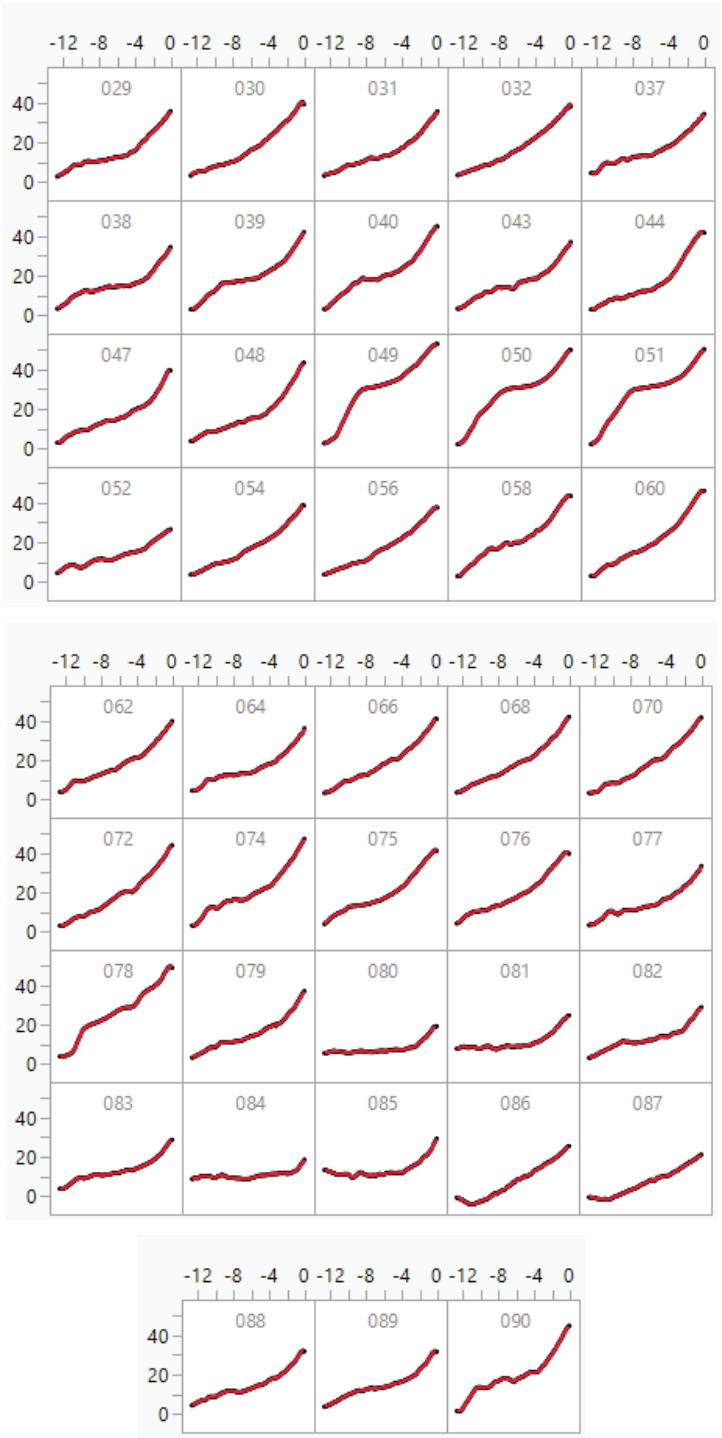

Figure 20. Wavelet Basis Models Overlayed on MDR Curves

The difference between the actual MDR functions and the wavelet fits are nearly impossible to see in Figure 20. The differences can be seen using diagnostic plots and are shown in Figure 21. The actual by predicted plot shows the actual MDR values (y-axis) versus the predicted MDR values using the wavelet basis model (x-axis). The residual by predicted plot shows that error in the wavelet basis predictions (y-axis) versus the MDR predictions (x-axis). This shows that the errors in the wavelet predictions of MDR are approximately less than 0.5-mil[1]/sec (see right plot in Figure 21).

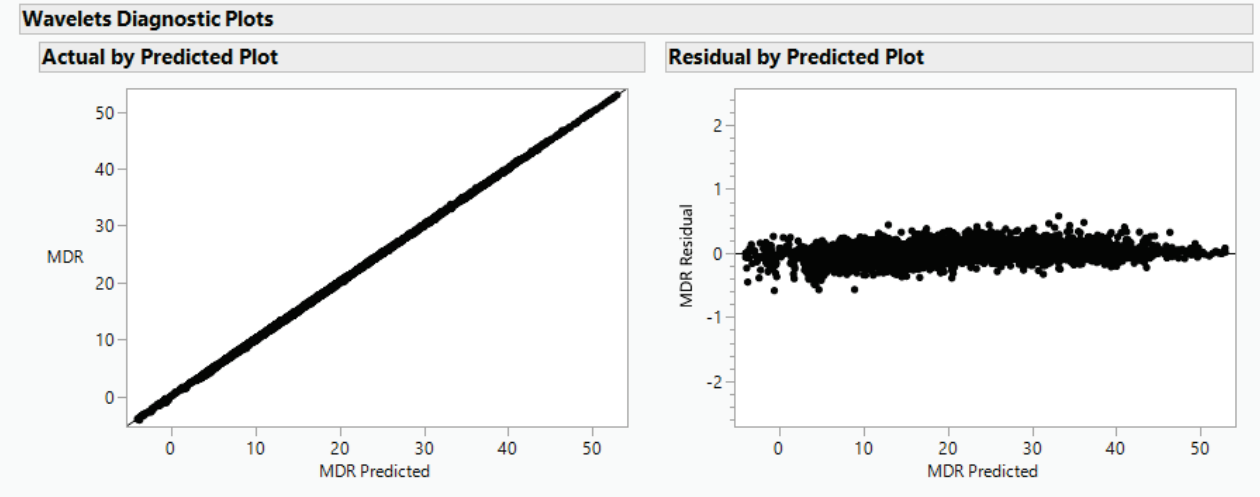

Figure 21. Wavelet Diagnostic Plots

7.4.2.2 Functional Principal Components Analysis (PCA)

Once a wavelet basis function is fitted to the MDR curves, the next step is to use PCA (or functional PCA) on the functional model (the wavelet basis model). This allows the exploring of features characterizing typical functions and modeling the functions as a linear combination of functions. Results from the functional PCA (e.g., the functional principal component (FPC) scores) are used with a specified set of covariate variables to fit a generalized regression model. The regression model will allow us to determine how the independent covariates affect the response and provide predictions of MDR curves for a given set of values of the covariates.

The functional PCA results are given in Figure 22. The functional PCA results selected 17 principal component functions (or shape functions) to fit the wavelet predictions of the MDR functions. Notice that the first four PCA functions model 99.2% of the variability on the wavelet predictions.

[1] Note “mil” equates to 0.001 in, or 0.5 mil = 0.0005 in.

Eigenvalues

FPC	Eigenvalue	20 40 60 80	Percent	Cumulative
1	3811.8		88.4%	88.4%
2	333.3		7.73%	96.1%
3	101.0		2.34%	98.5%
4	32.5		0.75%	99.2%
5	9.2		0.21%	99.5%
6	6.7		0.16%	99.6%
7	5.3		0.12%	99.7%
8	3.7		0.09%	99.8%
9	2.1		0.05%	99.9%
10	1.5		0.04%	99.9%
11	1.1		0.02%	99.9%
12	0.79134		0.02%	99.9%
13	0.61338		0.01%	100%
14	0.40786		0.01%	100%
15	0.24532		0.01%	100%
16	0.23208		0.01%	100%
17	0.19218		4e-3%	100%

Figure 22. Functional PCA Results

Figure 23 shows the PCA shape functions which are used to compute the functional PCA fits to the wavelet predictions. The PCA fits are computing from the shape functions by starting with the mean shape function and then adding the remaining shape functions scaled by the PCA score. Thus the MDR curves are represented by a linear combination of these 18 functions, which are tabulated in Appendix C.

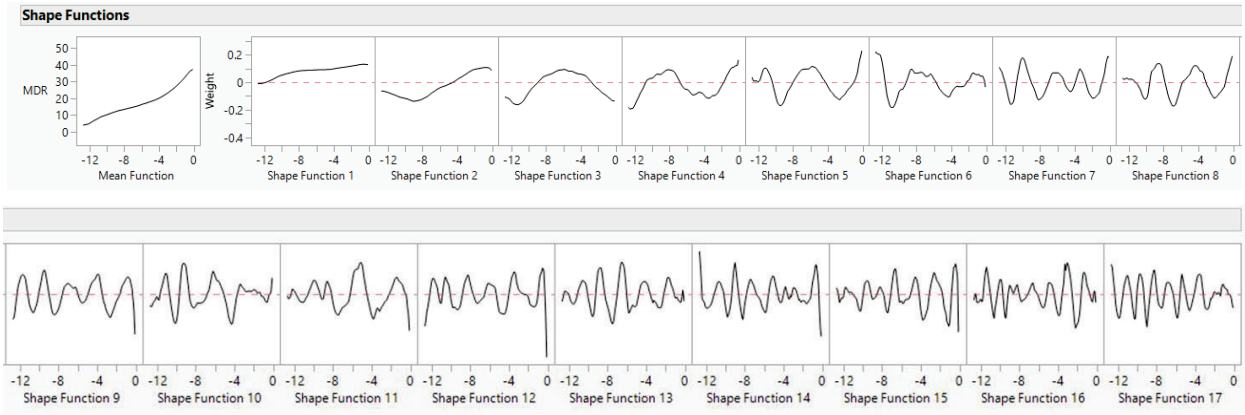

Figure 23. Functional PCA Shape Functions

Figure 24 shows the diagnostics plots of the functional PCA models to the measured MDR curves. These plots show the functional PCA fits to the MDR values are excellent and almost all fit errors less than 0.5 mil/s.

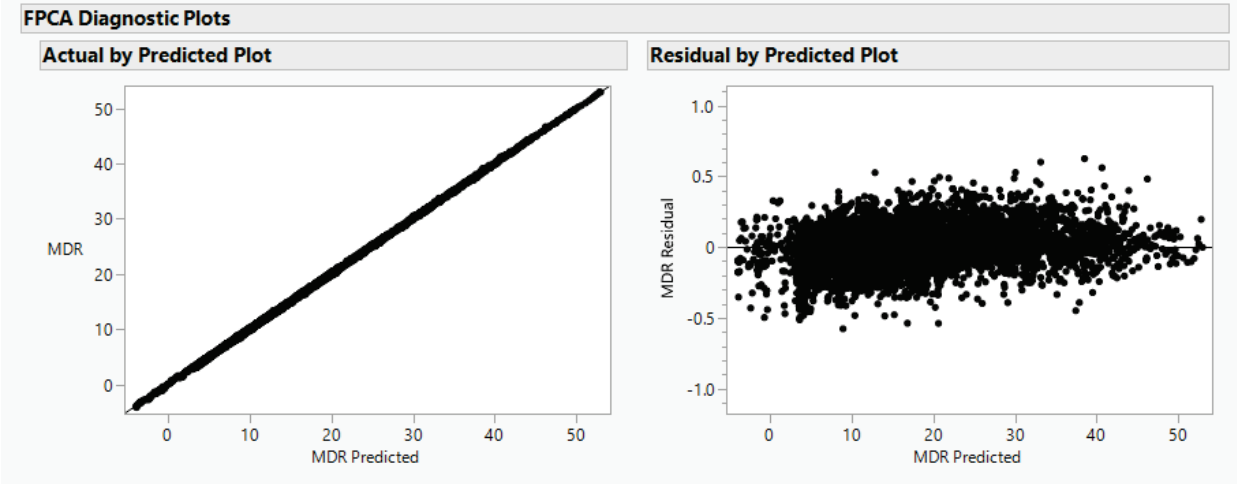

Figure 24. Functional PCA Diagnostic Plots

7.4.2.3 Generalized Regression for MDR

The final step in FDA is to fit regression models to each the 17 FPC models. Since each MDR function is now represented as a sum of the mean function plus a weighted sum of 17 shape functions, there are 43 coefficients (one for each test) for each FPC shape function. The objective is to fit a regression function of the six independent covariates to the 43 coefficients for each FPC shape function. This allows presenting the MDR as a function of the covariates.

Generalized regression using a normal pruned forward selection [ref. 25] was used to fit the 17 FPC models. The prediction expression for FPC 1 is given in Figure 25. This equation computes the predicted coefficient for the first shape function. The covariates selected were GOxFlow, Al_2O_3Content, and InsulMaterial 2.

Prediction Expression

-149.6585524

+ GOxFlow * (GOxFlow * 164.42355897)

+ GOxFlow * (Al203Content * 584.1643387)

+ Al203Content * Match(InsulMaterial 2, {"1" ⇒ -112.6587999, "2" ⇒ 84.58315698, "3" ⇒ 546.47030567, "4" ⇒ 28.953207133, "5" ⇒ 26.691532072, "6" ⇒ -207.8007025, "7" ⇒ -458.1984672, "8" ⇒ 444.68412601, "9" ⇒ -75.19656713, "10" ⇒ 0, else ⇒ . })

Figure 25. Prediction Expression for FPC 1 Coefficients

Similar prediction equations were computed for the remaining 16 FPC shape functions and are provided in Appendix C.

To compute the predicted MDR function for a set of covariates, sum the mean shape function with the weighted 17 shape functions at each location. The measured MDR is plotted against the predicted MDR in Figure 26. The error in the predictions is also plotted which shows most prediction errors are less than 2 mil/sec which is an excellent fit to this small set of 43 tests.

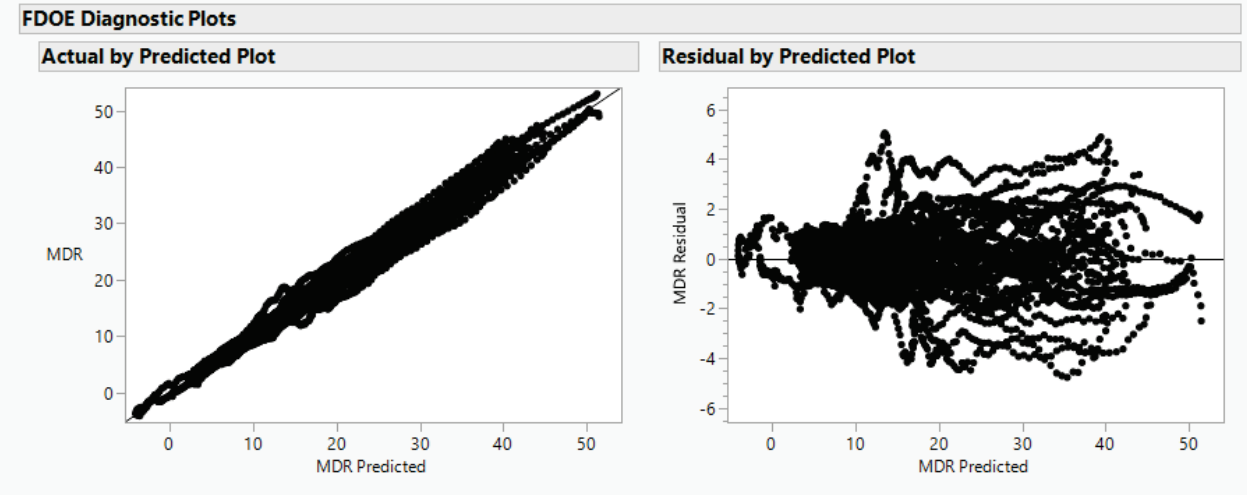

Figure 26. Regression Model Diagnostic Plots

7.4.2.4 MDR Regression Model Using Excel

The generalized regression model computed in Section 7.4.2.3 was recoded into a spreadsheet. The inputs are the values for the six independent covariates (GOxFlow, N_2Flow, OtotFTotalAvg, Al_2O_3Content, TotalAvgPress, and InsulMaterial 2) for each of three cases and are shown in Figure 27. This allows the user to compare three sets of factor values at one time to compare the factor effects on MDR.

Inputs						
	GOxFlow	N2Flow	OtotFTotalAvg	Al203Content	TotalAvgPress	InsulMaterial 2
Case1	0.5839631	0.75298218	2.704791027	0.23867	790.1748924	1
Case2	0.6339631	0.75298218	2.704791027	0.23867	790.1748924	1
Case3	0.6839631	0.75298218	2.704791027	0.23867	790.1748924	1

Figure 27. MDR Regression Model Inputs

The outputs are the MDR regression model predictions for each input case with a plot of the three MDR predictions as a function of location. Figure 28 shows an output plot for the inputs in Figure 27.

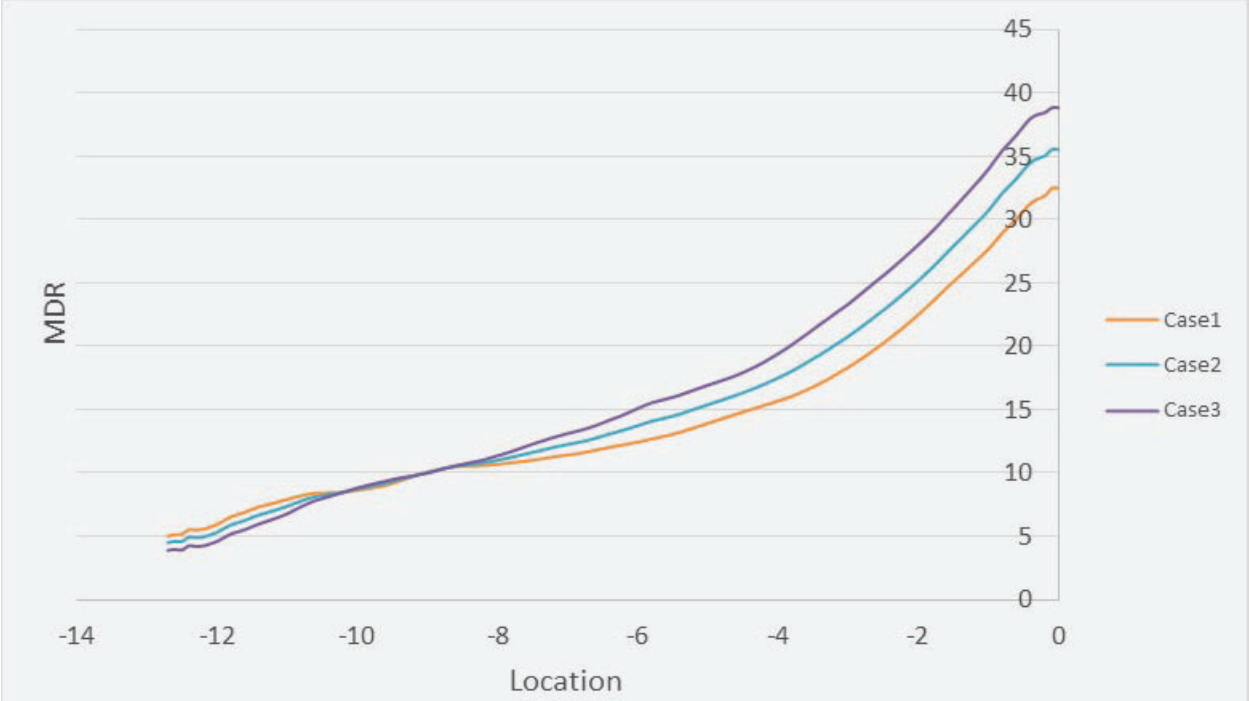

Figure 28. Excel Output Plot of Estimated MDR

By varying the factors one or more at a time, the user can determine the effects on MDR along all the locations. This tool can also be used to estimate the MDR for new cases that have not been tested. To do this, it is recommended to start inputs from with one of 43 test cases that is the closest match to the new case and then change the covariates that need to be changed to match the new case. If the covariates were only slightly changed, the predicted MDR should be a reasonable estimate. Users are highly recommended/cautioned NOT to use this tool for data outside the 43 test cases – in other words DO NOT extrapolate.

7.4.2.5 Variable Importance

The importance of each covariate variable is difficult to measure in this type of model due to the number of different regression models and the variable importance changes at different locations. Table 8 shows which covariate variables are included in each FPC prediction model.

Table 8. Covariates Used in Each FPC Regression Model

FPC Model	Covariates Used
FPC 1	GOxFlow, Al_2O_3Content, InsulMaterial 2
FPC 2	GOxFlow, N_2Flow, InsulMaterial 2, TotalAvgPress
FPC 3	N_2Flow, OtotFTotalAvg, Al_2O_3Content, InsulMaterial 2
FPC 4	N_2Flow, Al_2O_3Content, TotalAvgPress, InsulMaterial 2
FPC 5	Al203Content
FPC 6	N_2Flow, OtotFTotalAvg, Al_2O_3Content, TotalAvgPress
FPC 7	GOxFlow, TotalAvgPress, N_2Flow, Al_2O_3Content, InsulMaterial 2
FPC 8	NONE
FPC 9	NONE
FPC 10	NONE
FPC 11	NONE
FPC 12	NONE
FPC 13	GOxFlow, Al_2O_3Content, N_2Flow, OtotFTotalAvg
FPC 14	OtotFTotalAvg
FPC 15	N_2Flow
FPC 16	OtotFTotalAvg
FPC 17	NONE

Another method of assessing the covariate variable importance is using a prediction profiler. Figures 29 through 31 are prediction profilers at three different locations. The prediction profiler shows the predicted MDR from the regression model on the left along the vertical axis for the six independent factors settings. The curve of each factor shows the relationship between the factor and the response MDR.

At location -12.0, Figure 29 shows the factors TotalAvgPress, N_2Flow, and Al_2O_3Content are the most important factors (i.e., the steepest curves). In addition, GOxFlow and InsulMaterial 2 have a small effect on MDR, and OtotFTotalAvg has almost no MDR effect.

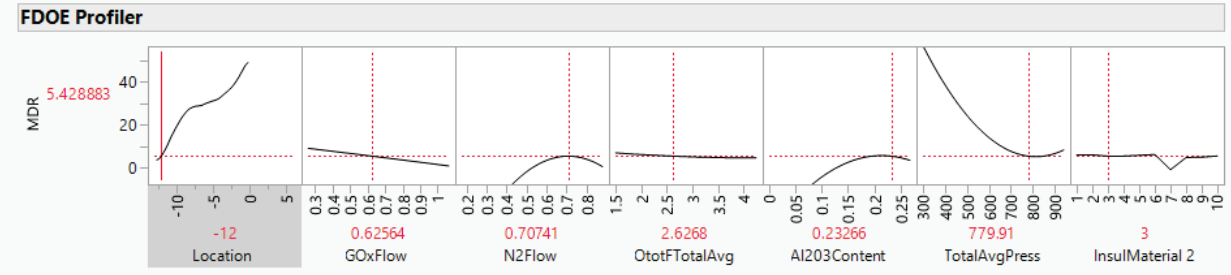

Figure 29. MDR Factor Effects at Location -12.0

At location -6.0, Figure 30 shows the factors Al_2O_3Content, GOxFlow, and InsulMaterial 2 are the most important factors. It is seen that N_2Flow and TotalAvgPress have a small to medium effect on MDR and OtotFTotalAvg has almost no MDR effect.

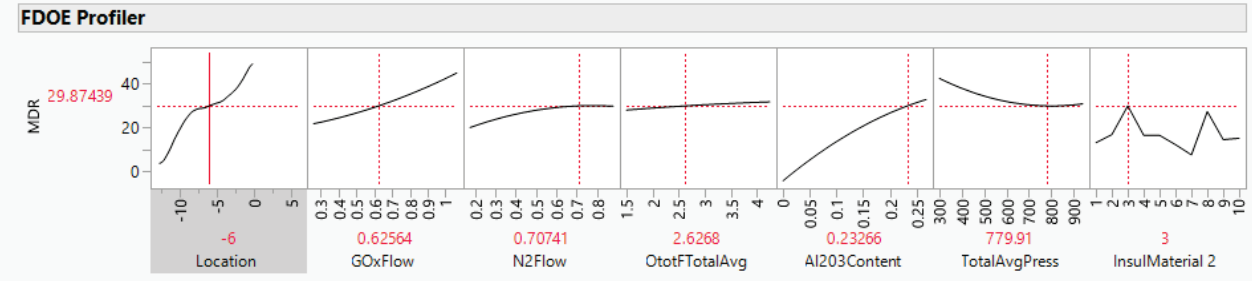

Figure 30. MDR Factor Effects at Location -6.0

At location -1.0, Figure 31 shows the factors GOxFlow, InsulMaterial 2, and Al_2O_3Content are the most important factors. Also shown is that TotalAvgPress and N_2Flow have a small to medium effect on MDR and OtotFTotalAvg has almost no MDR effect.

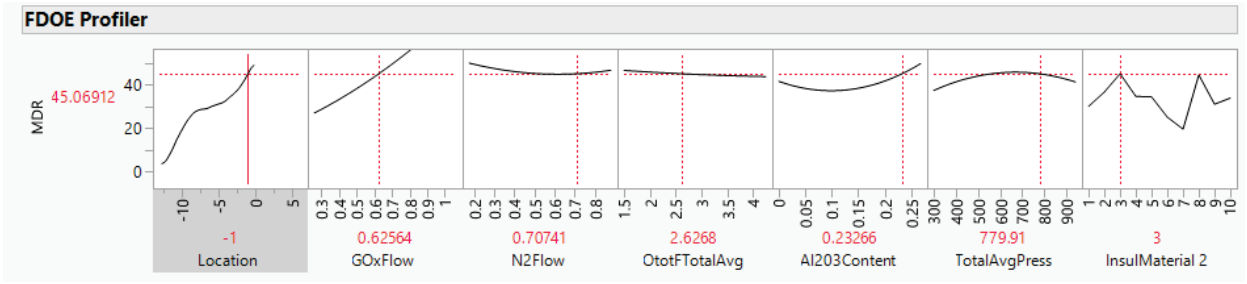

Figure 31. MDR Factor Effects at Location -1.0

7.4.3 Physical Implications of MDR Regression Equation

Though the complexity of the regression equation obfuscates the functional relationship among the MDR and the covariates, trends can be established by varying the value of a single covariate and noting the differences in the resulting MDR curves. The curves in Figures 32 through 36 show the results of varying each covariate independently by ±15% to gauge the sensitivity of MDR to each covariate. In each figure, "Case 2" is the MDR curve resulting from using the median values for the each of the five continuously varying covariates for PBI-NBR (i.e., InsulMaterial 2 = 1). "Case 1" is the MDR curve resulting from subtracting 15% from the median value of the covariate under study, while maintaining the median values for the other covariates, and "Case 3" is the MDR curve resulting from adding 15% to the median value of the covariate under study while maintaining the median values for the other covariates. The variation value of 15% was chosen to balance the need to produce a substantial response from the MDR function while staying within the bounds of the tested values. In only one case (maximum Al_2O_3 content) was the median ± 15% value outside the range of tested values. Table 9 displays the median and ±15% values for each continuous covariate. PBI-NBR was the material chosen for this study as it was tested at the broadest range of conditions, but each material group exhibits the same trends with the continuous covariates as PBI-NBR does.

Table 9. Median and ±15% Values for Each Continuous Covariate

	GOxFlow [lbm/s]	N_2Flow [lbm/s]	OtotFTotalAvg [-]	Al_2O_3Content [mass fraction]	TotalAvgPress [psia]
-15%	0.541	0.649	2.24	0.204	692
Median	0.636	0.764	2.64	0.240	814
+15%	0.731	0.879	3.04	0.276	936

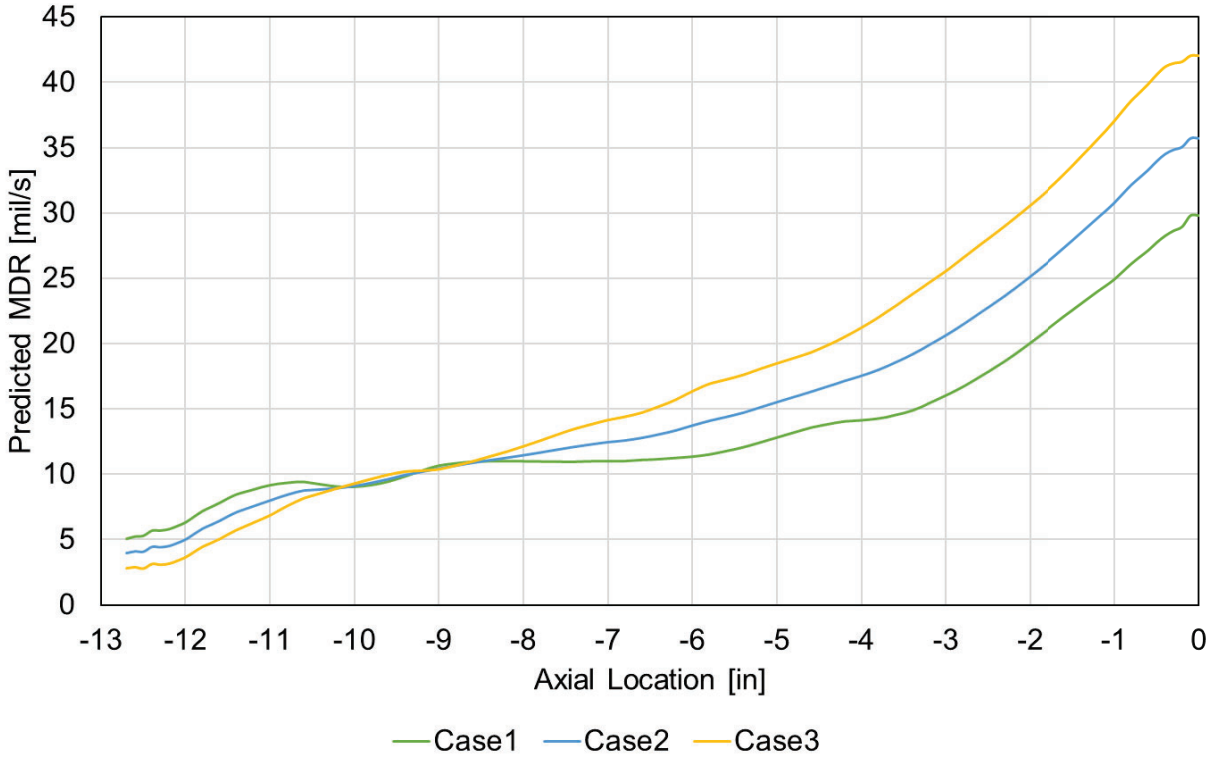

Figure 32. Regression-Model-Predicted MDR for Varying O_2 Mass Flow Rate (GOxFlow)

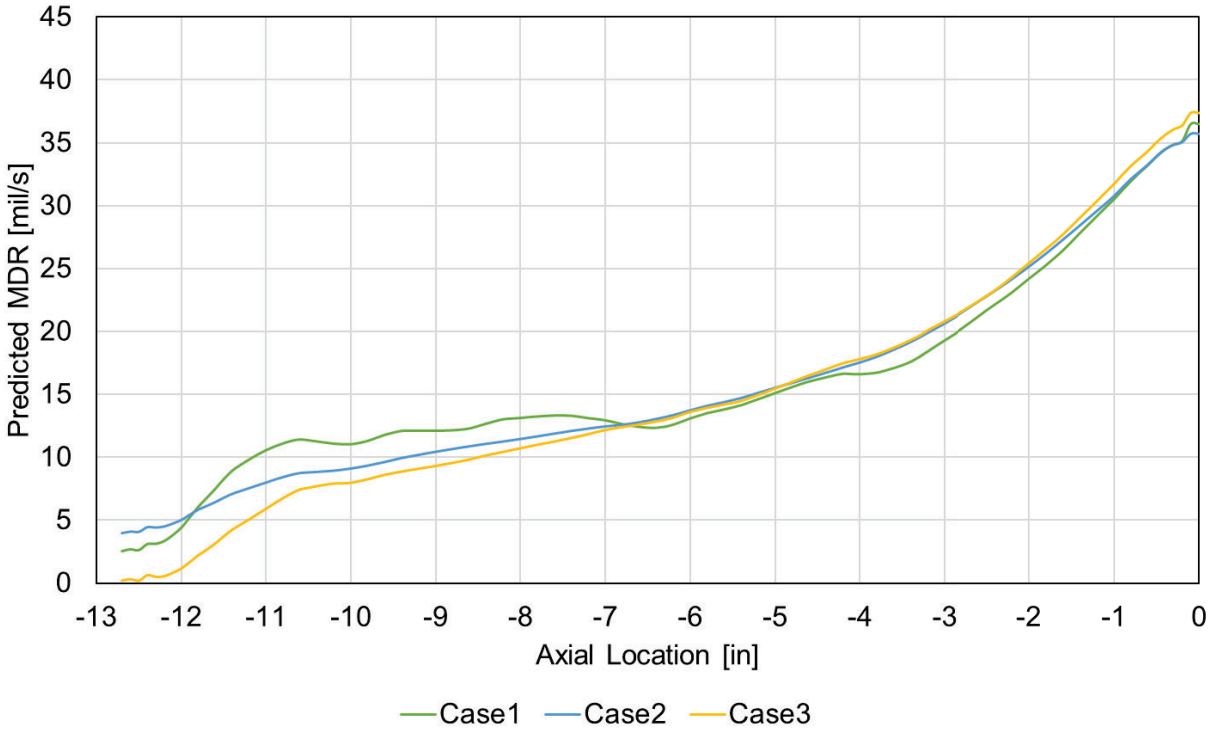

Figure 33. Regression-Model-Predicted MDR for Varying N_2 Mass Flow Rate (N_2Flow)

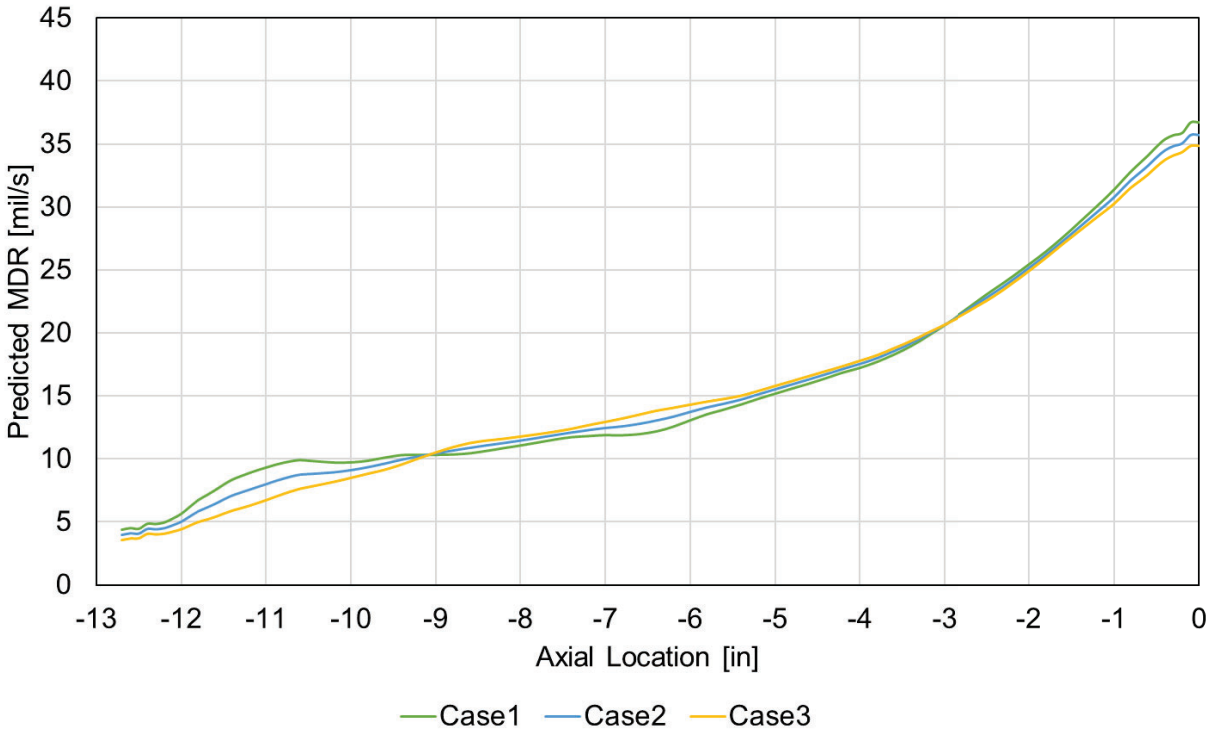

Figure 34. Regression-Model-Predicted MDR for Varying O/F (OtotFTotalAvg)

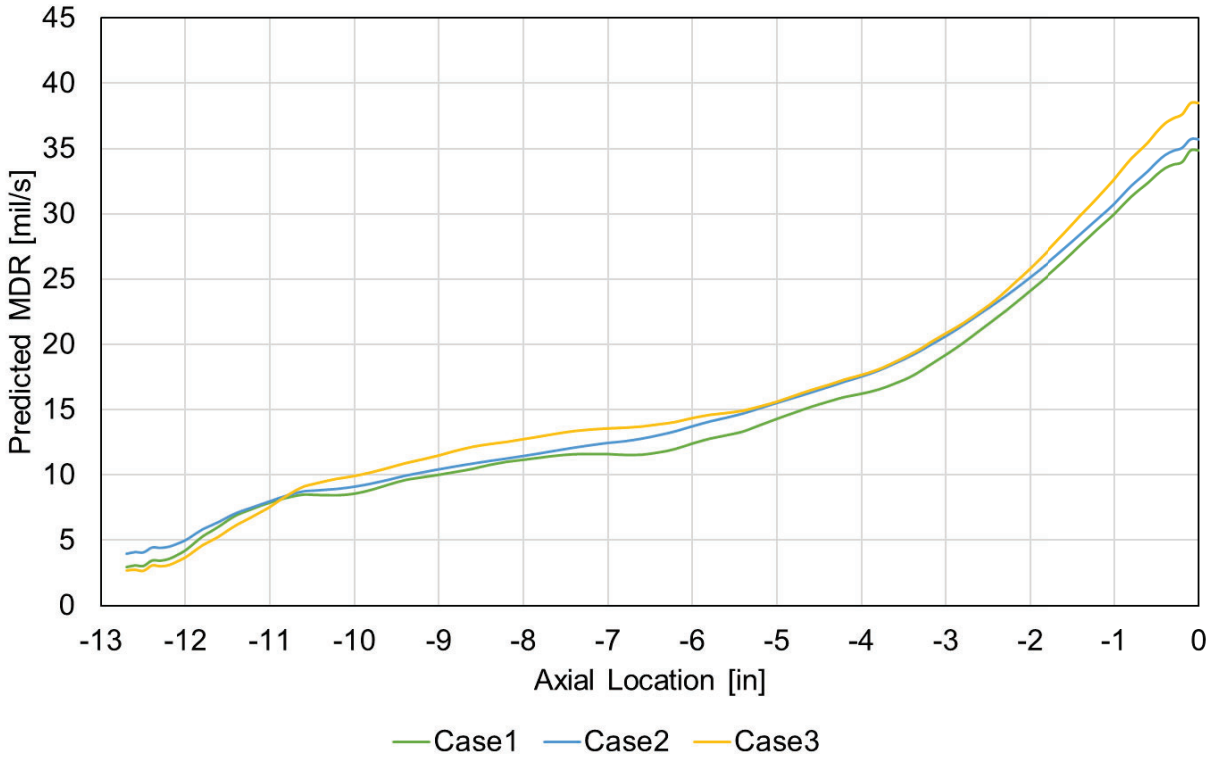

Figure 35. Regression-Model-Predicted MDR for varying Al_2O_3 Mass Fraction (Al_2O_3Content)

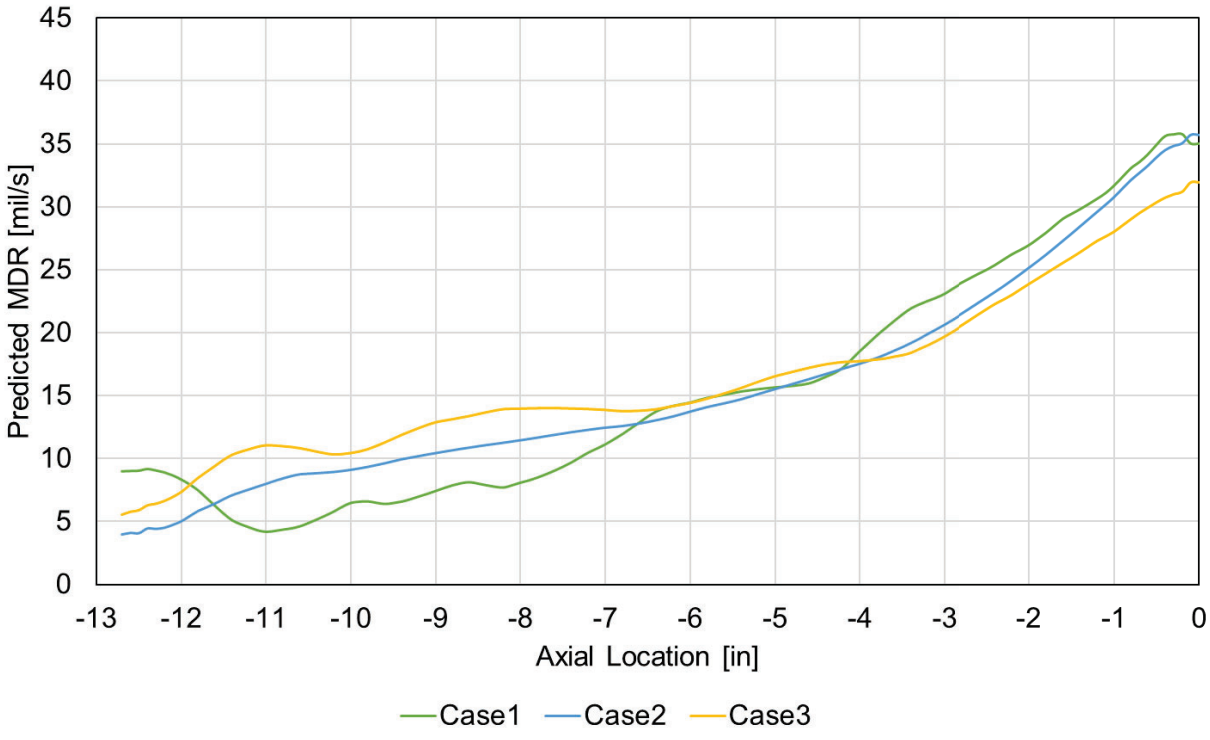

Figure 36. Regression-Model-Predicted MDR for Varying Average Chamber Pressure (TotalAvgPress)

From these figures, it appears that MDR is most sensitive to the O_2 mass flow rate, especially in the aft region of the test sample where flow is attached, mass fluxes are higher, and the effects of

higher mass fluxes (i.e., convective heat transfer and viscous shear rates), would be the dominant means of material degradation. In what is presumed to be the separated-flow region in the forward portion of the cone, the effect of additional O_2 mass flow rate is greatly diminished and even reversed in the forward-most part. This negative correlation between O_2 mass flow rate and MDR in the separated-flow region may indicate the effects of the flow straightener that was utilized only in the low-mass-flux tests. As illustrated in Figure 37, these four tests were conducted at lower pressures and mass flow rates than the remainder of those in the database. Therefore, these tests are likely to have an outsized effect on the relationship between MDR and those covariates in the regression equation. Since the flow straightener was only employed on the four low-mass flow, low-pressure tests, the effects of having attached versus separated flow in the forward region of the sample may be confounded with the effects of lowering mass flow rates and/or pressure. Therefore, though it appears that decreasing the O_2 mass flow rate increases MDR in the forward portion of the sample, it is actually the case that the presence of attached flow increases the MDR more effectively in this region than decreasing the O_2 mass flow rate tends to decrease it.

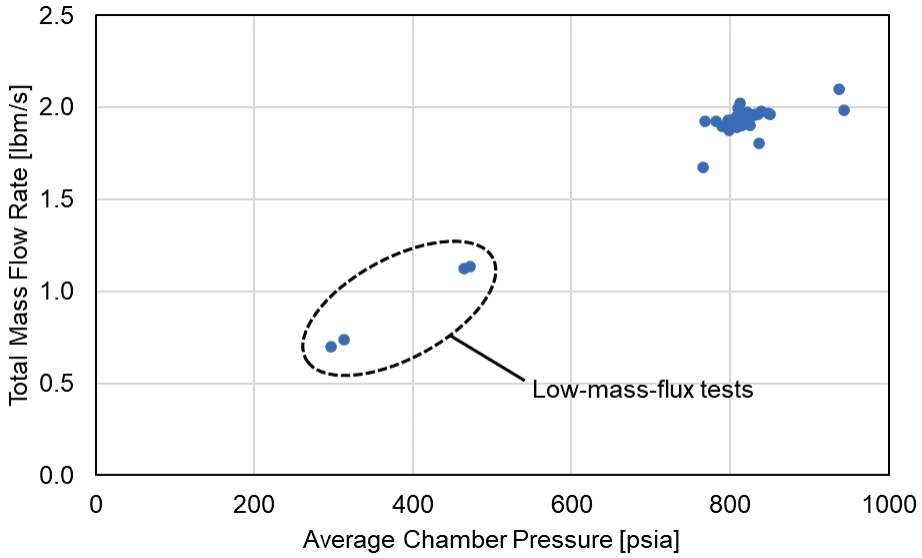

Figure 37. Total Mass Flow Rate versus Time-Average Chamber Pressure for Converging-cone SFT Tests

This same confounding affects the N_2 mass flow rate in the separated-flow region. Given that, what is surprising about the data in Figure 33 is how much less sensitive the MDR curve in the attached-flow region is to N_2 mass flow rate than it is to O_2 mass flow rate. It was expected that MDR would be more sensitive to O_2 than N_2 as the fuel regression rate was. However, the O_2/N_2 sensitivity difference demonstrated by the MDR goes well beyond what can be accounted for by the difference in fuel-regression-rate sensitivity. This fact indicates that increased O_2 flow rates have effects beyond those attributable to the mere increase in mass flow.

MDR is not sensitive to O/F, and the sign of the respective partial derivative changes twice over the length of the sample. On both the forward and aft ends of the sample, increasing O/F corresponds to decreasing MDR, but in the center, the opposite is true.

The relationship between MDR and the Al_2O_3 mass fraction in the SFT combustion-product flow revealed by the regression equation refines the understanding explicated in Section 7.1.

According to the results of the regression equation, increasing amounts of Al_2O_3 in the products *does* correlate with increasing insulation MDRs, *all other things being equal*. Nevertheless, the sensitivity of MDR to Al_2O_3 content is much lower than that of MDR to O_2 mass flow rate throughout the majority of the sample length, which is why Al_2O_3 content, which correlated negatively with O_2 mass flow rate in these tests (see Figure 16), appeared to correlate negatively with MDR when the other covariates were not controlled, as shown in Figure 4. Therefore, radiation, droplet impingement, and/or slag films do increase insulation MDRs, but only in the absence of a strong, oxidizing flow.

This relationship is reinforced by plotting PBI-NBR MDRs for the four different Al loading levels first with gas-phase mass flux (Figure 38) then with O_2 mass flux (Figure 39). For these plots, the mass flux at a given axial location is calculated by dividing the mass flow rate of interest (gas-phase or O_2) by the time-average cross-sectional area at that station. The gas-phase mass flow rate was computed by multiplying the total mass flow rate deduced from test data by the mass fraction of gas-phase products determined for chemical equilibrium of a uniform mixture of O_2, N_2, and fuel in the relative proportions deduced from the test data at the time-average chamber pressure. The mass flow rate of O_2 is simply that injected into the forward end of the motor. The time-average cross-sectional area was computed assuming a constant MDR throughout the test duration to be consistent with how time-average MDR is reported, though it is likely that MDR decreases in time. Regarding Figure 38, the relationship between MDR and gas-phase mass-flux appears roughly linear beyond the separated-flow region ($< \sim 0.3$ lbm/in^2-s) but with different slopes for each Al percentage. In Figure 39, however, three of the four Al-percentage curves essentially collapse into one, with the exception being that for 0% Al, which exhibits lower MDRs for a given O_2 mass flux than those with Al. All that is necessary to predict MDR for PBI-NBR for an Al-loaded fuel grain is O_2 mass flux is a deeply interesting result that warrants further inquiry. It must be noted that the computed O_2 mass flux is not truly the mass flux of O_2 at a given station since much of the O_2 injected into the motor will have reacted with fuel species to create other products before reaching the insulation sample. Nevertheless, this fictitious O_2 mass flux is clearly a key indicator of the dominant driver of MDR. Figure 40 presents the MDR versus O_2 mass flux curves for all 10 PBI-NBR tests performed in the converging-cone configuration of the SFT. Table 10 provides the key parameters for each of those tests. Though the curves for the three baseline tests and the 13% and 60% Al tests merge most neatly, the other five curves are also reasonably consolidated.

The difference between the non-aluminized (iSFT-075) and aluminized results may originate in radiative emissions from the Al_2O_3 droplets or from Al combustion occurring within the test sample, among other things, that become significant above a low threshold, but do not change much with further increases in Al concentration above this threshold. The long duration of iSFT-052 (21 s, approximately double the durations of the other tests in the database) likely explains its lower average MDRs, as MDR tends to decrease in time. The deviations of MDR curves from the low-mass-flux tests (iSFT-080 and iSFT-081) may be attributable to the use of the flow-straightener in those tests. Regardless, these results add confidence to the regression model's predictions and underscore the complexity of the SFT internal environment.

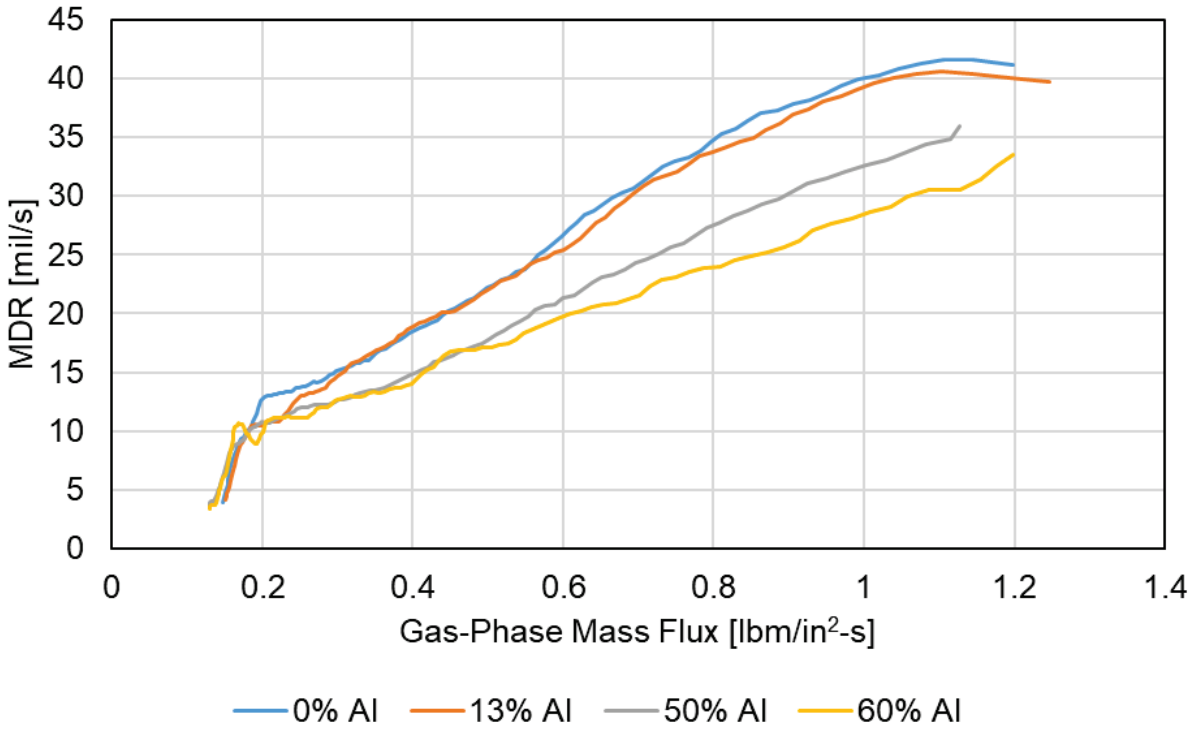

Figure 38. MDR versus Gas-Phase Mass Flux for PBI-NBR in Tests with Varying Al Loadings

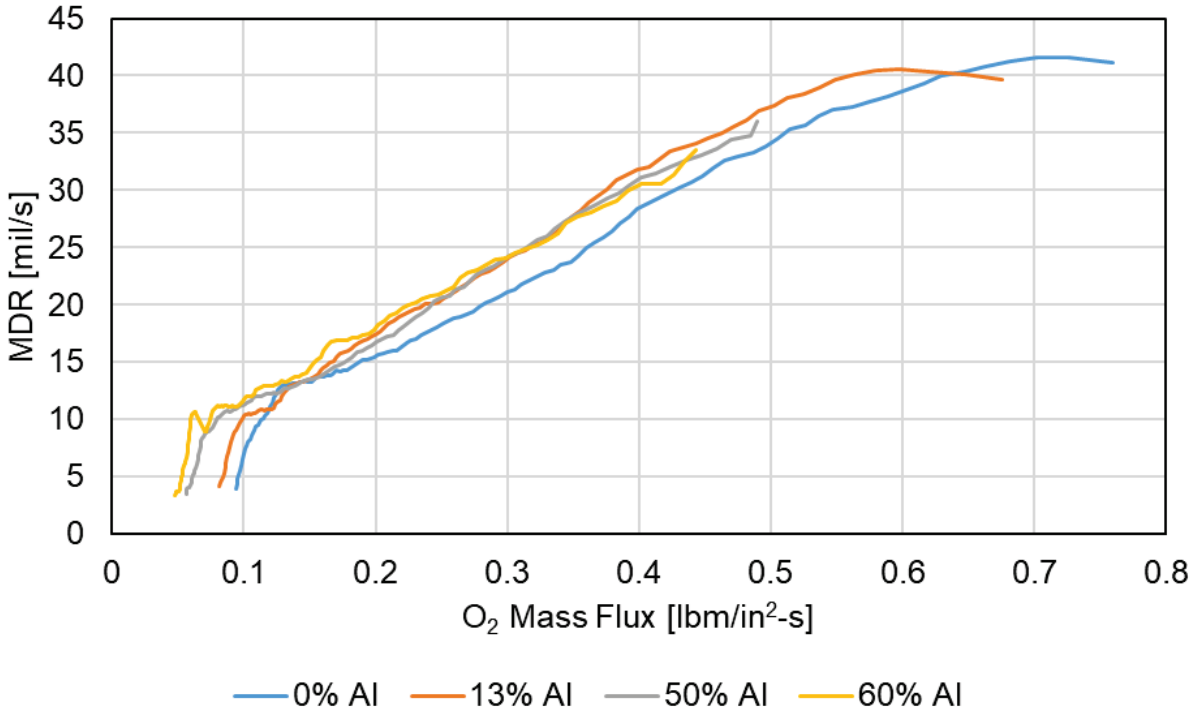

Figure 39. MDR versus O_2 Mass Flux for PBI-NBR in Tests with Varying Al Loadings

Table 10. As-measured Parameters for all PBI-NBR Tests

iSFT-	Al% in Solid Fuel	O_2 mass flow rate [lbm/s]	N_2% of Oxidizer	O/F	Pressure [psia]	Flame Temp. [K]	Al_2O_3% in products	Note
029	50	0.634	54	2.70	790	3736	24	Baseline
031	50	0.615	55	2.65	799	3704	24	Baseline
052	50	0.660	55	2.86	944	3751	23	2× duration
062	50	0.744	51	2.64	937	3830	24	High O_2 Flow
064	50	0.622	55	2.56	825	3708	25	Baseline
075	0	1.063	22	4.25	765	3530	0.0	0% Al
076	13	0.923	34	3.58	837	3574	5.1	13% Al
077	60	0.540	62	2.46	812	3606	27	60% Al
080	50	0.261	40	1.65	297	3617	27	low-mass-flux
081	50	0.376	49	1.94	464	3563	26	low-mass-flux

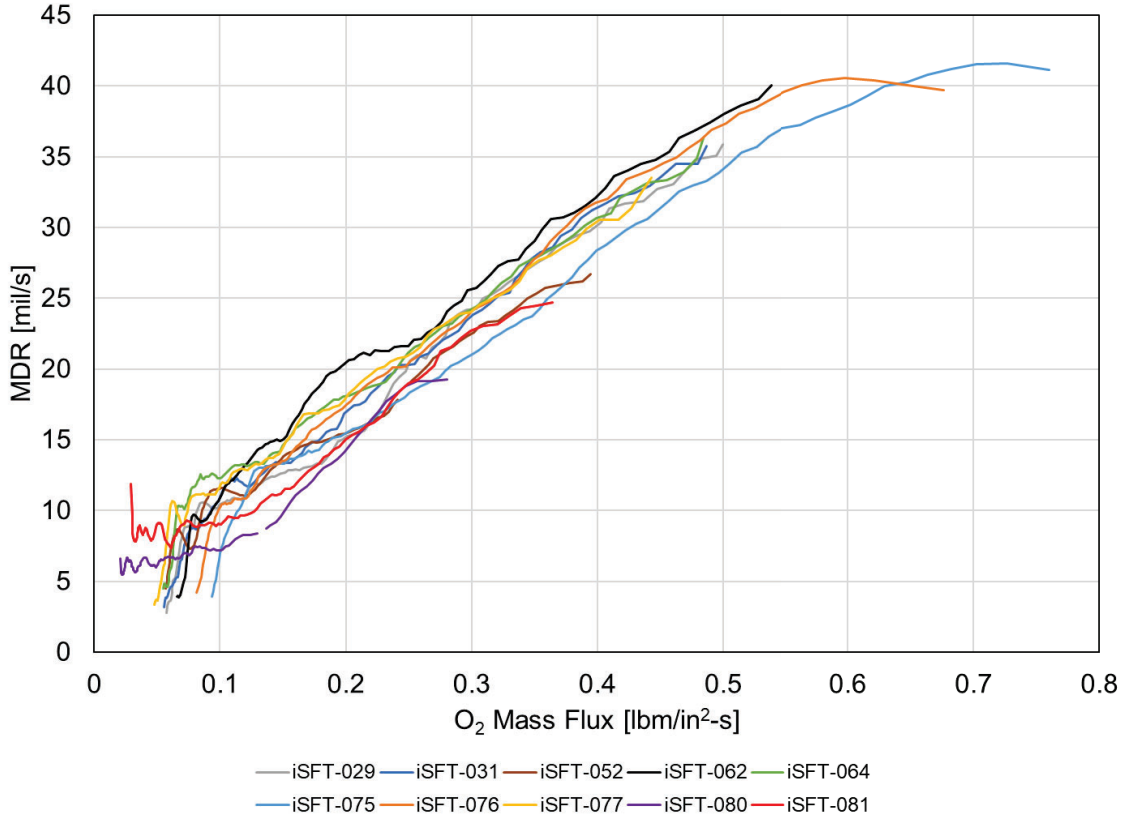

Figure 40. MDR versus O_2 Mass Flux for all PBI-NBR Tests

The correlation between pressure and MDR is positive in the forward portion of the insulation sample but negative in the aft portion. The negative correlation in the aft section may perhaps be explained by the fact that the pressure is being changed independently of the mass flux at a given location (O_2 mass flow rate, N_2 mass flow rate, and fuel mass flow rate (implicitly through O/F) are held constant), so the pressure is negatively correlated with velocity and therefore shear stress. In the forward section, as with O_2 and N_2 mass flow rates, the pressure effect may be confounded with the presence or absence of the flow-straightener, which leads to a positive correlation between pressure and MDR.

7.5 Conclusions

A test campaign was completed to hot-fire test four commonly used but previously untested SRM internal insulation materials in the MSFC SFT and to test PBI-NBR at three non-standard fuel-Al loadings. All seven tests were successfully performed, along with subsequent data analysis that revealed the thermal performance differences among the tested materials as well as some tested in other efforts. FDA was used to create a model of MDR as a function of six covariates: O_2 mass flow rate, N_2 mass flow rate, O/F, Al_2O_3 mass fraction, average chamber pressure, and material group. This model was then used to interrogate the relationships among these covariates and insulation thermal response.

Uncertainties in the precise fluid, thermal, and chemical environment in the insulation test sample complicate the effort to use SFT MDRs to predict insulation performance in SRMs. Coupled thermal-fluid-chemical modeling of the SFT and additional testing at non-standard conditions (e.g., other fuel Al loadings, pressures) and in the flow-straightened configuration would reduce uncertainties, expand the SFT material database, and increase its usefulness for SRM design and material development.

8.0 Findings and Observations

8.1 Findings

The following findings were identified:

F-1. The effect of condensed-phase Al_2O_3 in the combustion products of the SFT is to increase insulation MDRs over all but the forward-most locations of an insulation sample.

F-2. For all materials tested in the SFT, MDR is most sensitive to mass flow rate of O_2 among the covariates included in the FDA and, in the attached-flow region, its correlation is positive, meaning that greater O_2 mass flow rates produce greater MDRs.

8.2 Observations

The following observations were identified:

O-1. The SF-NBR performed roughly as expected, with higher MDRs than the other materials under consideration.

O-2. SF-EPDM performed unexpectedly well under high shear flow, given its lack of reinforcing fibers, with MDRs similar to those of PBI-NBR throughout the test sample.

O-3. The two SCP formulations tested exhibited lower MDRs throughout the test sample length than the rubber-matrix formulations and featured negative MDRs in the forward portion of the sample.

O-4. Uncertainty in the precise fluid, thermal, and chemical environment in the region of the insulation test sample due to separated flow, radially stratified flow, and axially distributed combustion complicates interpretation of the data and limits its usefulness to SRM design and material development.

1. Uncertainty in the near-wall velocity (and by analogy temperature) profile in the forward region of the sample prevents relating MDR to heat flux or shear force that would be translatable to other systems.

2. Non-uniform species distribution and/or energy release similarly confounds correlation of MDR data with environmental parameters.

9.0 Alternative Technical Opinion(s)

No alternative viewpoints were identified during the course of this assessment by the NESC team or the NRB quorum.

10.0 Other Deliverables

No unique hardware, software, or data packages, outside those contained in this report, were disseminated to other parties outside this assessment.

11.0 Recommendations for the NASA Lessons Learned Database

No lessons learned were identified during the course of this assessment.

12.0 Recommendations for NASA Standards, Specifications, Handbooks, and Procedures

No recommendations for NASA standards and specifications were identified as a result of this assessment.

13.0 Definition of Terms

Aluminum Content in Fuel	Weight percent of Al in the hybrid fuel grain. For a given test, the value of Aluminum Content in Fuel is established to produce an amount of Al_2O_3 in the combustion products of the SFT match that in the combustion products of the solid-propellant motor of interest.
Aluminum %	Weight percent of Al in the hybrid fuel grain. For a given test, the value of Aluminum % is established to produce an amount of Al_2O_3 in the combustion products of the SFT match that in the combustion products of the solid-propellant motor of interest.
Axial Location	Insulation test section station axial location defined with the origin at the throat and positive axis directed along the flow direction and out the nozzle. Negative axial locations correspond to stations upstream of the throat. This definition is reported with the white light (also called structured light) data measurements.
Bulk c* efficiency	A measure of the completeness of combustion in terms of various flow properties and geometries, depending on the mathematical definition. Higher c* efficiency implies higher chamber pressure and higher thrust.
Burke	Insulation material manufacturer.

Finding	A relevant factual conclusion and/or issue that is within the assessment scope and that the team has rigorously based on data from their independent analyses, tests, inspections, and/or reviews of technical documentation.
Gas Phase Mass Flow Rate	The mass flow rate through the SFT excluding the condensed-phase species. Computed by multiplying the total mass flow rate by the fraction of non-Al_2O_3 species as determined for chemical equilibrium of a uniform mixture of O_2, N_2, and fuel in the test-specific proportions at the time-averaged chamber pressure.
Gas Phase Mass Flux	Calculated at each axial station using the gas phase mass flow rate divided by the time-averaged cross-sectional area at that station. The time-averaged cross-sectional area calculation assumed a constant MDR calculated from inner diameter pre-test and post-test data and test duration. Constant MDR was applied during the entire test consistent with the time-averaged MDR reporting.
Insulation Material	Insulation test section material identifier providing information about the composition, history, form factor, manufacturer, etc.
Kirkhill	Insulation material manufacturer.
Max Pressure	Maximum chamber pressure measured during the test.
Max Smoothed Pressure	Maximum chamber pressure after the test data have been smoothed to remove noise.
Material Decomposition Depth	Depth of the insulation or the thickness of material that was either completely or partially decomposed.
Material Decomposition Rate	Rate of the insulation decomposition and defined as the material decomposition depth/test duration.
Observation	A noteworthy fact, issue, and/or risk, which may not be directly within the assessment scope, but could generate a separate issue or concern if not addressed. Alternatively, an observation can be a positive acknowledgement of a Center/Program/Project/Organization's operational structure, tools, and/or support provided.
Recommendation	A proposed measurable stakeholder action directly supported by specific Finding(s) and/or Observation(s) that will correct or mitigate an identified issue or risk.
REDAR	Insulation material manufacturer.
Regression Rate Coeff	Fuel grain regression rate coefficient used when calculating the regression rate. Note the units of in/s / (lbm/in^2-s)^n (e.g. n = 0.6652) depends on the regression rate

	relationship and specifically the regression rate exponent for a given formulation, etc.
Total Mass Flow Rate	Calculated using the constant GOx mass flow rate, the constant GN_2 diluent mass flow rate, and the time-averaged hybrid fuel grain mass flow rate calculated using the hybrid fuel grain mass burned divided by the actual duration burn time. The total mass flow rate includes the gas phase and alumina (Al_2O_3) particles.
Total Mass Flux	Calculated for each axial location as the total mass flow consisting of the constant GOx mass flow rate, constant GN_2 diluent mass flow rate, and hybrid fuel grain mass burned divided by the actual duration burn time resulting in a time-averaged fuel grain mass flow rate. The total mass flux includes the gas phase and alumina (Al_2O_3) particles.

14.0 Acronyms and Nomenclature List

°F	Degrees Fahrenheit
AF-EPDM	Aramid-Filled EPDM
Al	Aluminum
Al_2O_3	Aluminum Oxide, Alumina
BOLE	SLS Booster Obsolescence and Life Extension
EPDM	Ethylene-Propylene-Diene Monomers
FDA	Functional Data Analysis
FPC	Functional Principal Component
GN_2	Gaseous Nitrogen
GOx	Gaseous Oxygen
HTPB	Hydroxyl-Terminated Polybutadiene
in	Inch
in^2	Square Inch
iSFT	Insulation Configuration Solid Fuel Torch
K	Kelvin
KF-EPDM	Kevlar-Filled-Ethylene-Propylene-Diene Monomers
lbm	Pound Mass
lbs	Pounds
MAV	Mars Ascent Vehicle
MDD	Material Decomposition Depth
MDR	Material Decomposition Rate
MFD	Marshall Formulation Development
mil	Mil, $1/1{,}000^{th}$ of an Inch
MSFC	Marshall Space Flight Center
N_2	Nitrogen
NBR	Nitrile Butadiene Rubber
NESC	NASA Engineering and Safety Center
O	Oxygen Radical
OH	Hydroxyl Radical

O_2	Oxygen
O/F	Oxidizer to Fuel Ratio
PAL	Percent Aluminum Loading
PBI-NBR	Polybenzimidazole-Nitrile Butadiene Rubber
P_c	Chamber Pressure
PCA	Principal Components Analysis
psi	Pounds Force Per Square Inch
psia	Pounds Force Per Square Inch Absolute
psig	Pounds Force Per Square Inch Gauge
s	Second
SCP	Silica-Cloth Phenolic
SF-EPDM	Silica-Filled-Ethylene-Propylene-Diene Monomer
SF-NBR	Silica-Filled NBR
SFT	Solid Fuel Torch
SLS	Space Launch System
SRM	Solid Rocket Motor
Std	Standard
T_f	Flame Temperature
WEI	Wound Elastomeric Insulation

15.0 References

1. Peregrine Sounding Rocket Redesign, NESC-RP-15-01090, March 14, 2019.
2. McCollum, L. T., Schnell, A., Yaghoubi, D., Bean, Q., McCauley, R., and Prince, A., "Development Concepts for Mars Ascent Vehicle (MAV) Solid and Hybrid Vehicle Systems," M19-7230, March 1, 2019 https://ntrs.nasa.gov/api/citations/20190002123/downloads/20190002123.pdf
3. Yaghoubi, D., "Mars Ascent Vehicle Solid Propulsion Configuration," M20-7948, March 12, 2020, https://ntrs.nasa.gov/citations/20200002338
4. Prince, A., Kibbey, T., Karp, A., "A Design for a Two-Stage Solid Mars Ascent Vehicle." AIAA 2019-4149, AIAA Propulsion and Energy Forum, Indianapolis, IN, August 19-22, 2019.
5. Yaghoubi, D. and Ma, P., "Integrated Design for the MSR DAC-0.0 Mars Ascent Vehicle," IEEE Aerospace Conference, March 2021.
6. "Mars Ascent Vehicle (MAV) Mars Ascent Propulsion Systems (MAPS) First-Stage Solid Rocket Motor (SRM1) Development Motor 1 (DM-1) Static Test Report", Northrup Grumman Systems Corporation Propulsion Systems and Controls, Elkton, MD, RDTM-3293, August 3, 2023, submitted to NASA Marshall Space Flight Center (MSFC) under Government Contract 80FSFC21C0010.
7. "Mars Ascent Vehicle (MAV) Mars Ascent Propulsion Systems (MAPS) Second-Stage Solid Rocket Motor (SRM2) Development Motor 1 (DM-1) Static Test Report", Northrup Grumman Systems Corporation Propulsion Systems and Controls, Elkton, MD, RDTM-3294, August 3, 2023, submitted to NASA Marshall Space Flight Center (MSFC) under Government Contract 80FSFC21C0010

8. McCraw, S. J., Welsh, J. S., and Marsh, J. K., "Lessons Learned from the ORS-4 Mission and First Flight of the Super Strypi Launch System," SSC16-II-03, Small Satellite Conference, AIAA/Utah State University, August 8-13, 2016.
9. Foust, J., "Super Strypi Failure Blamed on First Stage Motor Malfunction," Space News, August 8, 2016, https://spacenews.com/super-strypi-failure-blamed-on-first-stage-motor-malfunction/
10. Nowakowski, T., "Chinese Startup Landspace Launches Zhuque-1 Rocket, Fails to Deliver Payload to Orbit," Spaceflight Insider, October 28, 2018, https://www.spaceflightinsider.com/organizations/china-national-space-administration/chinese-startup-landspace-launches-zhuque-1-rocket-fails-to-deliver-payload-to-orbit/
11. China's New Space Race: Landspace's Zhuque-1 Launch Fails in First Orbit Bid, Spacewatch Asia Pacific, October 28, 2018, https://spacewatch.global/2018/10/chinas-new-space-race-landspaces-zhuque-1-launch-fails-in-first-orbit-bid/
12. Erwin, S., "Northrop Grumman to Investigate Anomaly after OmegA's First Rocket Motor Test," Space News, May 30, 2019, https://spacenews.com/northrop-grumman-to-investigate-anomaly-after-omegas-first-rocket-motor-test/
13. Harwood, W., "Northrop Grumman Looking into Dramatic Nozzle Anomaly on OmegA Rocket Motor," Spaceflight Now, May 30, 2019, https://spaceflightnow.com/2019/05/30/northrop-grumman-looking-into-dramatic-nozzle-anomaly-on-omega-rocket-motor/
14. Failure Analysis of Solid Rocket Apogee Motors, Stanford Research Institute, Final Report, Contract 953298, SRI Project 1614, September 1972.
15. McBurnett, M. and Whitmore, A., "Rocket Autopsies Part I – Analysis of Motor Failures," Rockets Magazine, December 2010, pp. 12-15.
16. Richardson, E. H., Blackwood, J. M., Hays, M. J., and Skinner, T., "Solid Rocket Launch Vehicle Explosion Environments," JANNAF Conference, Albuquerque, NM, December 8-14, 2014, https://ntrs.nasa.gov/citations/20150002613
17. Eleazer, W., "Launch Failures: Titan Groundhog Day," The Space Review, October 26, 2015, https://www.thespacereview.com/article/2852/1
18. Coleno, R., Larrieu, J-M., and Zanelli, D., "IM Tactical Solid Rocket Motor Failure Mode Analysis Protocol," IMEMTS 2012, Paper 14101, Las Vegas, NV, May 14-17, 2012.
19. Bower, C.L., Martin, H.T., Colbert, J.D., Kibbey, T.P., Howse, S.A., and Westrich, S.K., "Subscale Motor Test Bed Development to Simulate Solid Rocket Motor Internal Environments for Material Characterization," Abstract No. 2023-0001JP, JANNAF Conference, Pittsburgh, PA, May 2023.
20. Risha G. A., Evans, B. J., Boyer, E., and Kuo, K. K., "Metals, Energetic Additives and Special Binders Used in Solid Fuels for Hybrid Rockets," *Fundamentals of Hybrid Rocket Combustion and Propulsion*, edited by M. J. Chiaverini and K. K. Kuo, Progress in Astronautics and Aeronautics, AIAA, Reston, VA, 2007, pp. 413-456.

21. Strand, L. D., Ray, R. L., and Cohen, N. S., “Hybrid Rocket Combustion Study,” AIAA Paper 93-2412, 29thAIAA/ASME/SAE/ASEE Joint Propulsion Conference, Monterey, CA, June 1993.

22. Ramsay, J. O., and Silverman, B. W., Functional Data Analysis, Second Edition, Springer 2005.

23. JMP, Version 17.1, SAS Institute Inc., Cary, NC, 1989–2023.

24. Nason, G. P., Wavelet Methods in Statistics with R, Springer, New York, 2008.

25. Barker, C., One Stop Model Building with the Generalized Regression Platform, Pruned Forward Stepwise Method in JMP, SAS Institute Inc., Cary, NC https://community.jmp.com/kvoqx44227/attachments/kvoqx44227/discovery-eu-2018-content/59/5/One-Stop Model Building with the Generalized Regression Platform.pdf.

Appendices

Appendix A. Sample Manufacturing Anomalies

Solid Fuel Torch Phenolic Convergent Cones for NESC Testing

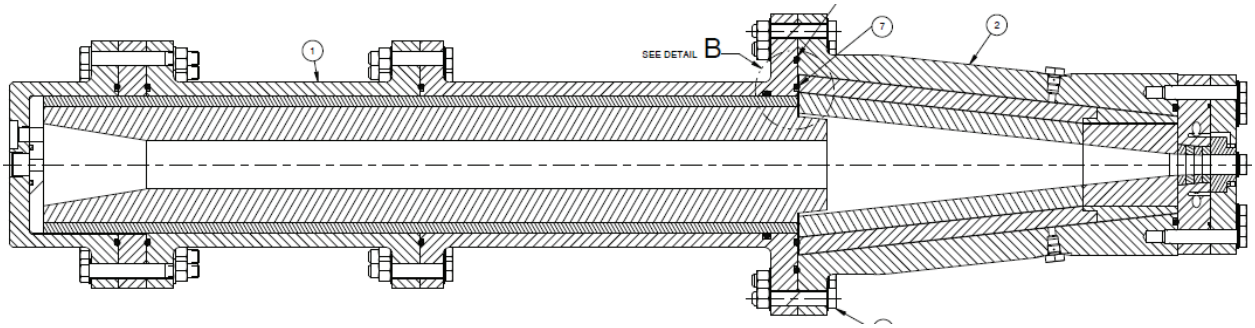

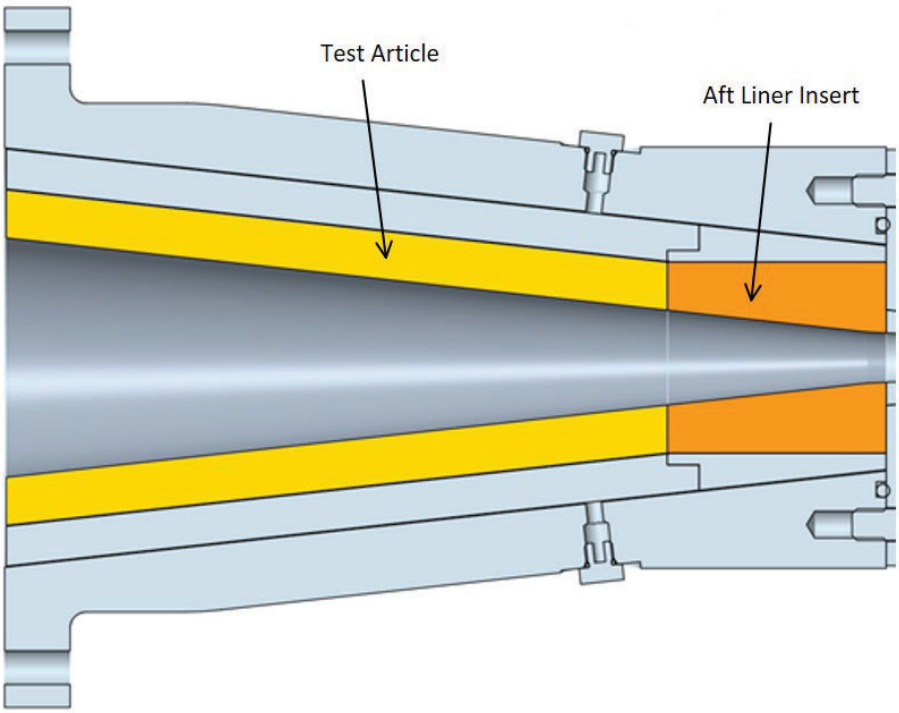

Two issues were noticed during machining of the parts:

1. Blemish on the inter diameter of FM5504 Test Article billet. It has a max depth of 0.1" and spans about 90 degrees circumferentially.
    a. Disposition: use as-is
    b. Rationale: Blemish is small in terms of both depth and circumferential extent.
2. The MXSE55 Aft Liner Insert billet has wavy plies. The outer diameter also did not fully clean up.
    a. Disposition: use as-is
    b. Rationale: Observed "waviness" on the OD of the billet does not necessarily entail an incorrect ply orientation within the part. The state of the OD will not affect the material response to the test conditions.

Issue #1 – FM5504 Test Article

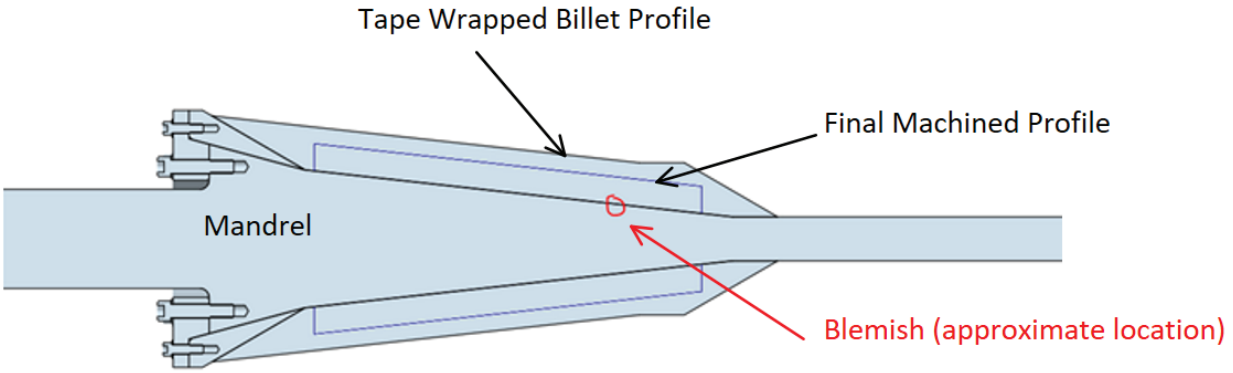

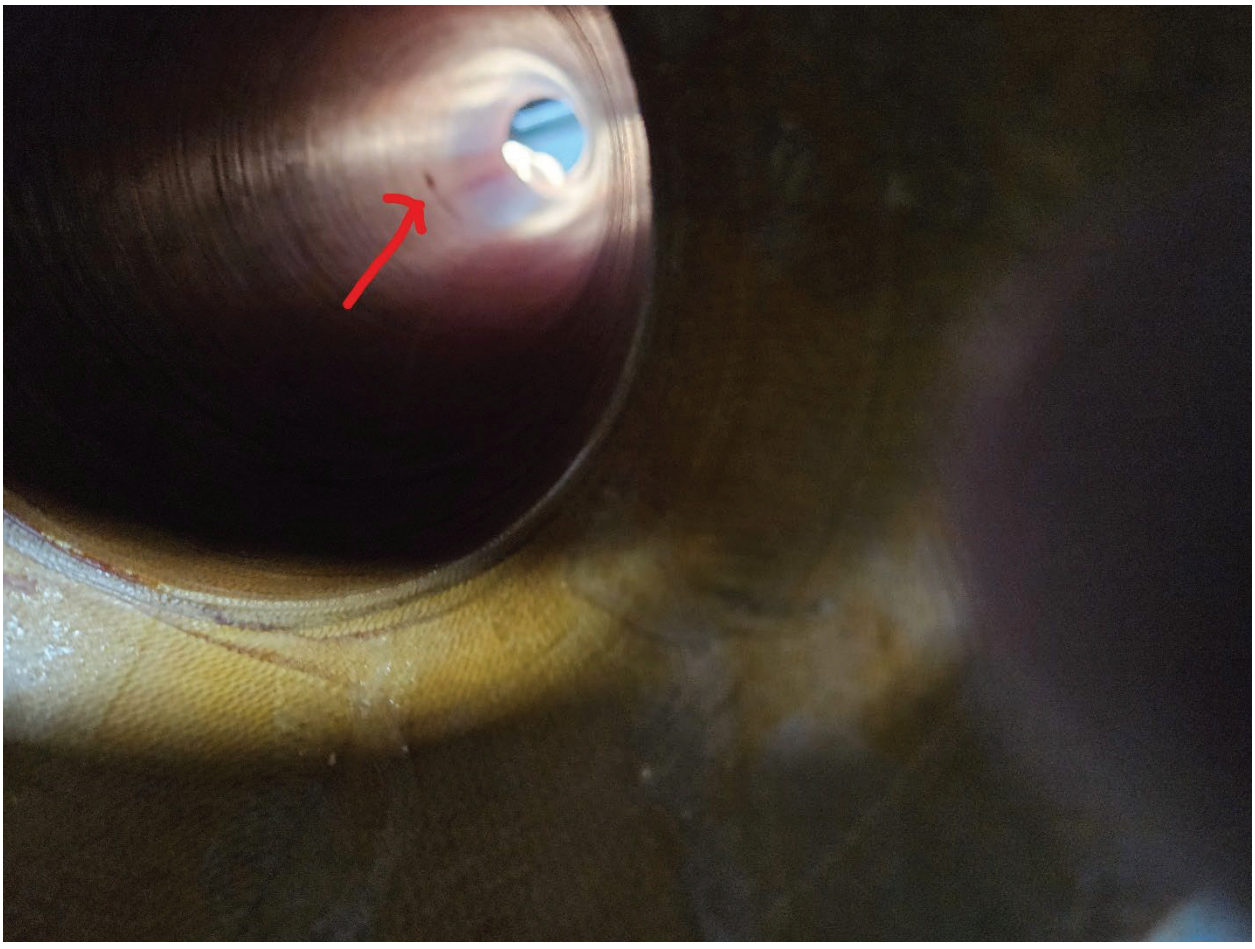

Issue #2 – MXSE55 Aft Liner Insert

National Aeronautics and Space Administration

George C. Marshall Space Flight Center
Propulsion Thermal Analysis Branch/ER43

NESC SFT Tests 1 & 2 (iSFT-075 & -076)

Heath T. Martin

June 6, 2022

National Aeronautics and Space Administration

George C. Marshall Space Flight Center
Propulsion Thermal Analysis Branch/ER43

Overview

- The first two NESC-funded SFT firings occurred on April 28, 2022.
- Both were part of the series intended to investigate the effect of propellant-aluminum mass fraction on insulation performance
- Both had lower aluminum loadings than previously tested in SFT

Material	Al% (Solid Propellant)	Al% (Solid Fuel)	O_2 mass flow rate [lbm/s]	N_2% of Oxidizer	Pressure [psia]	Flame Temperature [K]	Al_2O_3% of products
PBI-NBR	0	0	1.10	23	810	3582	0.0
PBI-NBR	3	13	0.95	34	809	3574	5.3
PBI-NBR	22	60	0.55	63	819	3647	27
SF-EPDM	16	50	0.65	55	810	3700	24
SF-NBR	16	50	0.65	55	810	3700	24
MX-2600 SCP	16	50	0.65	55	810	3700	24
MXSE 55	16	50	0.65	55	810	3700	24

12/6/23 2

National Aeronautics and Space Administration

George C. Marshall Space Flight Center
Propulsion Thermal Analysis Branch/ER43

Interior Ballistics

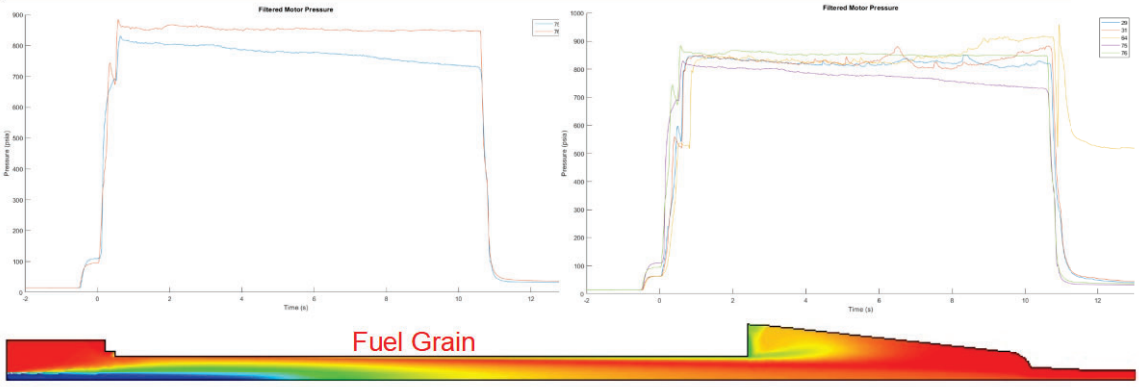

- Reducing Al loading resulted in higher-than-predicted O/F
  - 7% for 13% Al
  - 22% for 0% Al
- Hypothesis: reduced radiative heat feedback to fuel surface producing reduced regression rate
- Fuel less dense (O/F is mass ratio)
- Pressure & Temperature on-target for 13% test, about 5% low for 0% test

	0%	13%	50% (Avg)
P_c			
T_f			
O_2/F			

12/6/23 3

National Aeronautics and Space Administration

George C. Marshall Space Flight Center
Propulsion Thermal Analysis Branch/ER43

Insulation Performance

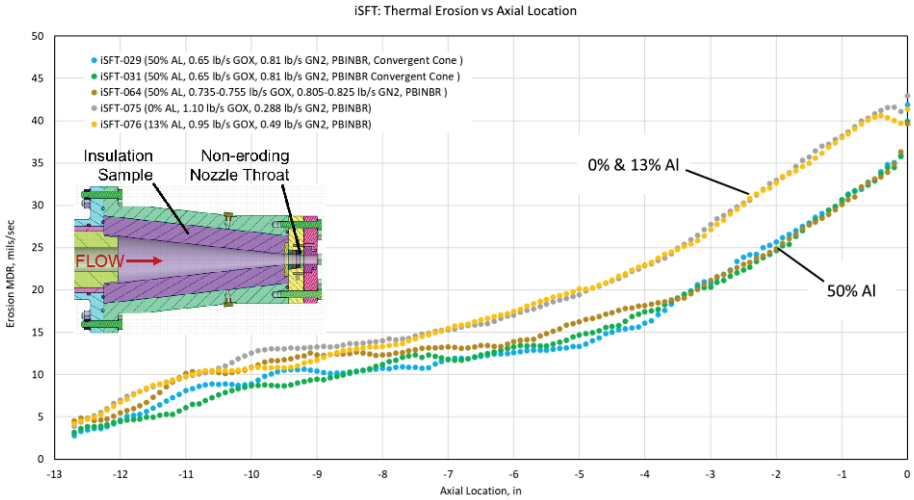

- Higher MDRs for lower-Al-loaded grains (remarkably similar to each other)
  - Higher gas-phase mass flux (17-19%), generally considered dominant
  - Higher oxidation potential, (9-14×), generally considered minor
- Little-to-no radiative heating
- Little-to-no slag interaction

12/6/23 4

NESC Update

Heath T. Martin

September 12, 2022

National Aeronautics and
Space Administration

George C. Marshall Space Flight Center
Propulsion Thermal Analysis Branch/ER43

Overview

- The second round of NESC-funded SFT firings occurred on July 27, 2022.
- The first, iSFT-077 was part of the series intended to investigate the effect of propellant-aluminum mass fraction on insulation performance and featured an aluminum loading greater than any previously used in an SFT.
- The second & third (iSFT-078 & -079) were intended to add materials to our database at baseline conditions.

Material	Al% (Solid Propellant)	Al% (Solid Fuel)	O_2 mass flow rate [lbm/s]	N_2% of Oxidizer	Pressure [psia]	Flame Temperature [K]	Al_2O_3% of products
PBI-NBR	0	0	1.10	23	810	3582	0.0
PBI-NBR	3	13	0.95	34	809	3574	5.3
PBI-NBR	22	60	0.55	63	819	3647	27
SF-EPDM	16	50	0.65	55	810	3700	24
SF-NBR	16	50	0.65	55	810	3700	24
MX-2600 SCP	16	50	0.65	55	810	3700	24
MXSE 55	16	50	0.65	55	810	3700	24

National Aeronautics and Space Administration

George C. Marshall Space Flight Center
Propulsion Thermal Analysis Branch/ER43

Interior Ballistics

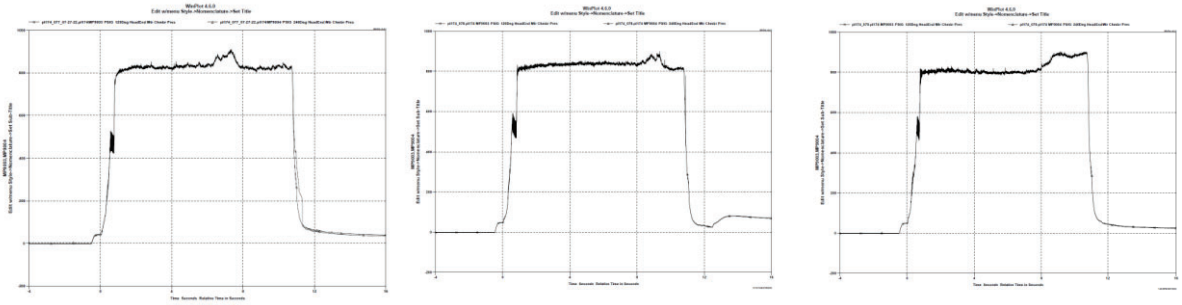

- Pressure & temperature targets met for each test.
- Blips in pressure histories, likely due to alumina slag flow through nozzle, have marginal effect on average values.
- Low delivered Gox flow rate (hot day)

Test	P_c	T_f	O/F
Target 77	**819**	**3647**	**2.68**
iSFT-077	812	3606	2.46
Target 78&79	**810**	**3700**	**2.67**
iSFT-078	815	3674	2.43
iSFT-079	809	3681	2.51

National Aeronautics and Space Administration

George C. Marshall Space Flight Center
Propulsion Thermal Analysis Branch/ER43

Aluminum Study

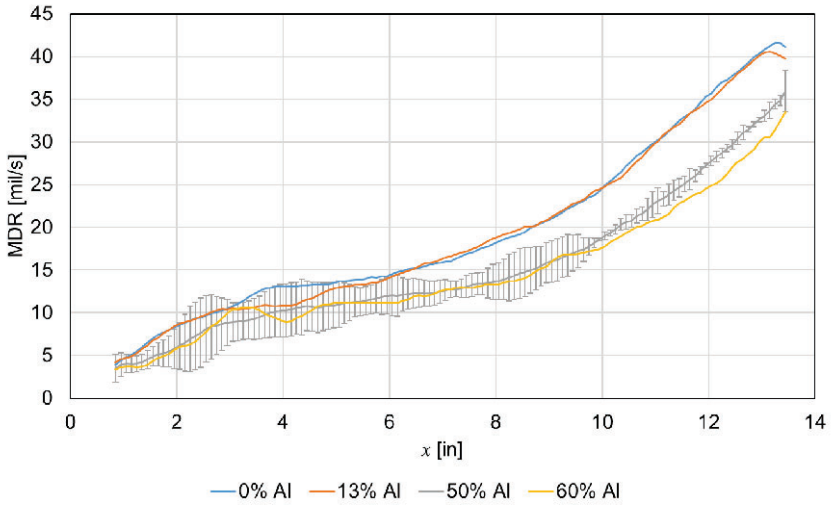

- Three tests at 50% Al from SFT database
- Error bars represent 2σ
- Hypothesis: Effects from slag impingement/flow and/or radiation are negligible

National Aeronautics and Space Administration

George C. Marshall Space Flight Center
Propulsion Thermal Analysis Branch/ER43

Aluminum Study

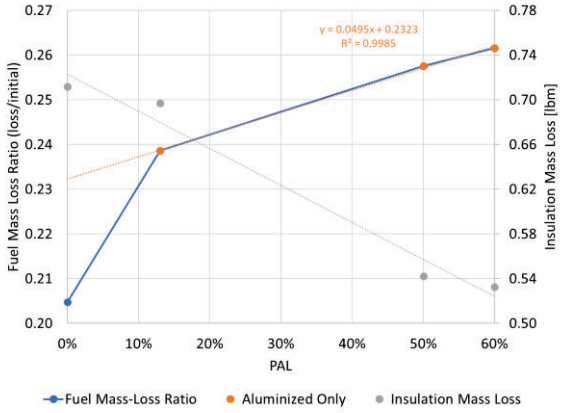

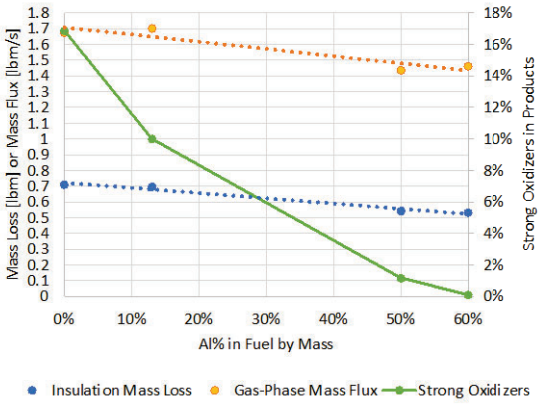

- Volume-basis fuel loss (essentially integrated regression rate) positively correlated with Al content
  - Relationship appears linear for Al-loaded grains
  - Hypothesis: big difference in regression rate between *no* Al and *some* Al owing to presence of broadband radiation emission from condensed-phase species
- Insulation mass loss negatively correlated with Al content
  - For these tests, Al% is negatively correlated with gas-phase mass flux, which is a useful proxy for both shear stress and convective heat flux and often used as a correlating parameter for insulation MDR.
- The burning of Al reduces the amount of oxidizing species in the combustion products, which could reduce MDRs, as well.

9/12/2022 5

National Aeronautics and Space Administration

George C. Marshall Space Flight Center
Propulsion Thermal Analysis Branch/ER43

Material Database Building

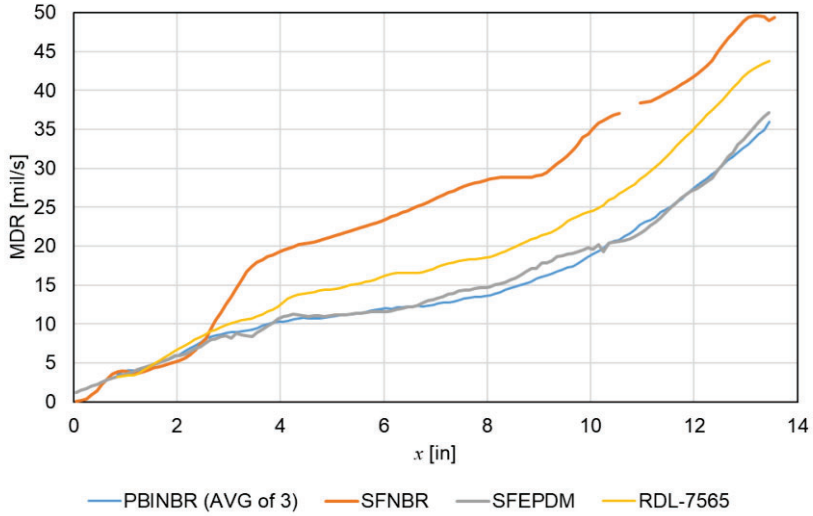

- SFNBR behaved as expected for a non-fiber-filled rubber
  - Good performance in radiation-dominated environments
  - Poor performance in convection-dominated environments
- SF-EPDM, however, performed as well as PBINBR in all environments
  - It was expected that SF-EPDM performance would be most similar to SF-NBR performance of the tested materials, given that it also doen not contain fibers to reinforce the char layer against mechanical removal.
  - KF-EPDMs have shown substantial test-to-test variability in the SFT, perhaps SF-EPDM behaves similarly.

9/12/2022 6

NESC SFT Tests 6 & 7 (iSFT-086 & -087)

Heath T. Martin

July 17, 2023

National Aeronautics and
Space Administration

George C. Marshall Space Flight Center
Propulsion Thermal Analysis Branch/ER43

Overview

- The last two NESC-funded SFT firings occurred on July 11, 2023.
- These were the first SFT tests of phenolic, rather than rubber, materials.
- Initial data review indicated nominal performance of SFT.
- Motors have been disassembled.
- Sample being prepared for post-test structured-light scan.

Material	Al% (Solid Propellant)	Al% (Solid Fuel)	O_2 mass flow rate [lbm/s]	N_2% of Oxidizer	Pressure [psia]	Flame Temperature [K]	Al_2O_3% of products
PBI-NBR	0	0	1.10	23	810	3582	0.0
PBI-NBR	3	13	0.95	34	809	3574	5.3
PBI-NBR	22	60	0.55	63	819	3647	27
SF-EPDM	16	50	0.65	55	810	3700	24
SF-NBR	16	50	0.65	55	810	3700	24
MX-2600 SCP	16	50	0.65	55	810	3700	24
MXSE 55	16	50	0.65	55	810	3700	24

National Aeronautics and
Space Administration

George C. Marshall Space Flight Center
Propulsion Thermal Analysis Branch/ER43

Unique Observation

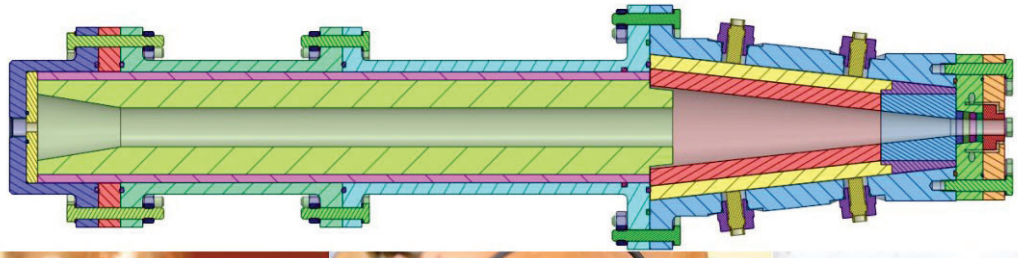

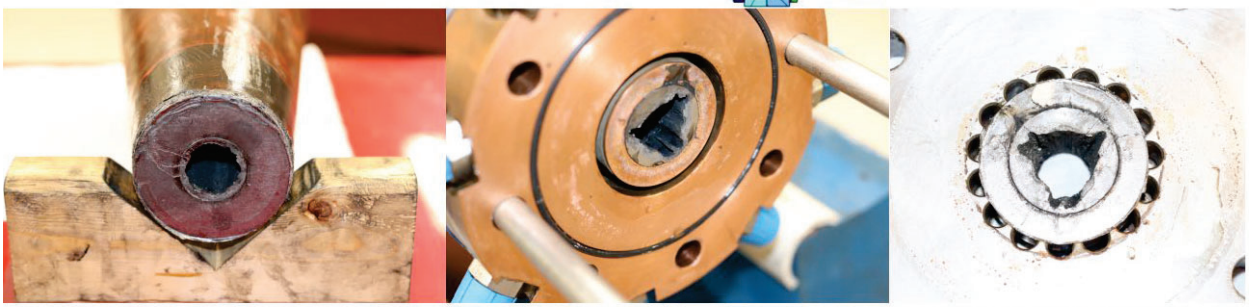

- Three-pointed erosion pattern in tungsten nozzle rings and nozzle retainer
- No pattern observed in MXSE-55 test specimen upstream.

Appendix C. Regression Model Details

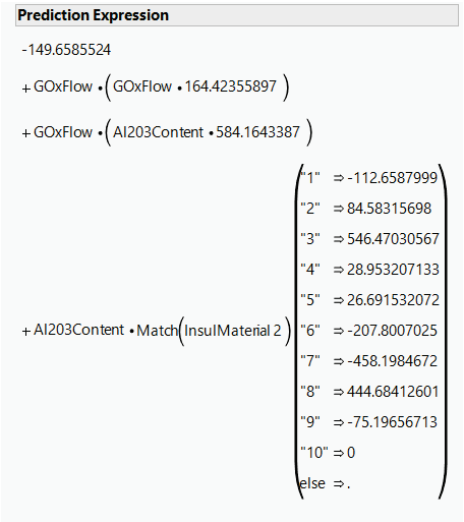

Figure C-1. Prediction Equation for FPC 1 Coefficient

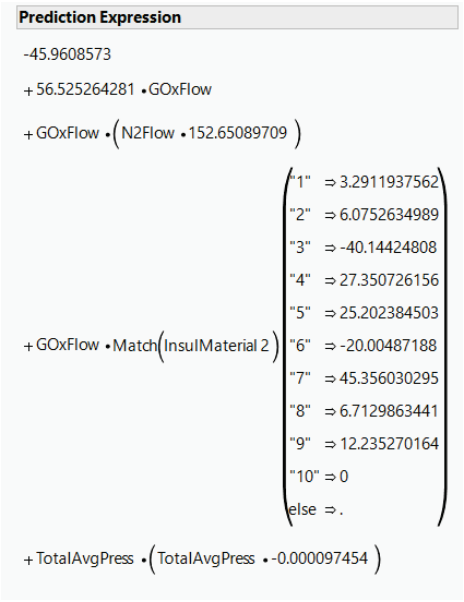

Figure C-2. Prediction Equation for FPC 2 Coefficient

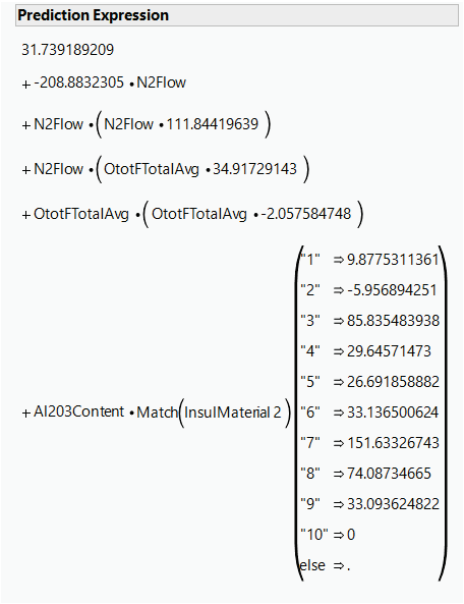

Figure C-3. Prediction Equation for FPC 3 Coefficient

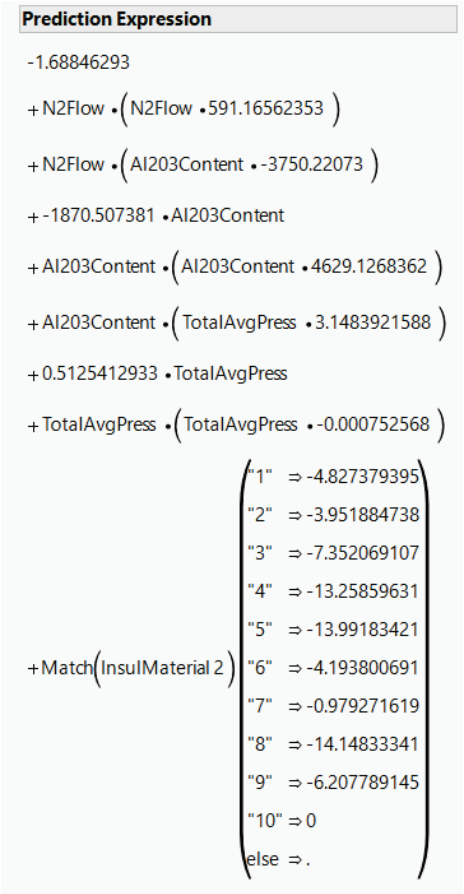

Figure C-4. Prediction Equation for FPC 4 Coefficient

Prediction Expression

$$-3.830062398 + 16.462008567 \cdot \text{Al203Content}$$

Figure C-5. Prediction Equation for FPC 5 Coefficient

Prediction Expression

$$\begin{aligned}
&78.228006204 \\
&+ 513.58996997 \cdot \text{N2Flow} \\
&+ \text{N2Flow} \cdot (\text{N2Flow} \cdot -332.8494223) \\
&+ 43.627232921 \cdot \text{OtotFTotalAvg} \\
&+ \text{OtotFTotalAvg} \cdot (\text{Al203Content} \cdot -164.1310746) \\
&+ \text{Al203Content} \cdot (\text{TotalAvgPress} \cdot 0.5554642146) \\
&+ -0.787240871 \cdot \text{TotalAvgPress} \\
&+ \text{TotalAvgPress} \cdot (\text{TotalAvgPress} \cdot 0.0003690369)
\end{aligned}$$

Figure C-6. Prediction Equation for FPC 6 Coefficient

Prediction Expression

$$\begin{aligned}
&-0.87141138 \\
&+ \text{GOxFlow} \cdot (\text{TotalAvgPress} \cdot 0.0244621986) \\
&+ \text{N2Flow} \cdot (\text{Al203Content} \cdot 55.765234806) \\
&+ \text{TotalAvgPress} \cdot (\text{TotalAvgPress} \cdot -0.000033279) \\
&+ \text{TotalAvgPress} \cdot \text{Match}(\text{InsulMaterial 2}, \\
&\quad \text{"1"} \Rightarrow -0.000681023, \\
&\quad \text{"2"} \Rightarrow -0.000809161, \\
&\quad \text{"3"} \Rightarrow -0.001603043, \\
&\quad \text{"4"} \Rightarrow 0.0012867648, \\
&\quad \text{"5"} \Rightarrow 0.0013302921, \\
&\quad \text{"6"} \Rightarrow 0.0010685378, \\
&\quad \text{"7"} \Rightarrow -0.003034917, \\
&\quad \text{"8"} \Rightarrow 0.009959342, \\
&\quad \text{"9"} \Rightarrow 0.0033181538, \\
&\quad \text{"10"} \Rightarrow 0, \\
&\quad \text{else} \Rightarrow .)
\end{aligned}$$

Figure C-7. Prediction Equation for FPC 7 Coefficient

Prediction Expression

$$5.551115e\text{-}15$$

Figure C-8. Prediction Equation for FPC 8 Coefficient

Prediction Expression

$$7.806256e\text{-}16$$

Figure C-9. Prediction Equation for FPC 9 Coefficient

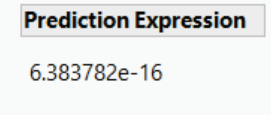

Figure C-10. Prediction Equation for FPC 10 Coefficient

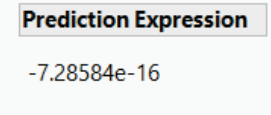

Figure C-11. Prediction Equation for FPC 11 Coefficient

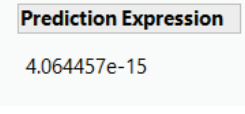

Figure C-12. Prediction Equation for FPC 12 Coefficient

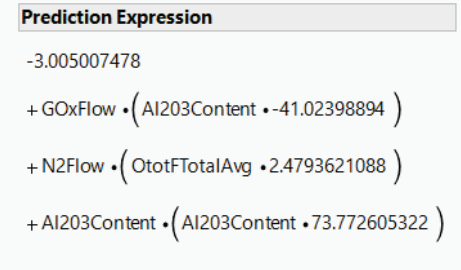

Figure C-13. Prediction Equation for FPC 13 Coefficient

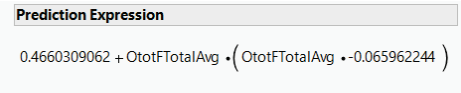

Figure C-14. Prediction Equation for FPC 14 Coefficient

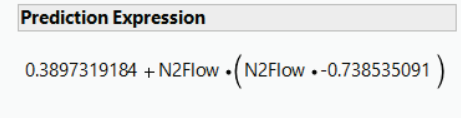

Figure C-15. Prediction Equation for FPC 15 Coefficient

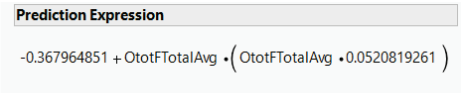

Figure C-16. Prediction Equation for FPC 16 Coefficient

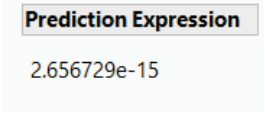

Figure C-17. Prediction Equation for FPC 17 Coefficient

Table C-1. Shape Functions for Mean and FPC 1-17

Location	Shape Mean	Shape 1	Shape 2	Shape 3	Shape 4	Shape 5	Shape 6	Shape 7	Shape 8	Shape 9	Shape 10	Shape 11	Shape 12	Shape 13	Shape 14	Shape 15	Shape 16	Shape 17
0	37.39562357	0.128348118	0.088203591	-0.13810426	0.161930127	0.228872076	-0.03265101	0.184444669	0.189597178	-0.26018016	0.106600373	-0.23681824	-0.41015573	-0.04306233	-0.27408268	-0.24505566	-0.05117608	-0.08742183
-0.1	37.39562357	0.128348118	0.088203591	-0.13810426	0.161930127	0.228872076	-0.03265101	0.184444669	0.189597178	-0.26018016	0.106600373	-0.23681824	-0.41015573	-0.04306233	-0.27408268	-0.24505566	-0.05117608	-0.08742183
-0.2	36.9100834	0.131028758	0.098794619	-0.13443478	0.124702049	0.198660889	0.015327107	0.190947995	0.172139973	-0.09506245	0.021488605	-0.1275133	-0.11852688	0.041249682	-0.21126209	0.123956388	0.025688163	-0.05786285
-0.3	36.69080389	0.131220271	0.103080544	-0.13477041	0.122057378	0.175227571	0.028829224	0.171955153	0.146324834	-0.0244574	0.004172266	-0.08701211	0.020554822	-0.01237062	-0.07815703	0.155536035	0.012081483	-0.01960533
-0.4	36.36808188	0.131651174	0.106164079	-0.13279549	0.121371141	0.146407795	0.049223513	0.145286369	0.122842872	0.043263785	-0.00140419	-0.01230524	0.157418686	-0.05685471	0.08264743	0.202535998	-0.05333798	-0.00596121
-0.5	35.82557493	0.132063435	0.107485641	-0.12750911	0.117602442	0.110043357	0.045856476	0.108361608	0.099114187	0.067994278	-0.02553241	0.004519294	0.176362818	-0.0485226	0.14450274	0.178449402	-0.04407218	0.001534899
-0.6	35.19524529	0.132317149	0.108019517	-0.12061843	0.111108606	0.07152506	0.042326053	0.068945187	0.078717065	0.095177713	-0.05149885	0.015378722	0.154863235	-0.04487426	0.191616786	0.18075739	-0.02769239	-0.00110717
-0.7	34.61576952	0.132033478	0.108535602	-0.11581874	0.110270446	0.049491155	0.047734513	0.038941469	0.053388593	0.107837847	-0.05029367	0.036745237	0.13229245	-0.03618088	0.19234385	0.097520423	-0.0006007	0.031725326
-0.8	34.03945962	0.131492	0.109456988	-0.11156923	0.108445154	0.030492735	0.057888434	0.018780083	0.029600715	0.115794593	-0.04487484	0.059722192	0.122068074	-0.01830247	0.141521544	0.019891899	0.018919411	0.033261519
-0.9	33.37485792	0.130736921	0.108395044	-0.10556597	0.102868079	0.014499516	0.05784389	-0.00272991	-0.0015611	0.110555273	-0.03081199	0.068826435	0.061571107	-0.02179019	0.107416635	-0.08214506	0.041505888	0.0424751
-1	32.69037318	0.129735423	0.106657447	-0.09933781	0.094984213	0.002725105	0.056335787	-0.0237766	-0.02788746	0.101486522	-0.01687672	0.076636318	-0.00381849	-0.02420247	0.077033121	-0.18637069	0.052131135	0.043098885
-1.1	32.08708999	0.128661658	0.105717836	-0.09440625	0.085953001	-0.00705909	0.056230382	-0.05141131	-0.04034587	0.089622702	-0.01210028	0.084153225	-0.04655945	-0.00217361	0.024456815	-0.21067127	0.096877071	0.065908662
-1.2	31.52501111	0.127458439	0.105311888	-0.09032911	0.073031123	-0.01620324	0.057911783	-0.07699455	-0.04737438	0.079754818	-0.01306774	0.088233228	-0.0706435	0.026655558	-0.02483947	-0.19209063	0.133263116	0.062682859
-1.3	30.95938314	0.126141566	0.104023659	-0.08614562	0.06206363	-0.02360778	0.061296867	-0.08582577	-0.05800208	0.066097612	0.003352646	0.101423504	-0.07932339	0.046136053	-0.03554391	-0.17758855	0.146201327	0.044806642
-1.4	30.40012341	0.124770966	0.102187154	-0.08205555	0.052048586	-0.03350444	0.065854737	-0.09081751	-0.06584521	0.057412482	0.018405411	0.112385432	-0.08360135	0.058980202	-0.04315386	-0.12385483	0.137560245	-0.01244482
-1.5	29.85185413	0.123631983	0.100812353	-0.07713334	0.037537832	-0.04025755	0.068024975	-0.09800676	-0.07482405	0.037705528	0.011802459	0.108797625	-0.08134535	0.083116599	-0.05565868	-0.10453063	0.085304479	0.006310482
-1.6	29.32287964	0.122646747	0.099746112	-0.07253466	0.022131745	-0.04577845	0.065705564	-0.1046441	-0.07946033	0.007556967	0.006042411	0.100894623	-0.07536991	0.106253806	-0.06323089	-0.07979918	0.005974914	0.014135964
-1.7	28.7865442	0.121751426	0.0985326	-0.06635665	0.010313921	-0.05444195	0.054757218	-0.11188863	-0.08905593	-0.00704424	0.014080055	0.080347788	-0.07319731	0.109718067	-0.05720487	-0.02323432	-0.07844032	0.00319811
-1.8	28.27127396	0.120951191	0.097826683	-0.05971364	-0.00262371	-0.06228312	0.038141919	-0.11522378	-0.09699278	-0.02015504	0.026422867	0.061605248	-0.06867178	0.110394469	-0.04420952	0.016566859	-0.14312466	0.0040166
-1.9	27.77231273	0.119901547	0.096673905	-0.05398135	-0.01394486	-0.07263219	0.026323053	-0.11567388	-0.10431844	-0.03225094	0.02996696	0.044330639	-0.0451484	0.087030706	-0.0416726	0.039225659	-0.17896384	0.01110475
-2	27.28941056	0.11877529	0.095246455	-0.04842849	-0.02489051	-0.08303258	0.015117026	-0.11315411	-0.1095104	-0.04431756	0.031348141	0.028764073	-0.01692813	0.053293069	-0.03920708	0.051277278	-0.19320153	0.019405274
-2.1	26.81492857	0.117686017	0.093498356	-0.04368489	-0.03603172	-0.09099915	0.010278344	-0.10603206	-0.11299103	-0.06101285	0.025095464	0.01310455	-0.00679719	0.026080993	-0.04659644	0.064434116	-0.20957834	0.009676022
-2.2	26.35246441	0.116597276	0.091241017	-0.03916232	-0.04592171	-0.09833167	0.007788704	-0.09500655	-0.11536617	-0.08114052	0.021180168	-0.00117114	-0.00128882	-0.00081666	-0.05188187	0.079190569	-0.22117285	-0.01496047
-2.3	25.90837744	0.115417531	0.088114254	-0.03302574	-0.05830522	-0.10186293	0.003463432	-0.08627953	-0.11957567	-0.09685051	0.018082129	-0.01101537	-0.00381463	-0.00416738	-0.0328228	0.085113534	-0.17725921	-0.00323303
-2.4	25.49241895	0.114226933	0.084886754	-0.02654505	-0.0708178	-0.10853035	-0.01734117	-0.07641168	-0.09601188	-0.11419408	0.021559026	-0.03420285	-0.00319434	-0.07549829	-0.04009678	0.102114657	-0.09893859	-0.02452031
-2.5	25.09047098	0.113256746	0.081524299	-0.01990419	-0.07925535	-0.11533631	-0.02578883	-0.05676961	-0.08710615	-0.13303853	0.02175669	-0.0412491	0.003017947	-0.09021167	-0.01764594	0.123522234	-0.02804613	-0.0550927
-2.6	24.70833761	0.112606212	0.077747243	-0.01209906	-0.08599243	-0.1257073	-0.02835806	-0.03520476	-0.07569183	-0.15165226	0.021377073	-0.04634593	0.004833614	-0.08726438	0.005855234	0.145517551	0.041778518	-0.08557442
-2.7	24.30833849	0.111743489	0.073721209	-0.00435786	-0.09112457	-0.12522509	-0.03007278	-0.01304429	-0.06141419	-0.14944505	0.018832266	-0.05541008	0.008047698	-0.08654414	0.025339447	0.131709852	0.096074268	-0.09859174
-2.8	23.91175332	0.11081197	0.069647989	0.003277517	-0.09521627	-0.12038317	-0.03110026	0.009078226	-0.04566049	-0.13766107	0.016654233	-0.06572943	0.014147355	-0.08404144	0.039424374	0.102671814	0.140540678	-0.09829802
-2.9	23.52192397	0.109909185	0.065048245	0.010296527	-0.09538796	-0.11606374	-0.03123402	0.029533536	-0.03448659	-0.12714787	0.023365054	-0.07781245	0.022230296	-0.06861122	0.042278467	0.077777372	0.177915694	-0.09544482
-3	23.14148618	0.109009036	0.060334957	0.017051991	-0.09505616	-0.10972339	-0.03143142	0.046886509	-0.02320976	-0.11392814	0.033628281	-0.08627829	0.030397165	-0.05243231	0.042537477	0.04698849	0.209765269	-0.08591522
-3.1	22.78899085	0.108041597	0.056422996	0.024412748	-0.09829067	-0.10634067	-0.03141635	0.064199841	-0.00722064	-0.09593929	0.042157695	-0.10073501	0.053949914	-0.04882528	0.015079033	0.007379268	0.201092856	-0.04150093
-3.2	22.47141901	0.107037911	0.052793411	0.032015572	-0.10413534	-0.10205735	-0.03067208	0.07983544	0.017749803	-0.06511931	0.04852584	-0.11324657	0.073802808	-0.03747591	-0.01832178	-0.04511259	0.153774461	0.018127141
-3.3	22.12203685	0.106191196	0.048532842	0.039183914	-0.11069303	-0.09372951	-0.02677332	0.086251797	0.025136904	-0.05754563	0.06091509	-0.0973227	0.128090908	-0.05727806	-0.00886308	-0.09660488	0.202346329	0.061905598
-3.4	21.80585935	0.105225247	0.044229163	0.045324777	-0.11486115	-0.08310532	-0.02967384	0.101306001	0.060125656	-0.02298357	0.069773996	-0.08647013	0.145929472	-0.0367631	-0.03483314	-0.11280004	0.077938243	0.118824941
-3.5	21.47810172	0.104287586	0.040484485	0.04917402	-0.11543192	-0.07561025	-0.03369177	0.091510556	0.070635737	0.010829186	0.053285556	-0.01082182	0.146689179	-0.02065483	-0.02075701	-0.13865427	0.036107916	0.133555553
-3.6	21.16055572	0.10335815	0.036666705	0.052013945	-0.1153631	-0.06906626	-0.03852197	0.072791696	0.079525231	0.046006751	0.024698534	-0.12254634	0.126460774	0.005804968	-0.00426128	-0.1540732	-0.01227878	0.131001937
-3.7	20.84922158	0.102499996	0.033288428	0.054956738	-0.11183543	-0.06335955	-0.04753201	0.056373317	0.081247655	0.088295389	0.001863842	-0.14327325	0.112717206	0.023071899	0.02772787	-0.16530228	-0.07461623	0.126547112
-3.8	20.54667796	0.101448633	0.029720708	0.056684197	-0.10920878	-0.05330866	-0.05482571	0.032549255	0.083442681	0.125271022	-0.0255768	-0.16328927	0.082368841	0.051666748	0.051372773	-0.16887855	-0.13087667	0.110104962
-3.9	20.26965972	0.100228272	0.025669662	0.058601903	-0.10279655	-0.04240933	-0.0650085	0.012344531	0.093460483	0.133048505	-0.0667269	-0.15649547	0.046464513	0.06712294	0.033822592	-0.14162815	-0.14223426	0.077960974
-4	20.00829363	0.09894955	0.021427705	0.06031659	-0.09527385	-0.03044612	-0.07503891	-0.00728739	0.105348105	0.128275324	-0.10958708	-0.13811557	0.006283408	0.078719442	0.002248587	-0.10101803	-0.1319869	0.03857476
-4.1	19.75861968	0.097751482	0.016645378	0.06077423	-0.08730922	-0.01846455	-0.08950983	-0.02613483	0.113826241	0.11628374	-0.15295188	-0.1143112	-0.03673786	0.083292611	-0.0261315	-0.04250742	-0.10976206	0.008061277
-4.2	19.52141038	0.096629365	0.011776602	0.060861532	-0.07954828	-0.00630006	-0.10343268	-0.0427975	0.120388487	0.099461075	-0.18995965	-0.08578362	-0.07772057	0.082649253	-0.0516778	0.020164941	-0.07861125	-0.02034133
-4.3	19.28904376	0.095765561	0.007815568	0.062779609	-0.07668901	0.002872108	-0.10695843	-0.05565556	0.122350866	0.093837232	-0.19661358	-0.05694593	-0.10526541	0.083005869	-0.05423248	0.062341212	-0.04039086	-0.04652333
-4.4	19.07228288	0.095068295	0.004480213	0.064724557	-0.07564968	0.013899988	-0.10430803	-0.06552035	0.12163788	0.089077732	-0.1836995	-0.03027804	-0.12558714	0.076182978	-0.04920634	0.092735449	-0.00138784	-0.0743938
-4.5	18.86126274	0.094400147	0.000619286	0.066762556	-0.07317812	0.021894671	-0.10169094	-0.06718525	0.119461057	0.081779005	-0.16796639	0.001908885	-0.13097816	0.06811081	-0.02859666	0.109154519	0.025962869	-0.0947332
-4.6	18.65722695	0.093830432	-0.00321223	0.068995976	-0.07133565	0.028804947	-0.09703708	-0.06544281	0.113396516	0.071093064	-0.14732171	0.037075201	-0.12696068	0.05458047	0.002455553	0.112785641	0.055995939	-0.10692015
-4.7	18.47497957	0.093434417	-0.00615578	0.071764861	-0.07409242	0.04164307	-0.09275726	-0.05872932	0.101983304	0.052677048	-0.11194226	0.076958346	-0.12706281	0.02342816	0.029836735	0.09347671	0.06956603	-0.09501866
-4.8	18.29989429	0.093147927	-0.00887991	0.074513596	-0.07828539	0.054825812	-0.08806371	-0.04937559	0.088695604	0.031575801	-0.07524142	0.116148723	-0.12409913	-0.01032536	0.055286275	0.065025249	0.071620058	-0.06768988
-4.9	18.12959622	0.092866532	-0.01140625	0.077996068	-0.08273335	0.0641921	-0.08209801	-0.04159557	0.073031782	0.011796809	-0.04690145	0.159532781	-0.1220484	-0.04205028	0.087699923	0.038321059	0.076092142	-0.03400646
-5	17.96067892	0.092640263	-0.01386961	0.081354494	-0.0870464	0.07223586	-0.07538055	-0.03283504	0.056965507	-0.00687035	-0.02230414	0.198169694	-0.11577574	-0.06989061	0.116536616	0.012602676	0.074964335	0.004423184
-5.1	17.77727298	0.092636967	-0.0166351	0.081838535	-0.08949179	0.080712729	-0.06845398	-0.01830041	0.049326539	-0.02446567	0.0011451	0.208238521	-0.08542861	-0.07996752	0.120114651	-0.00926869	0.036091991	0.039770876
-5.2	17.59129278	0.092693451	-0.01940473	0.08158306	-0.09037946	0.088579656	-0.06069888	-0.00216455	0.044661954	-0.03970112	0.022340265	0.205991445	-0.04798252	-0.08364633	0.109152413	-0.02767974	-0.01342393	0.0646044
-5.3	17.40082939	0.092737279	-0.02257186	0.08111995	-0.09058367	0.097699932	-0.0531678	0.015856809	0.036239062	-0.04864887	0.039971961	0.190489932	-0.00501026	-0.07693865	0.092329514	-0.03209966	-0.05029728	0.104979814
-5.4	17.21072464	0.0927716	-0.02568628	0.080737784	-0.0895825	0.106362626	-0.04427354	0.033433767	0.027670676	-0.05235716	0.053831864	0.168079289	0.034764029	-0.06913972	0.064696865	-0.03163371	-0.079854	0.133953586
-5.5	17.04814618	0.09247592	-0.02769468	0.08390907	-0.08339333	0.110470642	-0.03256535	0.04297755	0.021583038	-0.0555461	0.069303672	0.164767926	0.049913213	-0.08214135	0.022269052	-0.03416536	-0.08871315	0.072217261
-5.6	16.89331146	0.092076334	-0.02938816	0.08803718	-0.07537174	0.112155315	-0.01983634	0.049013077	0.015188138	-0.05515361	0.084367941	0.163845653	0.05495697	-0.09568553	-0.0234054	-0.03601308	-0.08607549	-0.01600271
-5.7	16.74428678	0.091720974	-0.0313952	0.091293673	-0.06733109	0.114997092	-0.00649669	0.057262312	0.011207001	-0.04757363	0.087934805	0.160518685	0.058295843	-0.11546138	-0.07194722	-0.04763185	-0.07621957	-0.0899438
-5.8	16.59465116	0.09137954	-0.03360351	0.093951997	-0.05958061	0.116879375	0.00708384	0.064649526	0.006170359	-0.03549696	0.088734429	0.153140797	0.058566435	-0.12789547	-0.11575134	-0.06121595	-0.06092983	-0.15229843
-5.9	16.41662572	0.091181611	-0.03619695	0.094807765	-0.05486663	0.113760952	0.016250595	0.068090734	-0.01022474	-0.01687809	0.102837762	0.125572004	0.064682596	-0.08293232	-0.1206909	-0.05638308	-0.0416139	-0.15333167
-6	16.22960528	0.091001258	-0.03907223	0.094819519	-0.05125419	0.108940861	0.023772893	0.069761883	-0.03115515	0.003036424	0.117447542	0.090012816	0.069631328	-0.01737713	-0.10885695	-0.04150971	-0.02052627	-0.12752448
-6.1	16.03762017	0.090897422	-0.04261581	0.093045995	-0.05022131	0.103212593	0.036084388	0.069497714	-0.05245894	0.025636544	0.137638687	0.04980164	0.072094595	0.058524722	-0.09751865	-0.04834235	-0.0052646	-0.08224772
-6.2	15.84574724	0.090793059	-0.04656075	0.09044823	-0.04918317	0.097569658	0.047649495	0.067986931	-0.07490779	0.047169465	0.153634038	0.009672736	0.07074446	0.142331445	-0.08224021	-0.05324544	0.008405031	-0.02798502
-6.3	15.6739237	0.090240331	-0.05002862	0.090669011	-0.04535195	0.09612891	0.056941953	0.069666933	-0.09529588	0.047296889	0.137098105	-0.02320673	0.053253204	0.179364498	-0.06262689	-0.0098	0.020092748	0.006422839
-6.4	15.51522807	0.089596147	-0.0535068	0.091148144	-0.0379133	0.09758602	0.062109622	0.070621554	-0.11579416	0.038554151	0.101093203	-0.04840712	0.028805716	0.199716243	-0.0370766	0.054050919	0.024307864	0.0271807
-6.5	15.35212187	0.089149727	-0.05821021	0.089334945	-0.0307918	0.097468617	0.056853142	0.069799108	-0.13711392	0.041951034	0.069294961	-0.05983967	0.005232813	0.211283655	-0.02603322	0.113201403	0.049373554	0.049690481
-6.6	15.19454681	0.088777313	-0.06329243	0.086620743	-0.02252918	0.09724593	0.047890536	0.066435256	-0.15641607	0.047832783	0.036369823	-0.0641764	-0.01783163	0.207462646	-0.01781944	0.164473837	0.075609235	0.067145478
-6.7	15.04747543	0.088531257	-0.06730709	0.084586412	-0.01071013	0.096687862	0.044480347	0.054909335	-0.16741149	0.054490745	0.017530095	-0.07141106	-0.02632071	0.170888385	-0.00880929	0.167129636	0.070186491	0.076537673
-6.8	14.90703018	0.088348281	-0.07114973	0.082425963	0.002553083	0.095478903	0.043363767	0.039504512	-0.17221443	0.060834354	0.004152681	-0.07845346	-0.02953444	0.118548518	0.00074189	0.146261347	0.053393051	0.077694743
-6.9	14.78574741	0.088149523	-0.07536992	0.078937299	0.014793593	0.094127734	0.04408259	0.02154722	-0.1728303	0.067733831	-0.01385266	-0.08147623	-0.03736961	0.061031165	0.020415388	0.105004115	0.036711583	0.077977685
-7	14.67049472	0.08795639	-0.07977947	0.074985456	0.026854499	0.091863911	0.046248159	0.002086193	-0.16904265	0.073324733	-0.03070954	-0.08404579	-0.0445752	-0.00021177	0.042751013	0.052138671	0.018408487	0.07203214
-7.1	14.54238481	0.087754115	-0.08485907	0.071331734	0.038699067	0.086741022	0.054833933	-0.01480795	-0.15829097	0.069659483	-0.04182107	-0.09428064	-0.0524103	-0.05007957	0.060778999	0.003185661	0.004608364	0.039747645
-7.2	14.40920145	0.087551959	-0.09023168	0.06752376	0.04977471	0.080095283	0.064582431	-0.03090784	-0.14327215	0.061395091	-0.04926214	-0.10543275	-0.05738534	-0.09140693	0.073908354	-0.04044233	-0.0055751	-5.0951E-05
-7.3	14.27079919	0.087324865	-0.09534553	0.0644584	0.061477118	0.07183461	0.069498263	-0.04731665	-0.12846338	0.055888048	-0.05310926	-0.12002395	-0.05723835	-0.14260595	0.089447378	-0.08584773	-0.01784738	-0.04439994
-7.4	14.13002725	0.087049765	-0.1002356	0.061735063	0.072292935	0.06250877	0.072293413	-0.06302755	-0.11165882	0.048178893	-0.05442921	-0.13336366	-0.05286613	-0.18742687	0.1003629	-0.12213909	-0.02934205	-0.0862173
-7.5	13.99260856	0.086627368	-0.10433075	0.059534116	0.079030717	0.053579958	0.074047138	-0.07777854	-0.08870713	0.026478386	-0.05663923	-0.13506	-0.05748912	0.139414309	0.089245593	-0.1167338	-0.03454857	-0.09277448
-7.6	13.85682663	0.086109579	-0.10802142	0.057594527	0.083649193	0.043878849	0.072536931	-0.09117033	-0.06257977	-0.00041795	-0.05937	-0.12968515	-0.01637419	-0.18334352	0.066853022	-0.09362989	-0.03479058	-0.08151897
-7.7	13.72220663	0.085526481	-0.1112391	0.055715146	0.086571244	0.033856273	0.070340561	-0.10204748	-0.03717153	-0.02719328	-0.05660641	-0.12143844	0.000399296	-0.15871968	0.04202499	-0.05475239	-0.0439733	-0.07687337
-7.8	13.58949109	0.084875041	-0.11420337	0.053808173	0.088229184	0.023329054	0.067541979	-0.11090051	-0.01080363	-0.05372162	-0.05311483	-0.10799944	0.017866755	-0.12576299	0.011788078	-0.00949709	-0.05108139	-0.06507797
-7.9	13.46103325	0.084127307	-0.11750224	0.051812811	0.089936721	0.012876164	0.067149717	-0.11773127	0.018136254	-0.07596569	-0.06312899	-0.08365597	0.043853227	-0.10243441	-0.02491288	0.011388115	-0.03169987	-0.02287192
-8	13.33560074	0.083278622	-0.12071804	0.049597798	0.091015876	0.002289872	0.068374402	-0.12154765	0.046623289	-0.09507933	-0.0760491	-0.05469638	0.06963832	-0.07866066	-0.05929075	0.02215809	-0.00545987	0.026450163
-8.1	13.21117609	0.082511352	-0.12404556	0.046845833	0.092033272	-0.01036368	0.067231418	-0.12599847	0.079460255	-0.11040535	-0.08463772	-0.01882343	0.099944667	-0.05742931	-0.11427837	0.038198023	0.029123057	0.093626638
-8.2	13.08734176	0.081681479	-0.12721145	0.043473885	0.09228711	-0.02343334	0.066386803	-0.12758302	0.110529923	-0.12176638	-0.08942224	0.018171791	0.126827767	-0.03406325	-0.1656238	0.05042967	0.062748043	0.157229796
-8.3	12.97174755	0.08043644	-0.12916579	0.040114514	0.090767446	-0.03451355	0.075345626	-0.11715211	0.126148934	-0.13003968	-0.08669328	0.041379378	0.122799348	0.00736844	-0.15025436	0.041791662	0.057864126	0.157758006
-8.4	12.85603092	0.07900273	-0.13059397	0.036290983	0.088120391	-0.04553942	0.085778513	-0.10146123	0.134236705	-0.13276449	-0.07569112	0.055787172	0.104671619	0.052590866	-0.10715268	0.025164016	0.041358142	0.129529588
-8.5	12.72992487	0.077601138	-0.1322518	0.029774691	0.08331724	-0.05421635	0.093999933	-0.08216644	0.137729724	-0.1320607	-0.06039712	0.075404241	0.090348491	0.106451801	-0.06751774	0.007210613	0.022235015	0.093591439
-8.6	12.59677537	0.076144003	-0.13377409	0.022193669	0.077551158	-0.06297063	0.098918286	-0.06100247	0.13652372	-0.12531697	-0.03802198	0.089397208	0.072204811	0.157073343	-0.02166276	-0.01122366	0.002981318	0.04631835
-8.7	12.45396171	0.074585003	-0.1350404	0.015714534	0.07257646	-0.07918329	0.09058044	-0.04523303	0.135354916	-0.09967721	0.011658255	0.072685107	0.041290632	0.17478063	0.03447701	-0.02139593	0.014930958	-0.01555963
-8.8	12.30360026	0.072986113	-0.13593807	0.009395724	0.068139344	-0.09764612	0.070641774	-0.03069597	0.132567361	-0.0648848	0.06891719	0.045670118	0.003475808	0.172767437	0.086355902	-0.02527846	0.033562253	-0.07384551
-8.9	12.14562814	0.071308238	-0.13687894	0.002305974	0.062818085	-0.11528873	0.056765754	-0.01630089	0.120650036	-0.02950125	0.125595907	0.008340064	-0.03035159	0.166327003	0.152720554	-0.03112762	0.050558825	-0.14961013
-9	11.98073071	0.069615489	-0.13742619	-0.00492607	0.057978544	-0.13194056	0.035074659	-0.00168506	0.105541771	0.00794967	0.177165832	-0.02877279	-0.06474765	0.147544021	0.208492194	-0.03288829	0.061441617	-0.21536542
-9.1	11.81366141	0.068121765	-0.13640887	-0.01130071	0.057377887	-0.14615813	0.016976899	0.015909235	0.098833816	0.047976188	0.198936573	-0.03515735	-0.08614745	0.091804033	0.18229429	-0.00883138	0.029460941	-0.17412262
-9.2	11.63975965	0.066672233	-0.13457195	-0.01731941	0.058011184	-0.15748156	0.000797713	0.035122618	0.091208525	0.085453359	0.201568738	-0.02805827	-0.0971663	0.024432492	0.122932783	0.022478469	-0.01272674	-0.09874312
-9.3	11.45942432	0.065217543	-0.1324862	-0.02370816	0.059721163	-0.16511466	-0.01468086	0.054062907	0.085574555	0.124604609	0.203037502	-0.00933995	-0.10049215	-0.05226898	0.047377839	0.052761395	-0.08787249	-0.02017138
-9.4	11.27365932	0.063710581	-0.13011403	-0.03026868	0.061213762	-0.16910256	-0.02810907	0.07355317	0.076677039	0.156789121	0.191968784	0.015950234	-0.09865064	-0.12423872	-0.03475854	0.079983907	-0.1612563	0.059119314
-9.5	11.07167327	0.062014077	-0.1273514	-0.03608216	0.058437915	-0.16893189	-0.04064085	0.095973254	0.041968239	0.158438823	0.140809338	0.036038119	-0.09222174	-0.14505538	-0.0818521	0.089242291	-0.13803307	0.010243032
-9.6	10.86438592	0.060217679	-0.12452553	-0.04198775	0.053947624	-0.1643789	-0.05183547	0.118208913	-0.00056824	0.144748047	0.073446626	0.053997562	-0.08126246	-0.14194485	-0.11044387	0.086569382	-0.08188702	0.121634491
-9.7	10.66604593	0.058174366	-0.12206423	-0.04939252	0.047360396	-0.15670913	-0.05305137	0.141676987	-0.04499541	0.117611625	-0.00581969	0.072266386	-0.08501762	-0.12097462	-0.13599965	0.080585108	-0.00569585	0.135137816
-9.8	10.47122079	0.056023025	-0.11979504	-0.05754613	0.040274812	-0.14519177	-0.05250977	0.162402732	-0.08736601	0.0818787	-0.08507981	0.08702982	-0.08819617	-0.0870256	-0.14938706	0.067236282	0.073576276	0.131303823
-9.9	10.28160456	0.05412178	-0.11831387	-0.06621943	0.034977333	-0.12454393	-0.05772205	0.174556555	-0.10807545	0.051136274	-0.14058179	0.092414246	-0.06557177	-0.05656191	-0.12184859	0.026938799	0.098541383	0.090389318
-10	10.0964213	0.052191004	-0.11714617	-0.07539342	0.030464988	-0.09940042	-0.06595278	0.179224799	-0.11789934	0.021075928	-0.17981669	0.091679341	-0.03426909	-0.02596633	-0.07832804	-0.01984926	0.098642373	0.037987828
-10.1	9.911545204	0.050218959	-0.1154093	-0.08477637	0.02968414	-0.07416646	-0.08583596	0.175541279	-0.1223903	-0.05152039	-0.19145623	0.080151023	0.009047446	0.015697078	-0.03232424	-0.06691608	0.07465732	-0.06105172
-10.2	9.728576061	0.048109735	-0.11356022	-0.09437146	0.029939732	-0.04846151	-0.1097797	0.164221226	-0.12075984	-0.05120944	-0.18481504	0.063191697	0.055352748	0.056858894	0.01513862	-0.10833197	0.036419165	-0.16312111
-10.3	9.558204559	0.045363415	-0.11215323	-0.10470707	0.027531538	-0.02154886	-0.12906093	0.139342375	-0.11295113	-0.07492943	-0.16480962	0.047938568	0.075864282	0.075454494	0.037409754	-0.11019308	-0.00693079	-0.16161038
-10.4

Appendix D. Material Information and Specifications

Test Number	Part	Material Name	Part Number	Lot/Roll Number	Manufacturer	Manufacture Date
iSFT-075	Insulation Assembly	PBINBR	STW5-11058-002	39861/1	Kirkhill	12/14/2019
iSFT-076	Insulation Assembly	PBINBR	STW5-11058-002	39861/1	Kirkhill	12/14/2019
iSFT-077	Insulation Assembly	PBINBR	STW5-11058-002	39861/1	Kirkhill	12/14/2019
iSFT-078	Insulation Assembly	SFNBR	80019252	0001/1	Kirkhill	1/1/2017
iSFT-079	Insulation Assembly	SFEPDM	80015196	0001/1	Kirkhill	9/14/2014
iSFT-086	Convergent Cone	MXSE55	40797249	1013910/0001B	Solvay	2/26/2020
	Aft Liner Insert	MXSE55	40797249	1013910/0001A	Solvay	2/26/2020
iSFT-087	Convergent Cone	FM5504	40786607	1012871/005	Solvay	5/23/2019
	Aft Liner Insert	FM5504	40786607	1012318/001A, 001D	Solvay	3/27/2018

Cytec Engineered Materials, Inc.
501 West 3rd Street
Winona, MN 55987
Tel. (507) 454-3611
FAX. (507) 452-8195

BROADGOODS AND TAPES

MATERIAL: FM-5504

DESCRIPTION: FM-5504 is a high-purity silica reinforced prepreg employing a MIL-R-9299 resin. The reinforcement is a leached silica of 99% purity and a melting point of approximately 2000°F (1093°C). FM-5504 is useful in intermediate temperature ablative applications where oxidation potential is high. FM-5504 is suitable for short-term insulation service in the range of 3000-4000°F (1650-2200°C).

November 2002

Property	Units	Nominal English	Nominal Metric	Test Method
Resin solids		30 – 34	30 – 34	R111
Volatiles	Wt %	5 – 7	5 – 7	V137
Flow	Wt %	9 - 19	9 - 19	F-26
Tape tensile strength	lb/in (kg/cm)	305	54	

LAMINATED PROPERTIES: The following properties were obtained on 1/8" (3.2 mm) panels molded at 1000 psi (6.9 GPa) for 30 minutes at 325°F (163°C).

Property	Units	Nominal English	Nominal Metric	Test Method
Permanence				
Specific Gravity	g/cm³	1.7	1.7	ASTM D792
Barcol Hardness	g/cm³	70	70	ASDM D2583
Mechanical				
Cured ply thickness	In (mm)	0.021	0.53	
Tensile strength, warp	Ksi (MPa)	16	110	ASTM D638
Tensile Modulus, warp	Msi (GPa)	2.8	19	ASTM D638
Tensile strength, fill	Ksi (MPa)	11.6	80	ASTM D638
Tensile Modulus, fill	Msi (GPa)	2.1	14	ASTM D638
Flexural strength, warp	Ksi (MPa)	24	166	ASTM D790
Flexural modulus, warp	Msi (GPa)	2.5	17	ASTM D790
Flexural strength, fill	Ksi (MPa)	24	166	ASTM D790
Flexural modulus, fill	Msi (GPa)	2.5	17	ASTM D790
Compression Strength, warp	Ksi (MPa)	36	248	ASTM D695
Compression Modulus, warp	Msi (GPa)	2.2	15	ASTM D695
Compression Strength, fill	Ksi (MPa)	19.2	132	ASTM D695
Double notch shear	Ksi (MPa)	4.5	31	ASTM D3684
Dowel shear	Ksi (MPa)	3.7	26	FTM 406/1041
Thermal				
Deflection temperature	°F (°C)			ASTM D648
Glass transition temperature	°F (°C)			TMA
Thermal conductivity @ 250°F (121°C)		@ 250°F	@ 121°C	
With ply	W/m°K	0.47	0.47	F433
Across ply	W/m°K	0.57	0.57	F433
Coefficient of thermal expansion		@ 75 - 400°F	@ 24 - 204°C	
With ply @ 250°F (121°C)	10^{-6} in/in/°F (10^{-6} cm/cm/°C)	3.5	6.3	ASTM D3386

Cytec Engineered Materials, Inc.
501 West 3rd Street
Winona, MN 55987
Tel. (507) 454-3611
FAX. (507) 452-8195

Across ply @ 250°F (121°C)	10^{-6} in/in/°F (10^{-6} cm/cm/°C)	7.8	14	ASTM D3386

Cytec Engineered Materials
Winona Division
501 West Third Street
Winona, MN 55987
Tel. (507) 454-3611
Fax. (507) 452-8195

BROADGOODS AND TAPES

November 11, 2002

MATERIAL: MXSE-55

DESCRIPTION: MXSE-55 is a nominal 19-ounce per square silica fabric impregnated with a rubber modified phenolic resin. It has been found suitable as external ablative insulation in an aerodynamic heating environment. In solid rocket motors, it may be used internally as case, closure and submerged nozzle insulation.

PROPERTIES:

Uncured	Value	Test Method
Resin Solids, %	27-33	R-45
Volatile Content, %	2.5-4.5	V-1
Nominal Uncured Thickness, in	0.040	
Nominal Weight, lb/Lin yard	1.5	
Nominal Broadgoods Width, I	33	
Nominal Rubber to Phenolic Ratio	1:2	

Cured: The following properties were obtained from panels that were press cured at 500 psi for one hour at 325° F and cooled to ambient temperature under pressure. Other cure cycles can be used depending on part geometry and use.

Tensile Strength (Warp) psi	15,000	D-638
Modulus, Msi	2.0	D-638
Elongation, %	0.9	D-638
Tensile Strength 90°,psi	12,000	D-638
Tensile Strength 45°,psi	8,000	D-638
Elongation, %	3.3	D-638
Compression Strength (Warp) psi	13,000	D-695
Interlaminar Dowel Shear, psi	2,000	FTMS/406-1041
Specific Gravity	1.50	D-792
Cured Ply Thickness, in	0.022	
Specific Heat @ 150°F	0.25	C-351
Thermal Conductivity BTU/ft-hr-°F @ 300°F	0.18	C-177

REPORT DOCUMENTATION PAGE

Form Approved
OMB No. 0704-0188

1. REPORT DATE *(DD-MM-YYYY)*	2. REPORT TYPE	3. DATES COVERED *(From - To)*
07/29/2024	Technical Memorandum	

4. TITLE AND SUBTITLE
Characterization of Internal Insulation Thermal Performance

5a. CONTRACT NUMBER

5b. GRANT NUMBER

5c. PROGRAM ELEMENT NUMBER

6. AUTHOR(S)
Jones, Jonathan E.; Martin, Heath T.; Womack, James M.; Hiatt, Andrew T.

5d. PROJECT NUMBER

5e. TASK NUMBER

5f. WORK UNIT NUMBER

7. PERFORMING ORGANIZATION NAME(S) AND ADDRESS(ES)
NASA Langley Research Center
Hampton, VA 23681-2199

8. PERFORMING ORGANIZATION REPORT NUMBER
NESC-RP-19-01482

9. SPONSORING/MONITORING AGENCY NAME(S) AND ADDRESS(ES)
National Aeronautics and Space Administration
Washington, DC 20546-0001

10. SPONSOR/MONITOR'S ACRONYM(S)
NASA

11. SPONSOR/MONITOR'S REPORT NUMBER(S)
NASA/TM-20240009657

12. DISTRIBUTION/AVAILABILITY STATEMENT
Unclassified - Unlimited
Subject Category Fluid Mechanics and Thermodynamics
Availability: NASA STI Program (757) 864-9658

13. SUPPLEMENTARY NOTES

14. ABSTRACT

A test campaign was performed to build an SRM-insulation-material thermal-performance database using MSFC's Solid Fuel Torch that could be leveraged to enhance understanding of the relationship between ablation rates and internal-environment parameters and improve insulation performance predictions. Seven hot-fire tests were performed along with data analysis that revealed the thermal performance differences among the tested materials. Functional Data Analysis was employed to create a model of material ablation rate as a function of six covariates. The relative importance of several environmental parameters was indicated, and the gaps in the operational space covered by the database were identified.

15. SUBJECT TERMS
Ablation; Insulation; Solid Rocket Motor; Hybrid Rocket Motor; Functional Data Analysis

16. SECURITY CLASSIFICATION OF:			17. LIMITATION OF ABSTRACT	18. NUMBER OF PAGES	19a. NAME OF RESPONSIBLE PERSON
a. REPORT	b. ABSTRACT	c. THIS PAGE			STI Help Desk (email: help@sti.nasa.gov)
					19b. TELEPHONE NUMBER *(Include area code)*
U	U	U	UU	75	(443) 757-5802